AI

Global to Regional Atlas

Coordinating Editors: Hans-Otto Pörtner (Germany), Andrés Alegría (Germany/Honduras)

Editorial Team: Vincent Möller (Germany), Elvira S. Poloczanska (UK/Australia), Katja Mintenbeck (Germany), Sandra Götze (Germany)

AR6 WGII Chapter Representatives: Aditi Mukherji (Chapter 4), Carolina Adler (Chapter 17/CCP5), Christopher H. Trisos (Chapter 9), Christopher Lennard (Chapter 9), David S. Gutzler (Chapter 14), David Wrathall (Chapter 8), Delphine Deryng (Chapter 5), Donovan Campbell (Chapter 15), Elham Ali (Chapter 4), Gerald Nelson (Chapter 5), Guéladio Cissé (Chapter 7), Jamon Van Den Hoek (Chapter 8), Jeff Price (Chapter 2/CCP1), Joanna McMillan (Chapter 8), Joern Birkmann (Chapter 8), John Pinnegar (Chapter 15), Kevin Hennessy (Chapter 11), Kirstin Holsman (Chapter 14/CCP6), Laura Ramajo Gallardo (Chapter 12), Laurent Bopp (Chapter 3), Lea Berrang Ford (Chapter 16), M. Silvia Muylaert de Araujo (Chapter 18), Marie-Fanny Racault (Chapter 3), Marjolijn Hassnoot (Chapter 13), Mark Costello (Chapter 11/CCP1) Mark Pelling (Chapter 6), Nicholas P. Simpson (Chapter 9), Nicola Stevens (Chapter 2/CCP4), Piero Lionello (Chapter 13/CCP4), Rebecca Harris (Chapter 2/CCP3), Richard Dawson (Chapter 6/CCP2), Tabea Katharina Lissner (Chapter 4), Timon McPhearson (Chapter 6), Valeria Moreno Rudloff (CCP5) Veruska Muccione (Chapter 13), Winston Chow (Chapter 6/CCP2), Wolfgang Cramer (Chapter 1/CCP4), Wolfgang Kiessling (Chapter 3/CCP1), Yukiko Hirabayashi (Chapter 4), Zelina Zaiton Ibrahim (Chapter 16)

This annex should be cited as:

IPCC, 2022: Annex I: Global to Regional Atlas [Pörtner, H.-O., A. Alegría, V. Möller, E.S. Poloczanska, K. Mintenbeck, S. Götze (eds.)]. In: *Climate Change 2022: Impacts, Adaptation and Vulnerability.* Contribution of Working Group II to the Sixth Assessment Report of the Intergovernmental Panel on Climate Change [H.-O. Pörtner, D.C. Roberts, M. Tignor, E.S. Poloczanska, K. Mintenbeck, A. Alegría, M. Craig, S. Langsdorf, S. Löschke, V. Möller, A. Okem, B. Rama (eds.)]. Cambridge University Press, Cambridge, UK and New York, NY, USA, pp. 2811–2896, doi:10.1017/9781009325844.028.

AI

AI.1 Introduction

The WGII Global to Regional Atlas integrates and expands on the key messages in WGII chapters and cross-chapter papers to provide summaries of vulnerability, impacts, exposure, adaptation and risk complementing the narrative in the Summary for Policymakers. Where useful for a more complete storyline, complementary maps and figures from the three AR6 Special Reports are included. Figures are grouped in topical clusters: (1) Biodiversity, Biogeography, Habitability, Health, (a) Wild Species, (b) Humans, (c) Livestock and Crop Production, (d) Fish Stocks and Fisheries (Section AI.2.1); (2) Water-Related Challenges for Cities, Settlements and Key Infrastructure, (a) Drought, (b) Flooding (Section AI.2.2); (3) Global to Regional Risks (including economic), and Adaptive Capacities (Section AI.2.3); and (4) From Adaptation to Climate Resilient Development (Section AI.2.4). Within each topical cluster, the Summary for Policymakers (SPM) storyline is followed depending on the material available, from observed impacts (and adaptation) and projected impacts and risks, adaptation and enabling conditions to climate resilient development.

The Atlas provides visual support to key findings of the Assessment Report, allowing a broader display of material and case studies. The Atlas is not intended to be comprehensive. The underlying scientific basis for each figure/map is indicated by references to sections of the underlying report. These references are listed within curly brackets { and } at the end the corresponding caption texts.

AI.1.1 Risk Framework

The Atlas includes mapping of the different components of risk. Risk in this report is defined as the potential for adverse consequences for human or ecological systems, recognising the diversity of values and objectives associated with such systems. In the context of climate change impacts, risks result from dynamic interactions between climate-related hazards with the exposure and vulnerability of the affected human or ecological system. In the context of climate change responses, risks result from the potential for such responses not achieving the intended objective(s), or from potential trade-offs or negative side effects (Annex II: Glossary). Risk management is defined as plans, actions, strategies or policies to reduce the likelihood and/or magnitude of adverse potential consequences, based on assessed or perceived risks (Annex II: Glossary). {1.2.1.1}

Vulnerability is a component of risk, but also an important focus independently. Vulnerability in this report is defined as the propensity or predisposition to be adversely affected. Vulnerability encompasses a variety of concepts and elements including sensitivity or susceptibility to harm and lack of capacity to cope and adapt (Annex II: Glossary). Over the past several decades, approaches to analysing and assessing vulnerability have evolved. An early emphasis on top-down, biophysical evaluation of vulnerability included—and often started with—exposure to climate hazards in assessing vulnerability. From this starting point, attention to bottom-up, social and contextual determinants of vulnerability, which often differ, has emerged, although this approach is incompletely applied or integrated across contexts (Rufat et al., 2015; Spielman et al., 2020; Taberna et al., 2020). Vulnerability is now widely understood to differ within communities and across societies, also changing through time (Jurgilevich et al., 2017; Kienberger et al., 2013;

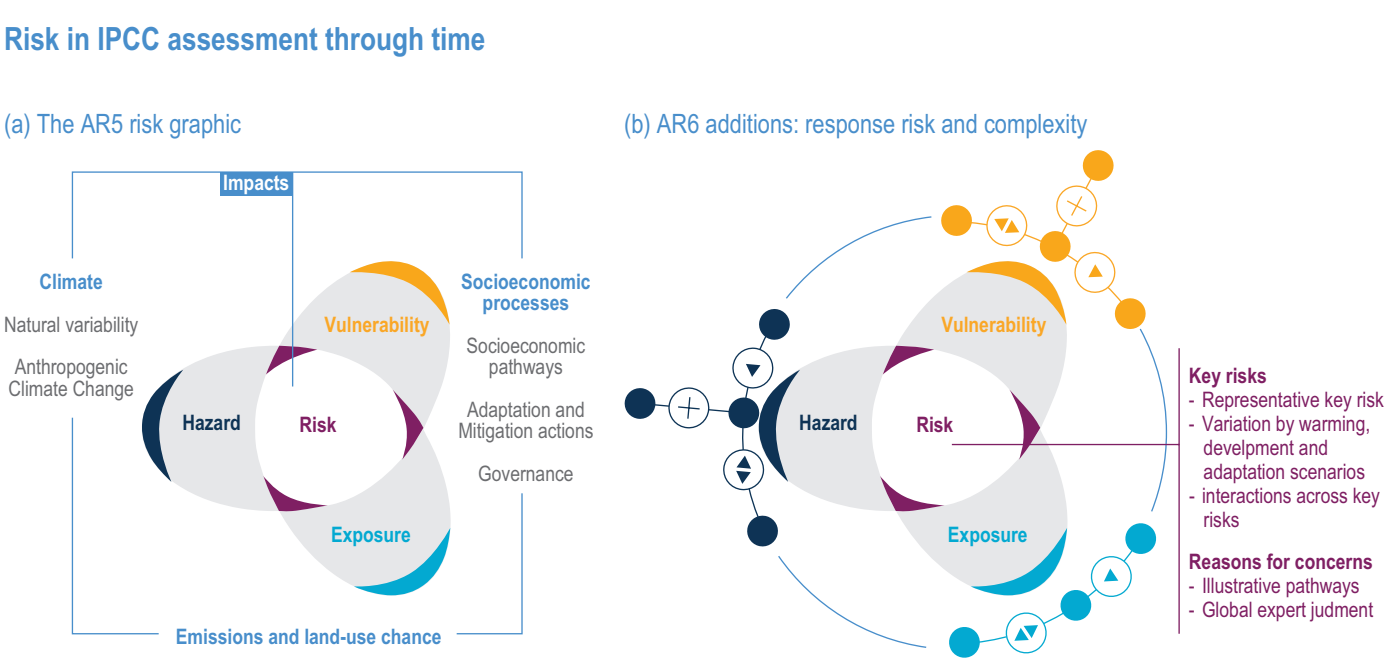

Figure AI.1 | Risk in IPCC assessments.

(a) An explicit risk framing emerged in the IPCC SREX (IPCC, 2012) and WGII AR5 (IPCC, 2014).

(b) In the current AR6 assessment, the role of responses in modulating the determinants of risk is a new emphasis (the 'wings' of the hazard, vulnerability and exposure 'propellers' represent the ways in which responses modulate each of these risk determinants {Figure 1.5}

https://doi.org/10.1017/9781009325844.028

see also Chapter 16). In the WGII AR6, assessment of the vulnerability of people and ecosystems encompasses the differing approaches that exist within the literature, both critiquing and harmonising them based on available evidence. In this context, **exposure** is defined as the presence of people; livelihoods; species or ecosystems; environmental functions, services and resources; infrastructure; or economic, social or cultural assets in places and settings that could be adversely affected (Annex II: Glossary). Potentially affected places and settings can be defined geographically, as well as more dynamically, for example through transmission or interconnections through markets or flows of people. {1.2.1.1}

The WGII AR6 assessment focuses primarily on adverse consequences of climate change. However, climate change also has positive implications (benefits and opportunities) for certain people and systems. {16.1.2}

AI.1.2 Regionalisation

As climate change is a multi-scale phenomenon from the local to the global, the assessment of climate risks and climate change impacts is strongly spatial, with a focus on regional climate change. The term 'regions' is used in different ways throughout the interdisciplinary AR6 assessment as the use of the term varies across disciplines. It is alternately used to point to a particular geography, relate physical distance or proximity, or categorise areas based on common biological, topographical characteristics, or elevation in relation to sea level. Its meaning depends on context. {1.3.3}

First, there are chapters dedicated to regional assessment in AR6 WGII (Chapters 9–15 and Cross-Chapter Paper 4), and within the content of these and other chapters of AR6, the term region is often used to describe continental and sub-continental regions, oceanic regions, hemispheres, or more specific localities within these geographic areas. Building on the continental domains defined in AR5 WGII (IPCC, 2014) and to ensure consistency with the AR6 WGI Atlas (Gutiérrez et al., 2021), AR6 WGII uses a Continental Set of Regions, namely Africa, Asia, Australasia, Europe, North America, Central and South America, Small Islands, Polar Regions and the Ocean. For AR6, the continental regions include the land together with the coastal ocean. {1.3.3}

Second, the term regions is used to categorise areas around the globe with common topographical characteristics or biological characteristics. For example, Chapter 2 introduces regions in its discussion of biomes, as in arid, grassland, savanna, tundra regions, tropical, temperate and boreal forested regions. Chapter 3 adds reference to an area's orientation with bodies of water, using terms such as deltaic, coastal, intercoastal, freshwater and salty. On top of this, Cross-Chapter 2 uses a coastal region typology based on physical geomorphology considering elevation, coastal type and topography (see Cross-Chapter Paper 2; Barragán and de Andrés, 2015; Haasnoot et al., 2019a; Kay and Adler, 2017). {1.3.3}

Third, cross-chapter papers are dedicated to typological regions, defined in the AR6 Glossary (Annex II) as regions that share one or more specific features (known as 'typologies'), such as geographic location (e.g., coastal), physical processes (e.g., monsoons), and biological (e.g., coral reefs, tropical forests), geological (e.g., mountains) or anthropogenic (e.g., megacities) formation, and for which it is useful to consider the common climate features. Typological regions are generally discontinuous (such as monsoon areas, mountains and megacities) and are specifically used to integrate across similar climatological, geological and human domains. {1.3.3}

Fourth, the IPCC-WGI reference regions have been used for the regional synthesis of historical trends and future climate change projections. A recent update of these regions presented in AR6 WGI Atlas and used throughout AR6, offer an opportunity for refinement due to the higher atmospheric model resolution (including CMIP6). The number of land and ocean regions is 46 and 15, respectively, representing consistent regional climate features.

AI.1.3 Links to Working Group I

The WGII Atlas links to WGI through global and regional climate information {WGI Chapter 12 [Ranasinghe et al., 2021], WGI Atlas [Gutiérrez et al., 2021]}. Regional climate change information for impacts and for risk assessment draws on analysis of global and regional climatic variables that link climate conditions to sectors.

https://doi.org/10.1017/9781009325844.028

Physical drivers of climate change: Temperature

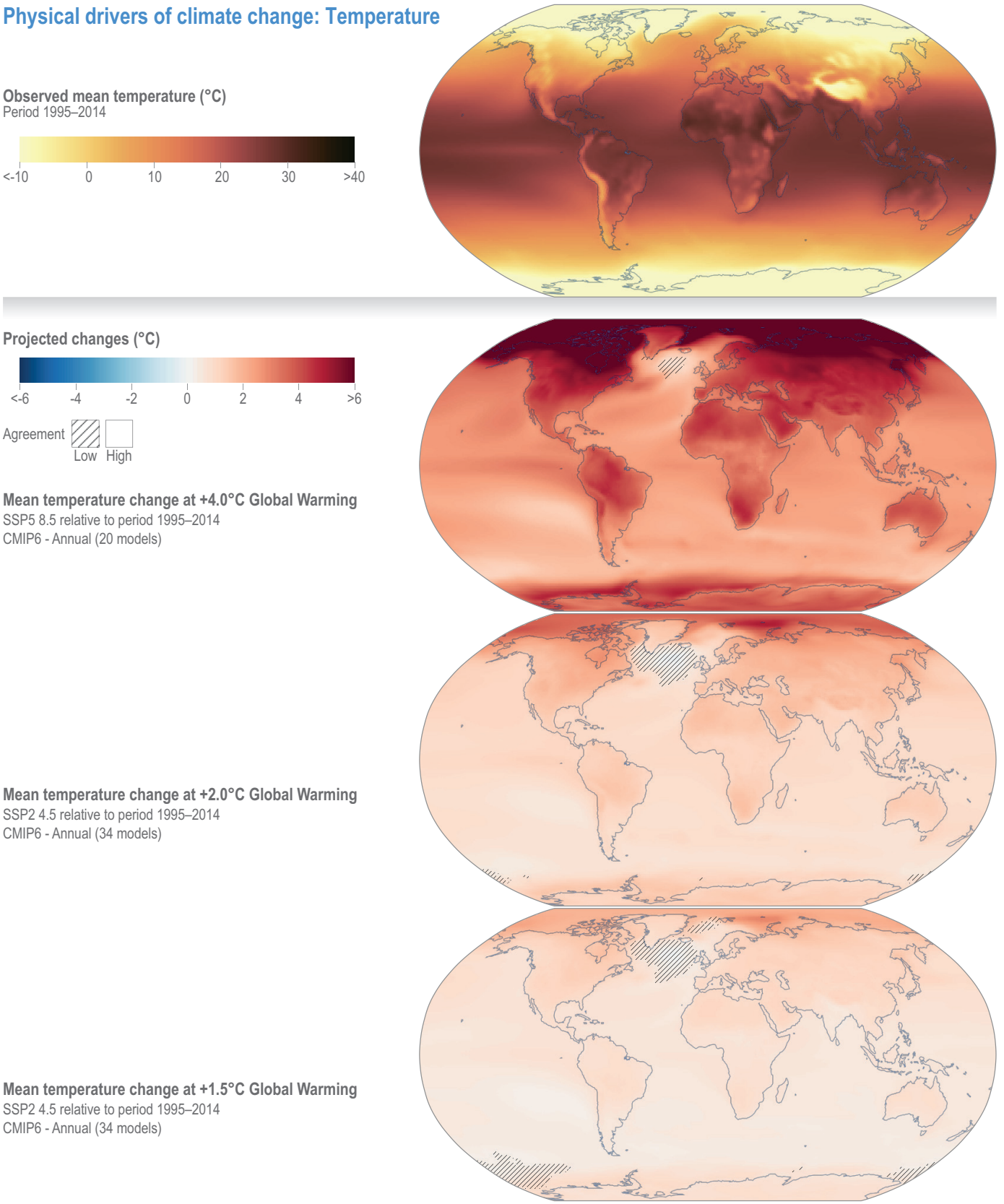

Figure AI.02 | Physical drivers of climate change: Temperature. {AR6 WGI Interactive Atlas, Gutiérrez et al., 2021}

https://doi.org/10.1017/9781009325844.028

Physical drivers of climate change: Precipitation

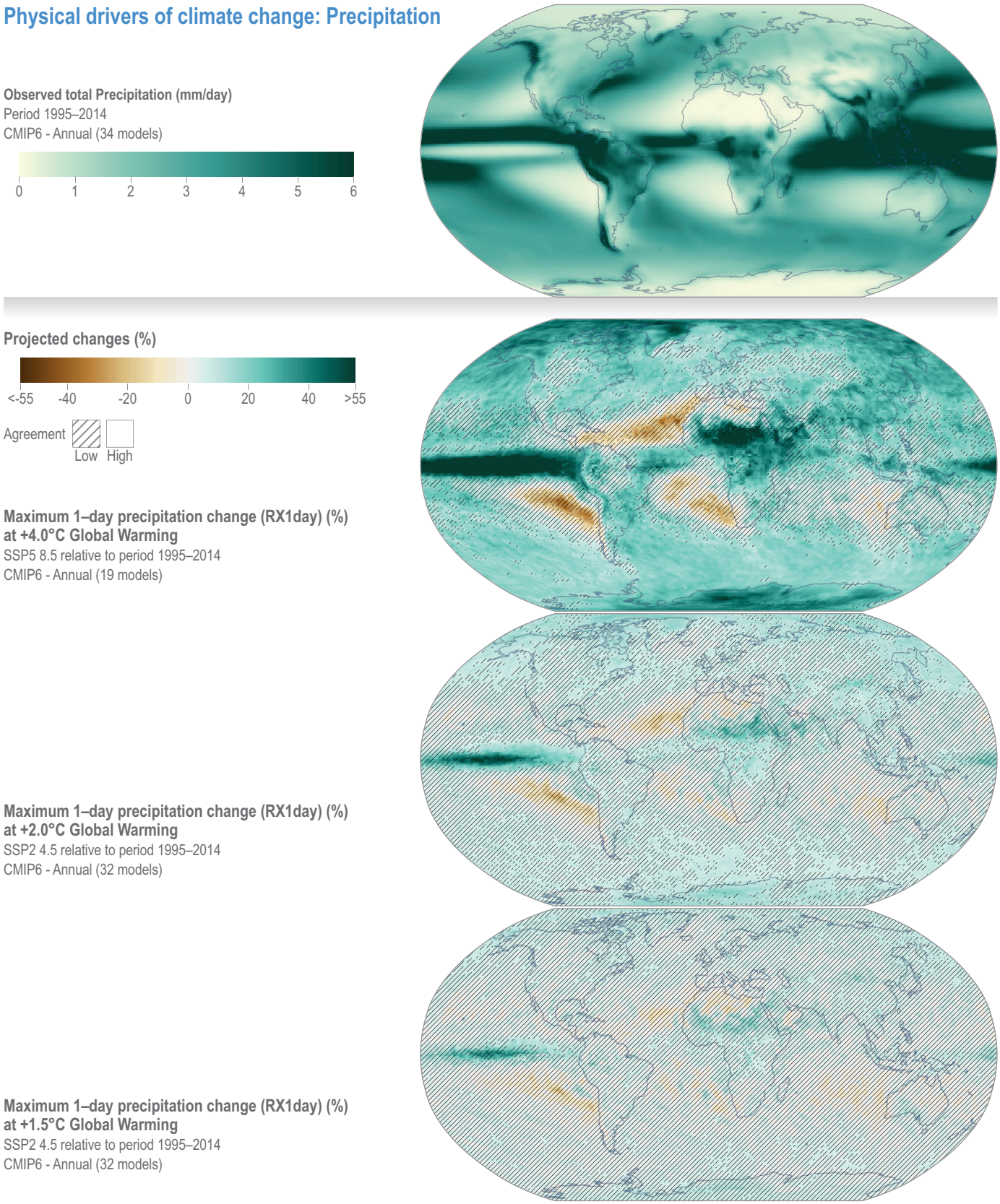

Figure AI.03 | Physical drivers of climate change: Precipitation. {AR6 WGI Interactive Atlas, Gutiérrez et al., 2021}

Physical drivers of climate change: Dissolved oxygen in the ocean

Oxygen concentrations affect aerobic processes, such as energy metabolism, and anaerobic microbial processes, such as denitrification. Hence, projected decreases in dissolved oxygen concentration will impact organisms and their geographic distribution patterns in ways that depend upon their oxygen requirements, which are highest for large, multicellular organisms.

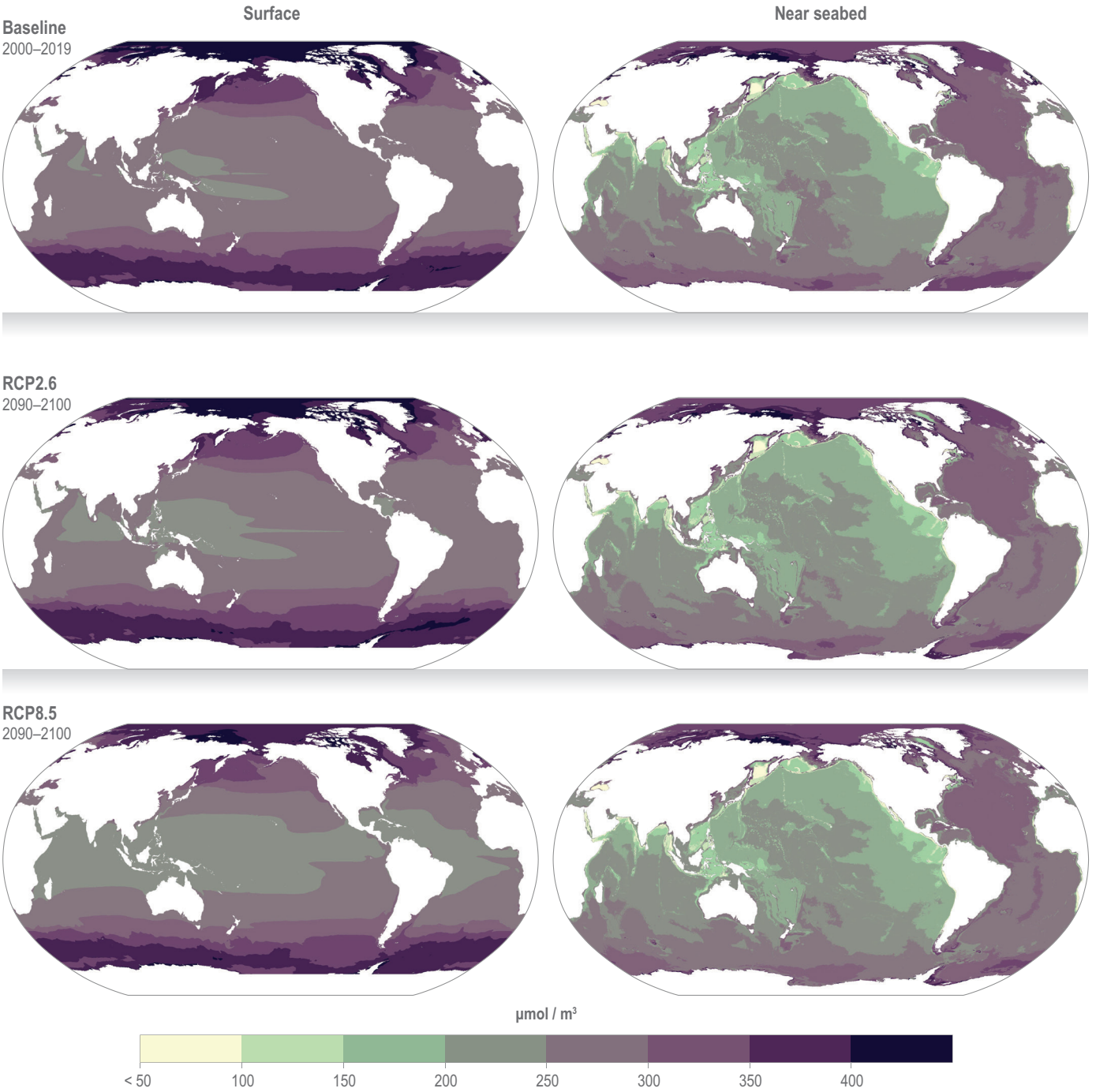

Figure AI.04 | Physical drivers of climate change: Dissolved oxygen in the ocean. {Assis et al., 2017}

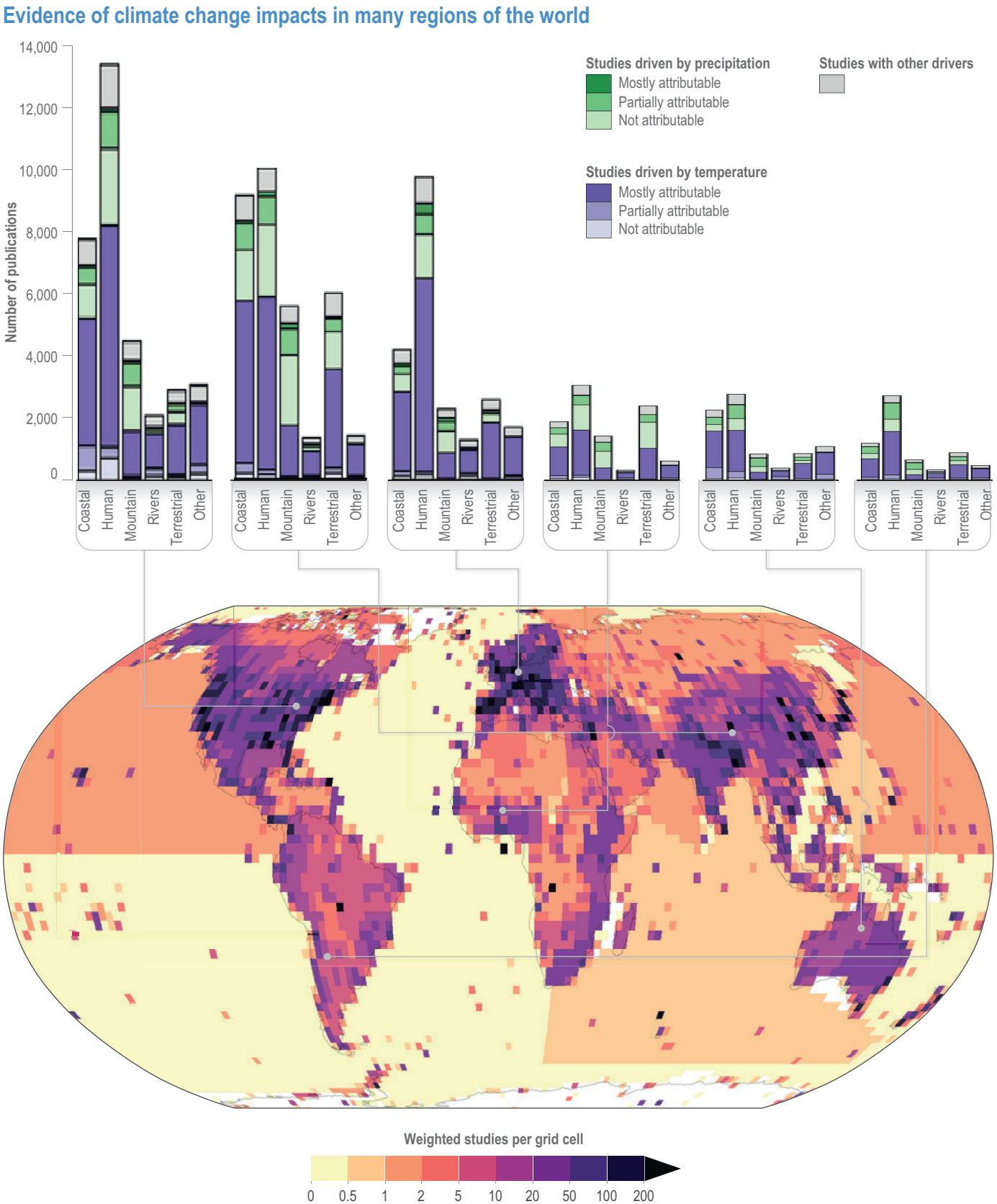

Figure AI.05 | Evidence of climate change impacts in many regions of the world. Global density map shows climate impact evidence, derived by machine learning from 77,785 studies. Bar charts show the number of studies per continent and impact category. Bars are coloured by the climate variable predicted to drive impacts. Colour intensity indicates the percentage of cells a study refers to where a trend in the climate variable can be attributed (partially attributable: >0% of grid cells, mostly attributable: >50% of grid cells). From Callaghan et al. (2021). {Figure 1.1}

Projected changes in global marine species richness in 2100 compared to 2006

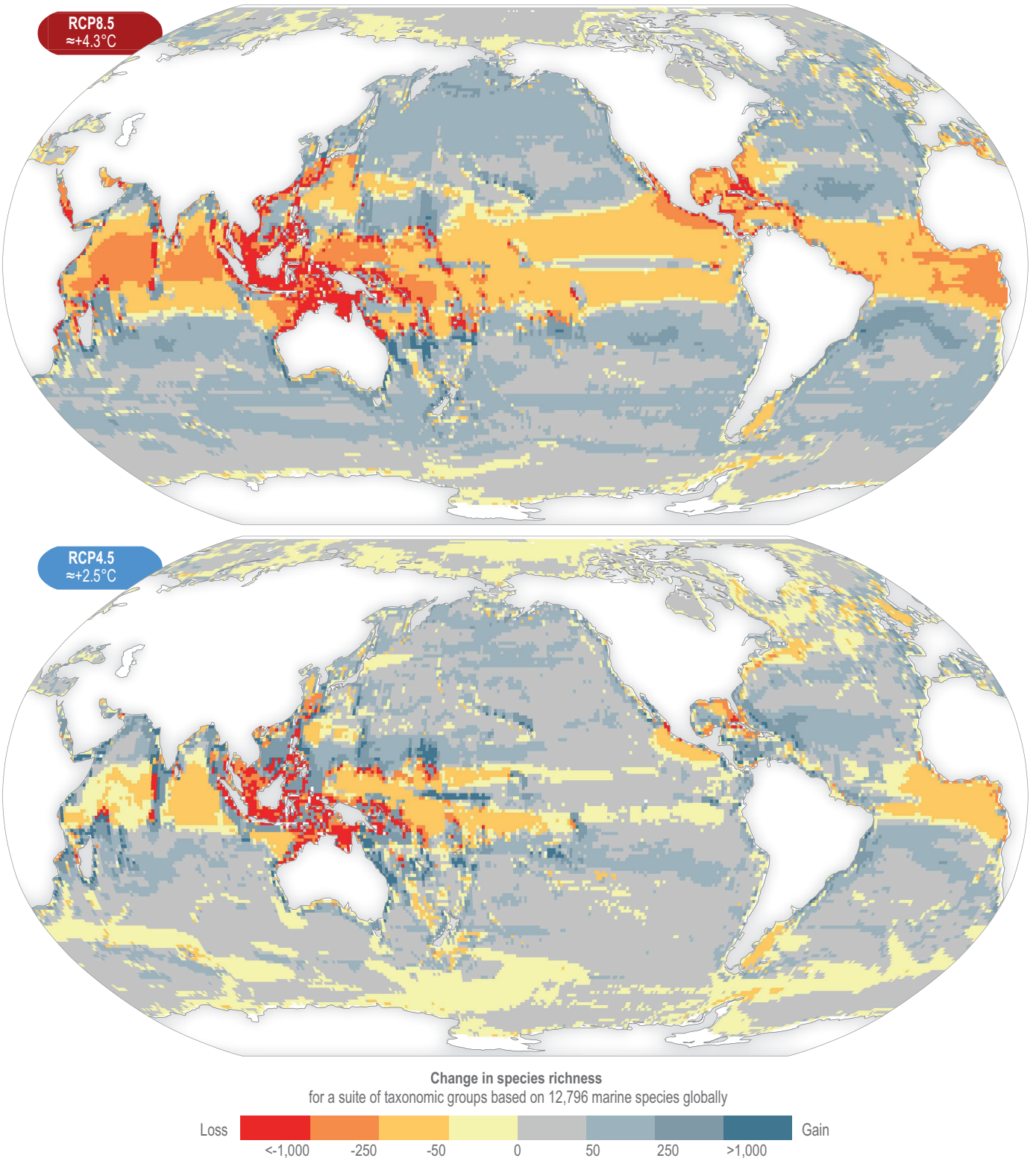

Figure AI.6 | Projected changes in global marine richness in 2100 compared with 2006. Differences between current (year 2006) and projected (year 2100) species richness for Representative Concentration Pathways RCP4.5 and RCP8.5 (García Molinos et al., 2016).

AI.2 Global to Regional Maps

AI.2.1 Biodiversity, Biogeography, Habitability, Health

AI.2.1.1 Wild Species

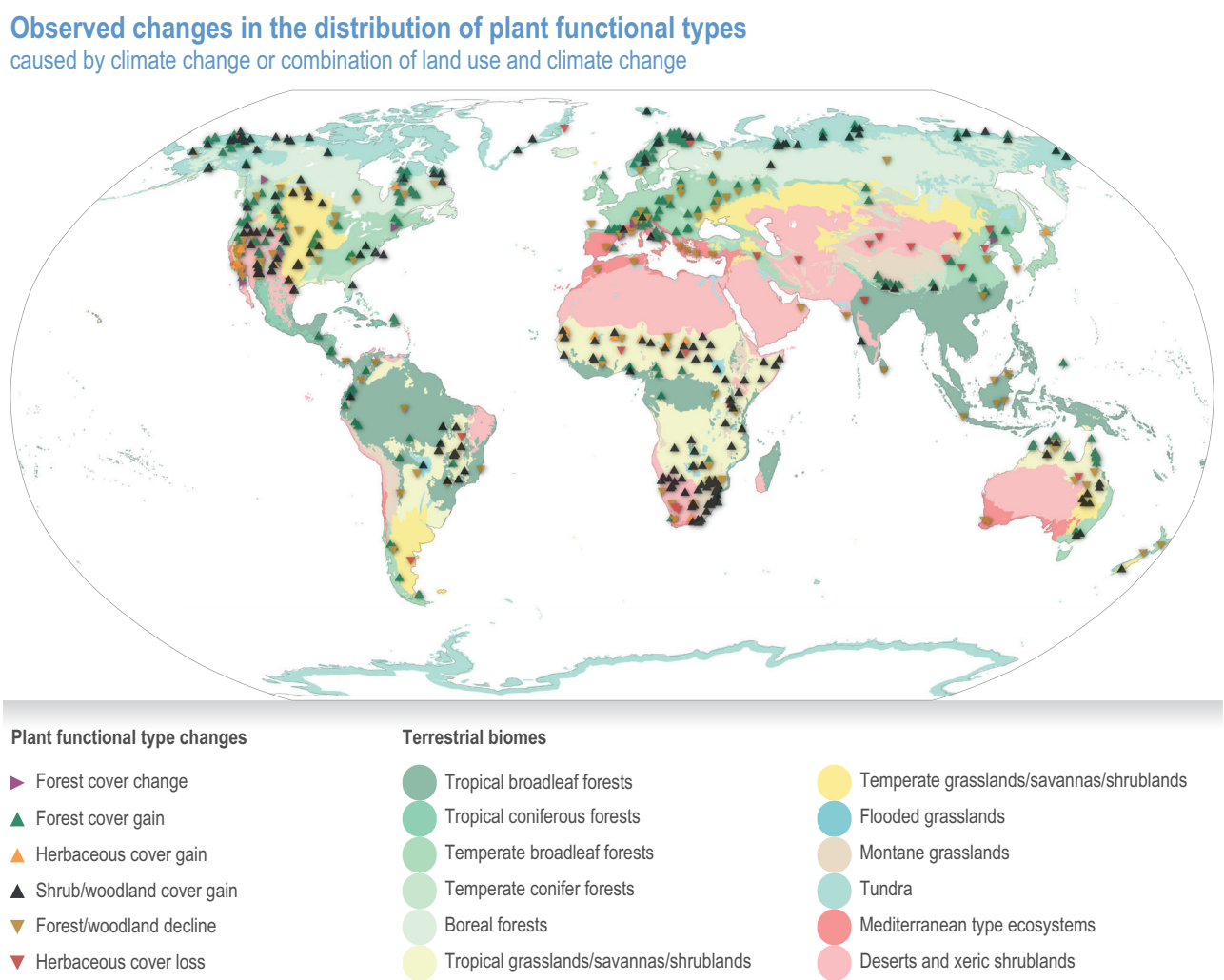

Figure AI.07 | Observed shifts in distribution of plant functional types. Observed shifts in the distribution of plant functional types over 1700–2020. Shifts in plant functional types are indicative of shift in biome function and structure. {Box 2.1, Figure Box 2.1.1}

Projected responses of rangeland plants to CO_2 fertilization

Changes in 2050 under RCP8.5 relative to 1971–2000

Figure AI.08 | Projected responses of rangeland plants to CO_2 fertilization. Regional percent changes in land cover and soil carbon from ensemble simulation results and plant responses to CO_2 fertilization. Regions as defined by the United Nations Statistics Division. (Boone et al., 2018) {5.5.3; Figure 5.11}

https://doi.org/10.1017/9781009325844.028

People living in land area of high conservation importance

These are a priority areas for nature conservation because they contain a high number of (endemic) species that occur nowhere else.

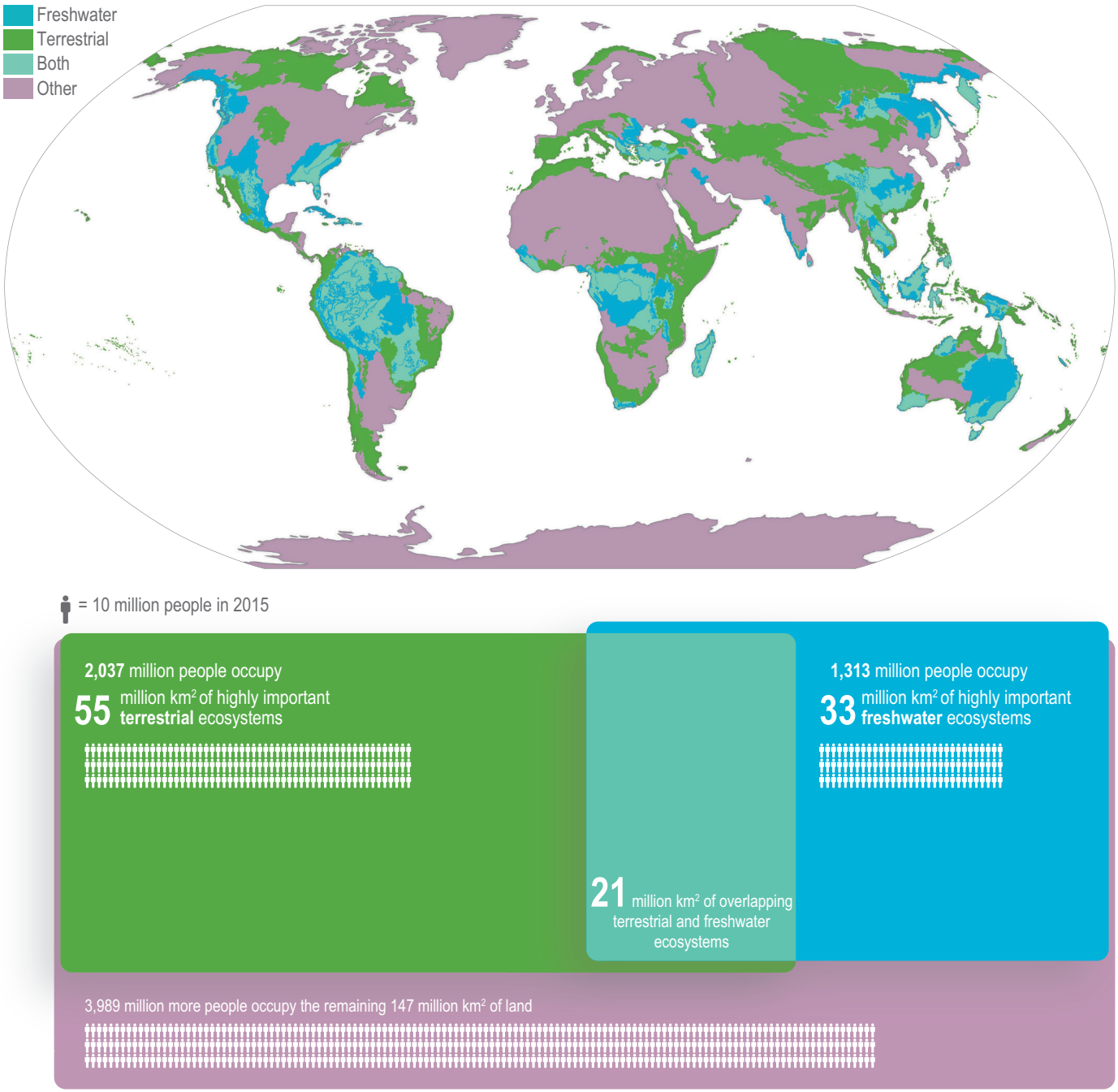

Figure AI.09 | People living in land area of high conservation importance. {CCP1.2.1.3, Figures CCP1.1, CCP1.2}

Present and projected habitat losses

of climatically suitable space across areas of high importance for biodiversity conservation

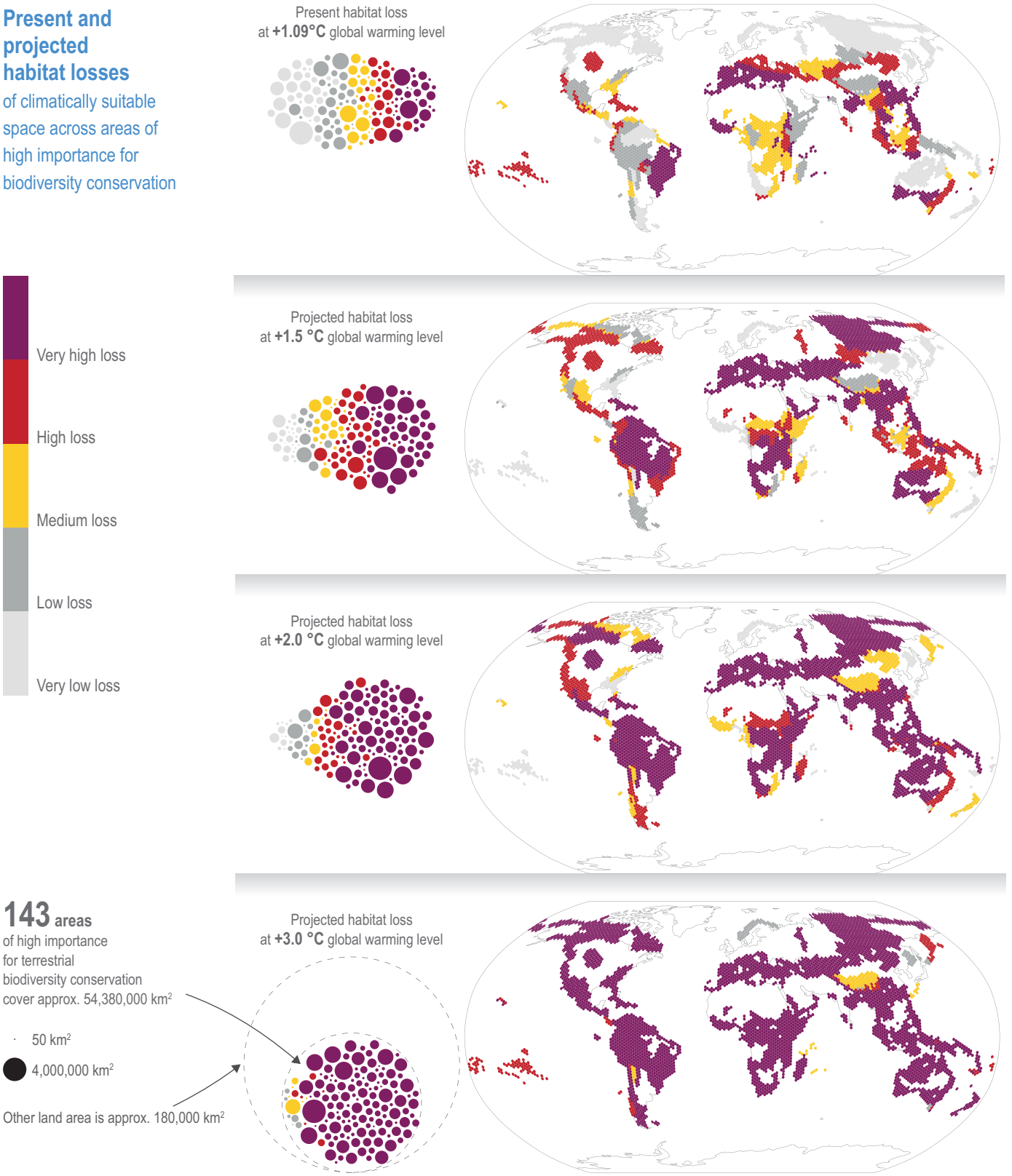

Figure AI.10 | Present and projected habitat losses of climatically suitable area in terrestrial biodiversity hotspots. Projected loss for present day (around 1°C warming) and at global warming levels of 1.5°C, 2°C and 3°C. Maps (right-hand column) show the regional distribution of losses in five categories of loss (very low loss 0–20%, low loss 20–40%, medium loss 40–60%, high loss 60–80%, very high loss 80–100%). The clusters of circles (middle column) show losses in the five categories of loss in each of the 143 hotspot areas of high importance for terrestrial biodiversity conservation with circles scaled by area size. {CCP1, Figure CCP1.6; Table CCP1.1}

https://doi.org/10.1017/9781009325844.028

Projected change in marine fish biomass

Simulated change averaged over 2090–2099, relative to 1990–1999

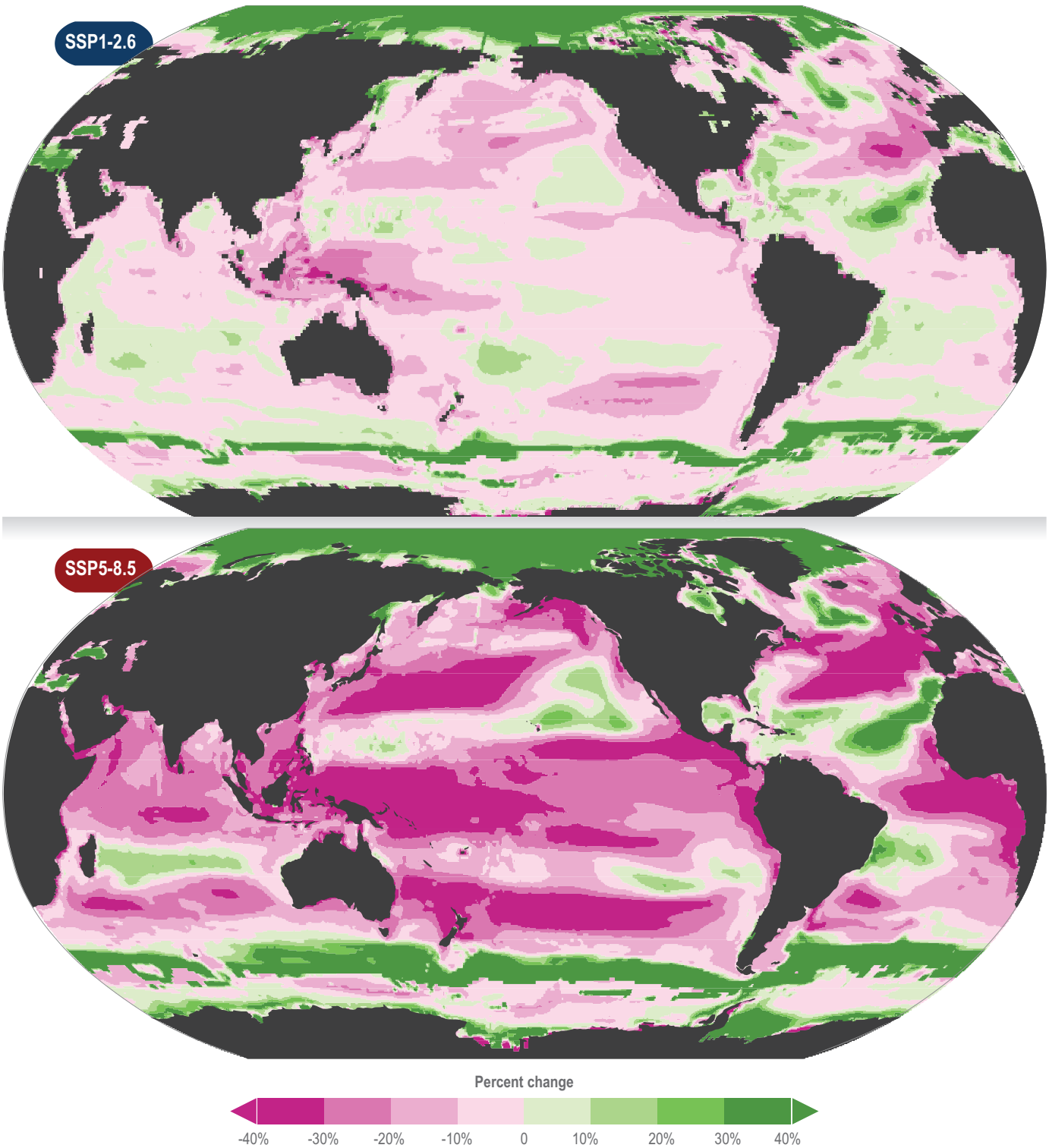

Figure AI.11 | Projected change in marine animal biomass. Simulated global biomass changes of animals. Spatial patterns of simulated change by 2090–2099 are calculated relative to 1995–2014 for SSP1-2.6 and SSP5-8.5. The ensemble projections of global changes in total animal biomass updated based on Tittensor et al. (2021) include 6–9 published global fisheries and marine ecosystem models from the Fisheries and Marine Ecosystem Model Intercomparison Project (Fish-MIP, Tittensor et al., 2018, 2021), forced with standardised outputs from two Coupled Model Intercomparison Project 6 (CMIP6) Earth System Models (ESMs). {3.4.3; Figure 3.21}

Projected change in marine zooplankton biomass

Simulated change by 2090–2099, relative to 1995–2014

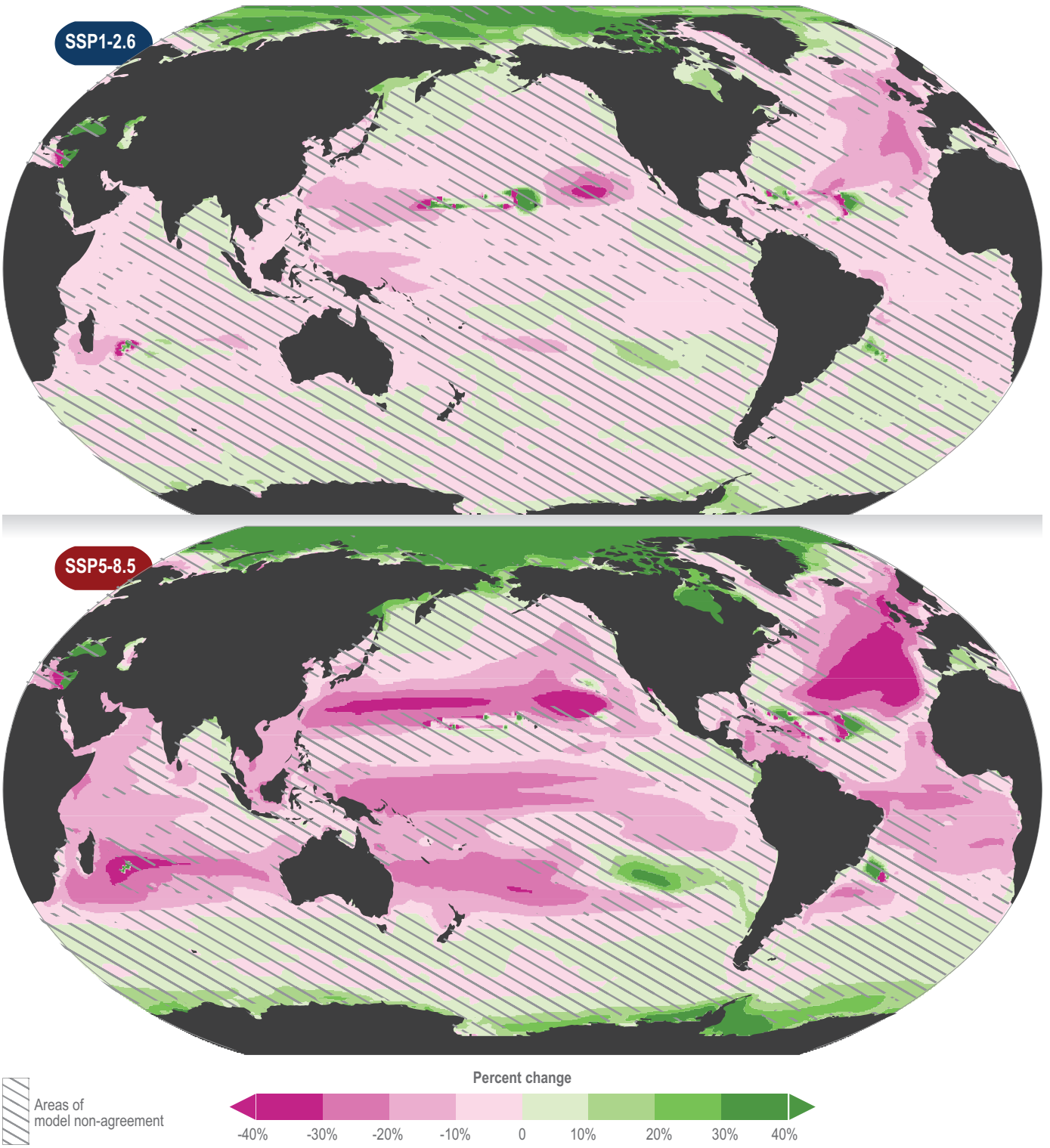

Figure AI.12 | Projected change in marine zooplankton biomass. Spatial patterns of simulated change by 2090–2099 are calculated relative to 1995–2014 for SSP1-2.6 and SSP5-8.5. The ensemble projections of global changes in zooplankton biomasses updated based on Kwiatkowski et al. (2019) include, under SSP1-2.6 and SSP5-8.5, respectively, a total of 9 and 10 Coupled Model Intercomparison Project 6 (CMIP6) Earth System Models (ESMs). Unhatched areas represent regions where at least 80% of models agree on the sign of biomass anomaly. {3.4.3.4, Figure 3.21}

Projected change in marine phytoplankton biomass

Simulated change averaged over 2090–2099, relative to 1995–2014

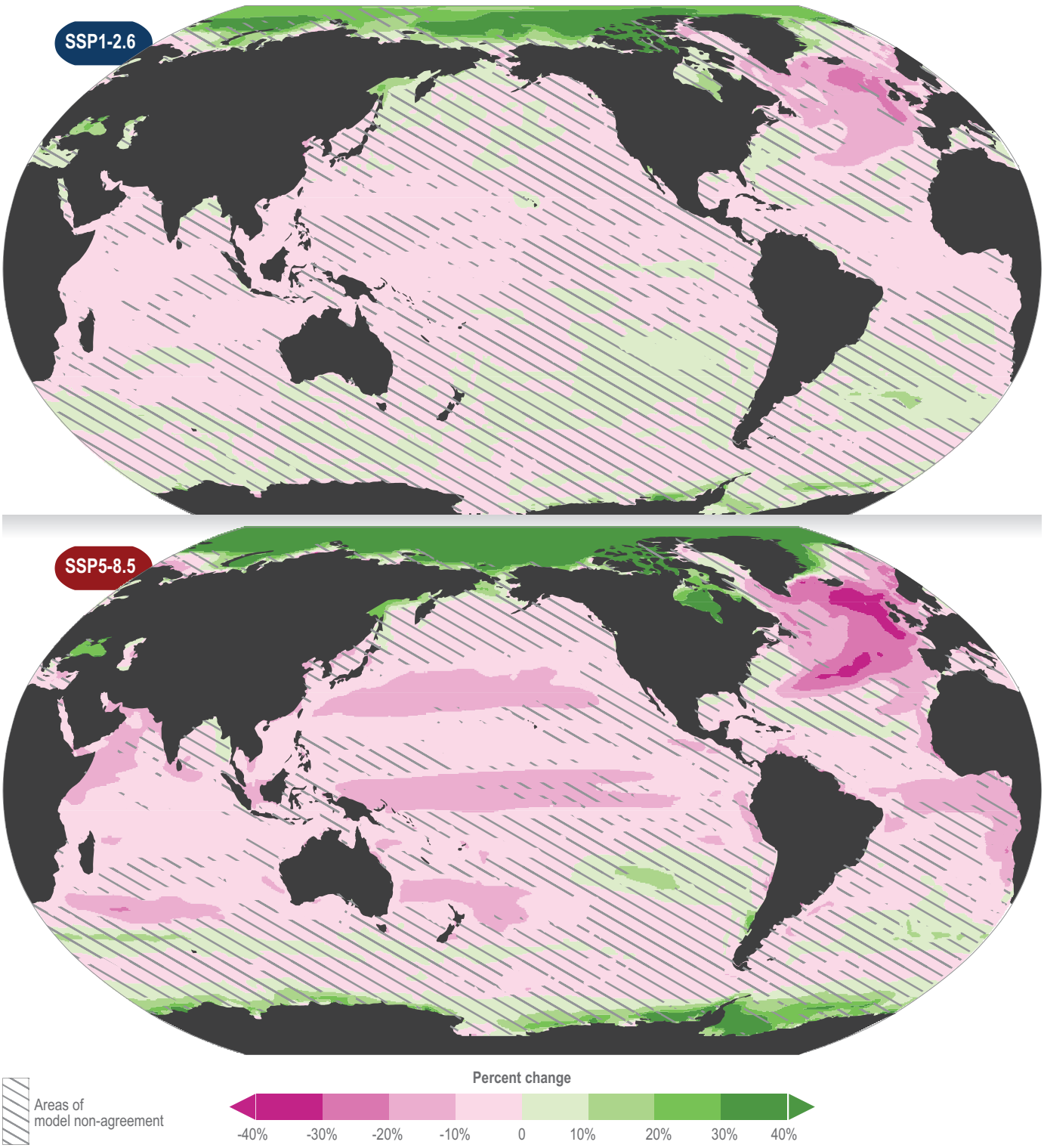

Figure AI.13 | Spatial patterns of simulated change in total phytoplankton biomass. Spatial patterns of simulated change by 2090–2099 are calculated relative to 1995–2014 for SSP1-2.6 and SSP5-8.5. The ensemble projections of global changes in phytoplankton biomasses updated based on Kwiatkowski et al. (2019) include, under SSP1-2.6 and SSP5-8.5, respectively, a total of 9 and 10 Coupled Model Intercomparison Project 6 (CMIP6) Earth System Models (ESMs). Unhatched areas represent regions where at least 80% of models agree on the sign of biomass anomaly. {3.4.3.4, Figure 3.21}

Projected change in marine benthic animal biomass

Simulated change averaged over 2090–2099, relative to 1990–1999

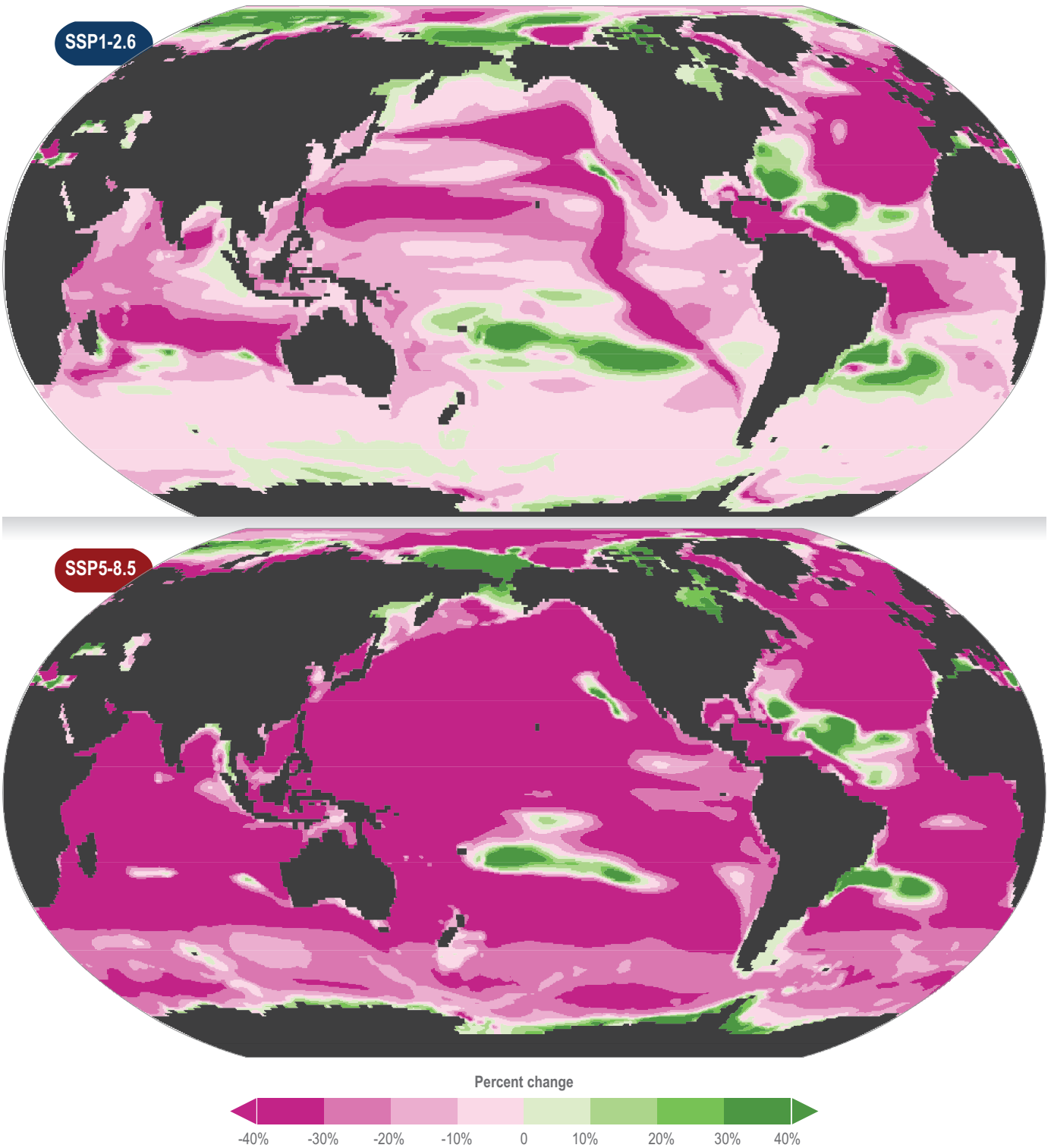

Figure AI.14 | Spatial patterns of simulated change in total benthic animal biomass. Spatial patterns of simulated change by 2090–2099 are calculated relative to 1995–2014 for SSP1-2.6 and SSP5-8.5. Globally integrated changes in total seafloor benthos biomass have been updated based on Yool et al. (2017) with one benthic model (Kelly-Gerreyn et al., 2014) forced with the Coupled Model Intercomparison Project 6 (CMIP6) Earth System Models (ESMs). {3.4.3.4, Figure 3.21}

Percentage of species exposed to potentially dangerous climate conditions

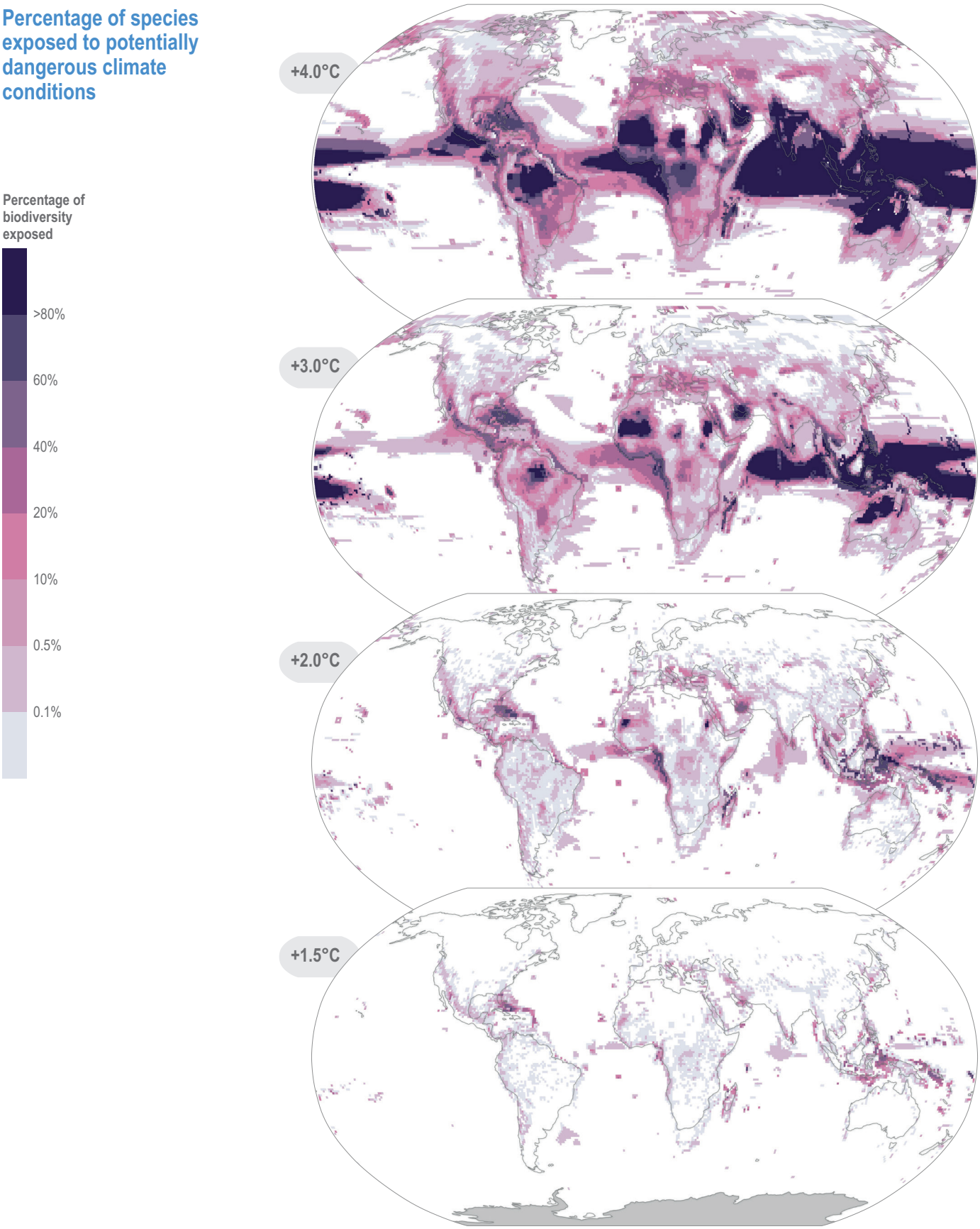

Figure AI.15 | Projected exposure of biodiversity. Global warming levels modelled across the ranges of more than 30,000 marine and terrestrial species. Figure based on Trisos et al. (2020). {CCP1; Figure 3.20}

Projected loss of terrestrial and freshwater biodiversity

at different global warming levels compared to pre-industrial period

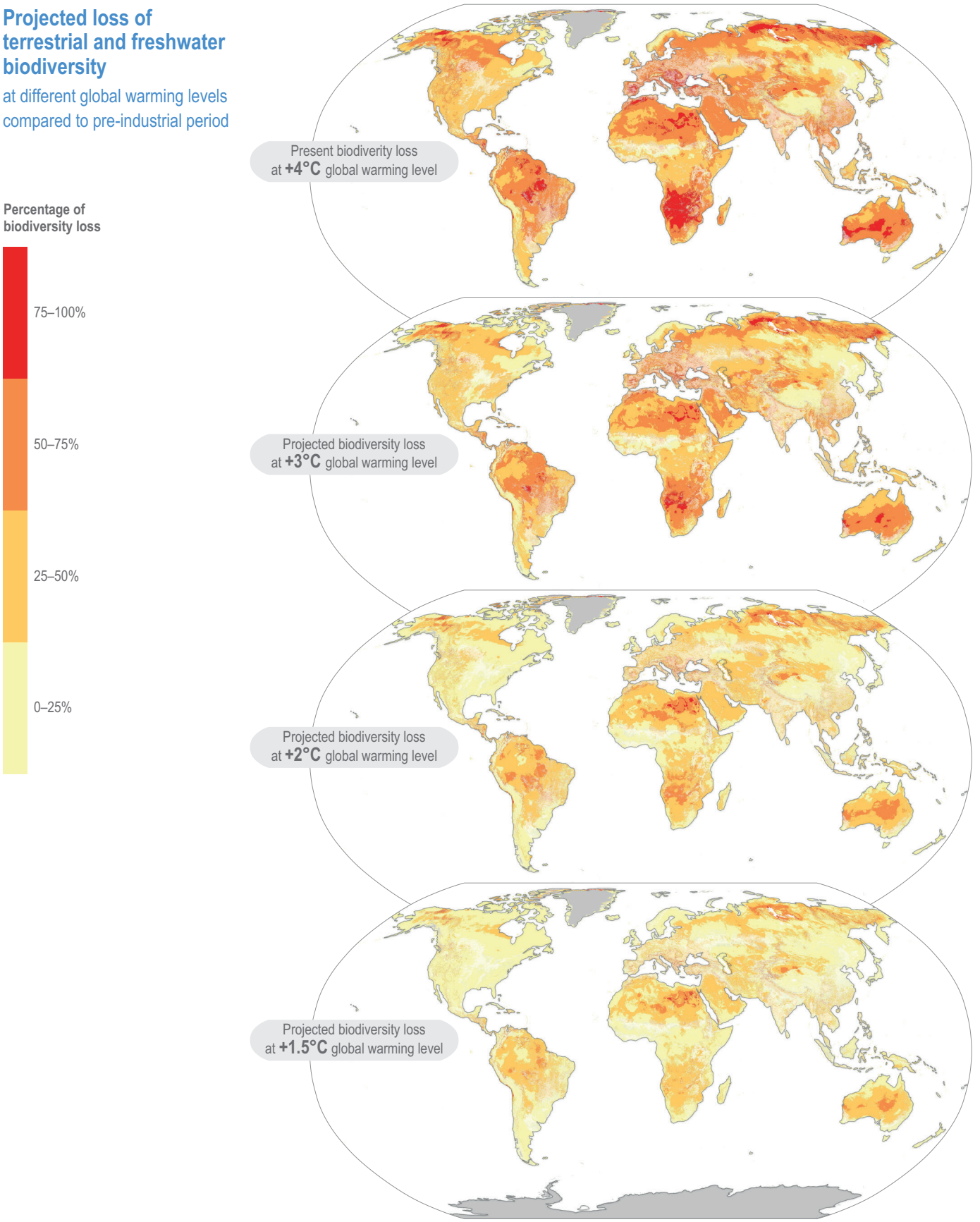

Figure AI.16 | Projected loss of terrestrial and freshwater biodiversity compared to pre-industrial period. Change indicated by the proportion of species (modelled n = 119,813 species globally) for which the climate is projected to become unsuitable across their current distributions. {Figure 2.6}

https://doi.org/10.1017/9781009325844.028

AI.2.1.2 Livestock and Crop Production

Regional impacts to major crop yields and food production loss events

Sudden losses of production in all food production systems have been increasing since 1960s. The major drivers of the increase are climate hazards including droughts, floods and storms.

Over the past 30 years, major crop yields decreased by 4–10% globally due to climate change (*high confidence*).

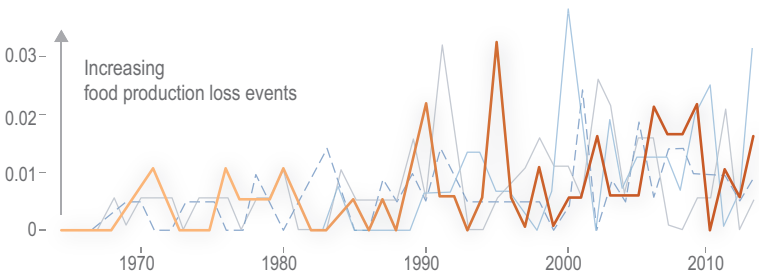

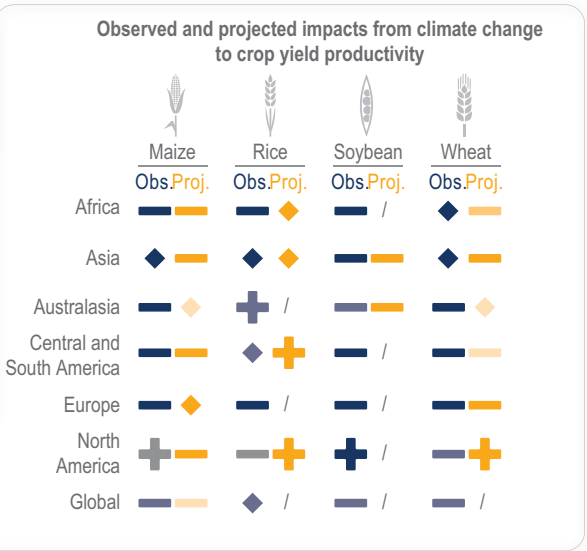

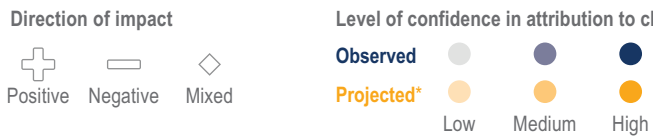

/ = not observed or insufficient evidence

*Mid-century at RCP4.5 (~2°C Global Warming Level)

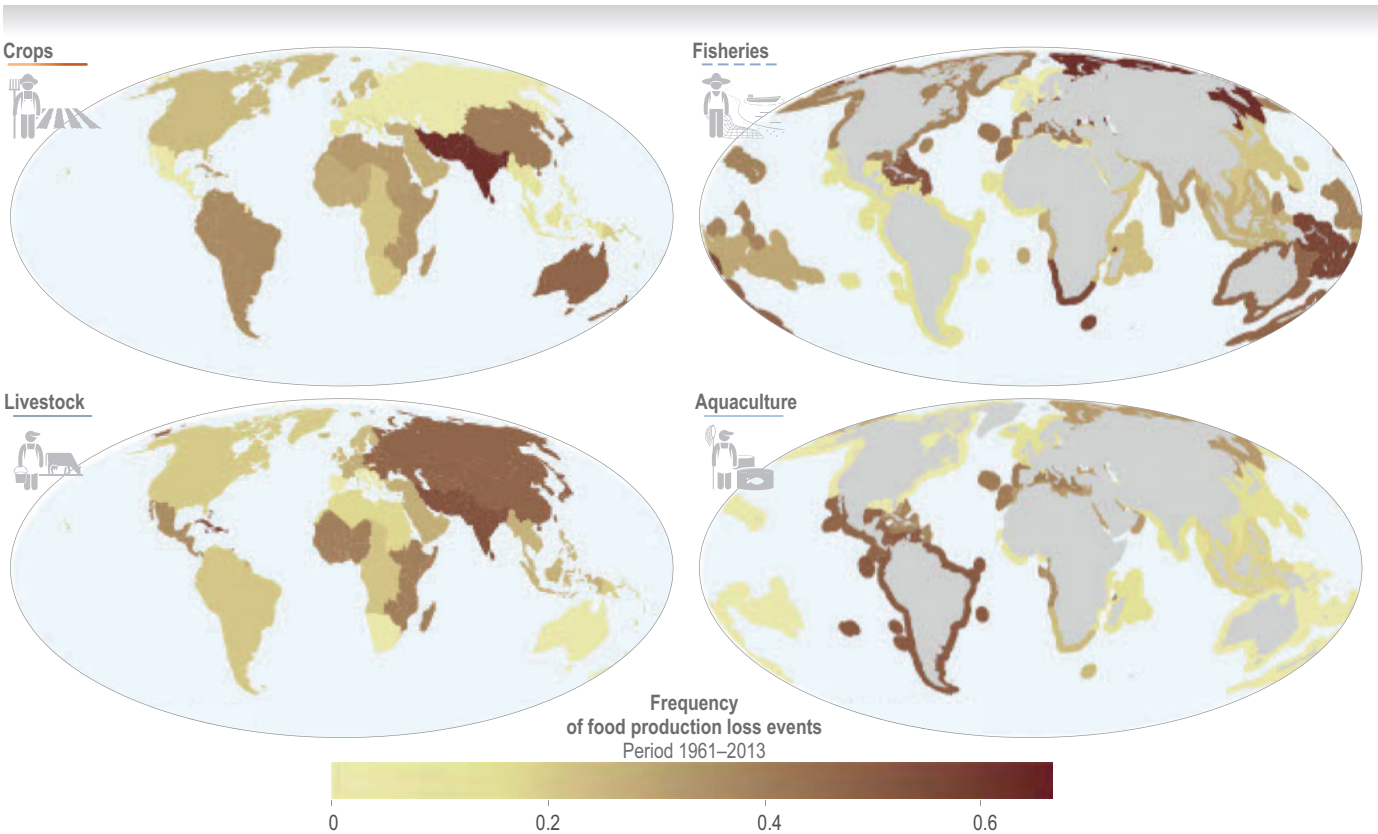

Figure AI.17 | Regional impacts to major crop yields and food production loss events. Trends in food production shocks in different food supply sectors since 1961 (Cottrell et al., 2019). Projected impacts are for Representative Concentration Pathway RCP4.5 mid-21st century, taking into account adaptation and CO_2 fertilization for crop yield productivity. {Figure 5.3; Sections 5.5.3, 5.4.1; Figure FAQ 5.1; Figure 9.22; Sections 15.3.4, 15.3.3}

https://doi.org/10.1017/9781009325844.028

AI

Climatic and environmental stresses on global production of wheat

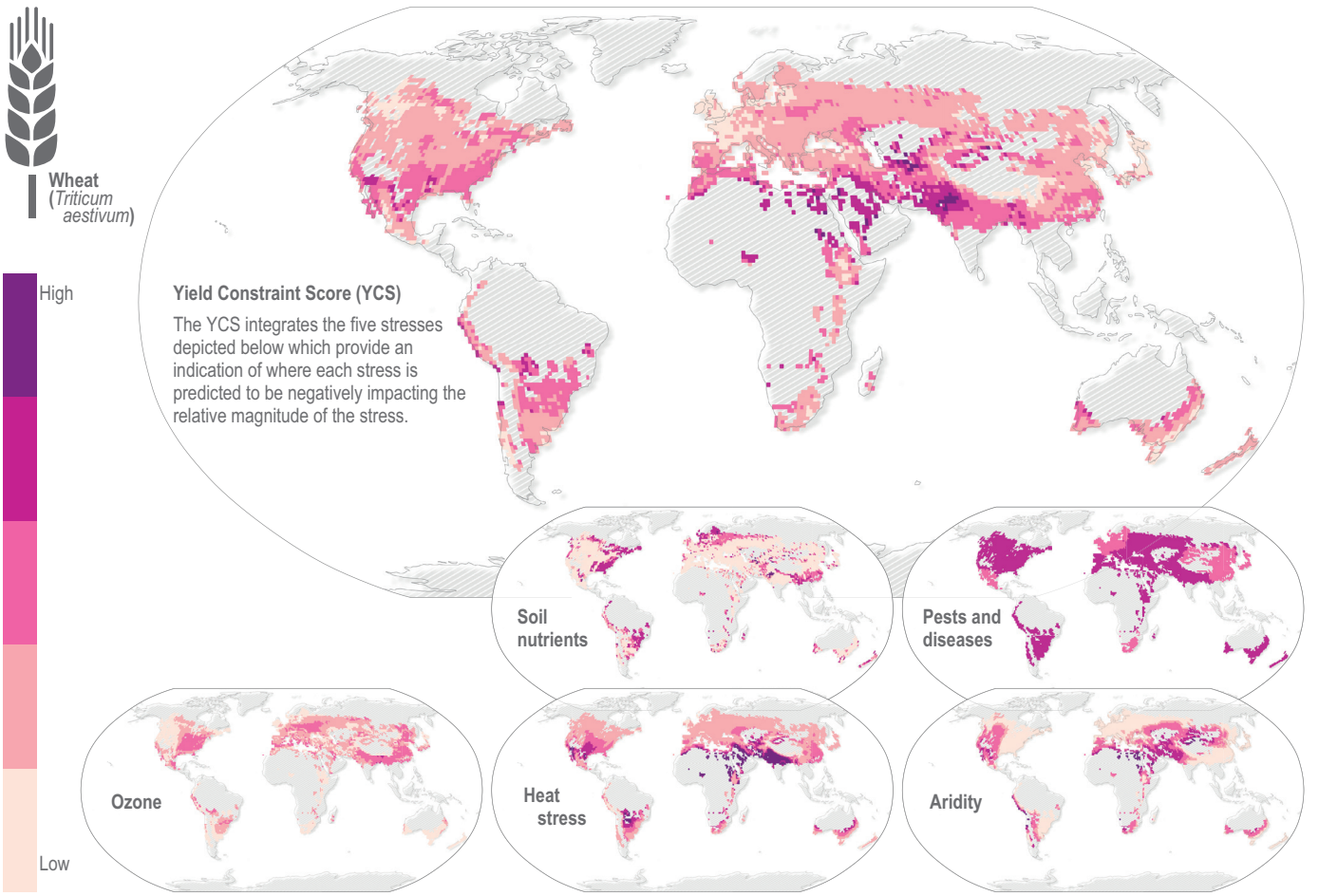

Figure AI.18 | Climatic and environmental stresses on global production of wheat. Larger map depicts the combined effect of five stresses on yield represented as a Yield Constraint Score (YCS) on a five-category scale from low stress to high stress (Mills et al., 2018). Higher temperatures enhance not only ozone production but also ozone uptake by plants, thus exacerbating yield loss and quality damage. Data are available at Sharps et al. (2020). All data are presented for the 1 × 1° (latitude and longitude) grid squares where the mean production of wheat was >500 tonnes (0.0005 Tg). {5.4.1; Figure 5.4}

Climatic and environmental stresses on global production of soybean

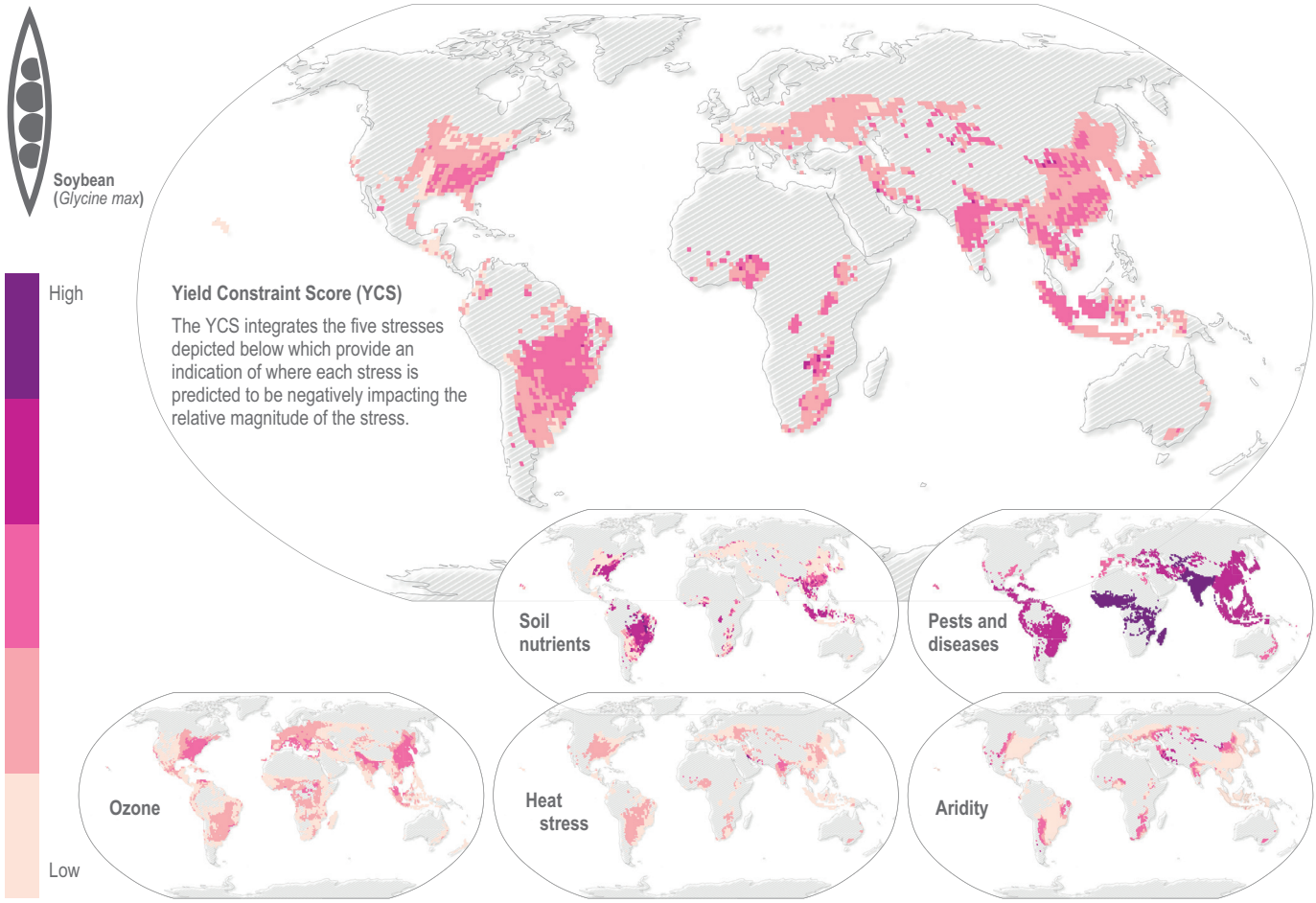

Figure AI.19 | Climatic and environmental stresses on global production of soybean. Larger map depicts the combined effect of five stresses on yield represented as a Yield Constraint Score (YCS) on a five-category scale from low stress to high stress (Mills et al., 2018). Higher temperatures enhance not only ozone production but also ozone uptake by plants, thus exacerbating yield loss and quality damage. Data are available at Sharps et al. (2020). All data are presented for the 1 × 1° (latitude and longitude) grid squares where the mean production of soybean was >500 tonnes (0.0005 Tg). {5.4.1; Figure 5.4}

https://doi.org/10.1017/9781009325844.028

AI

Climatic and environmental stresses on global production of rice

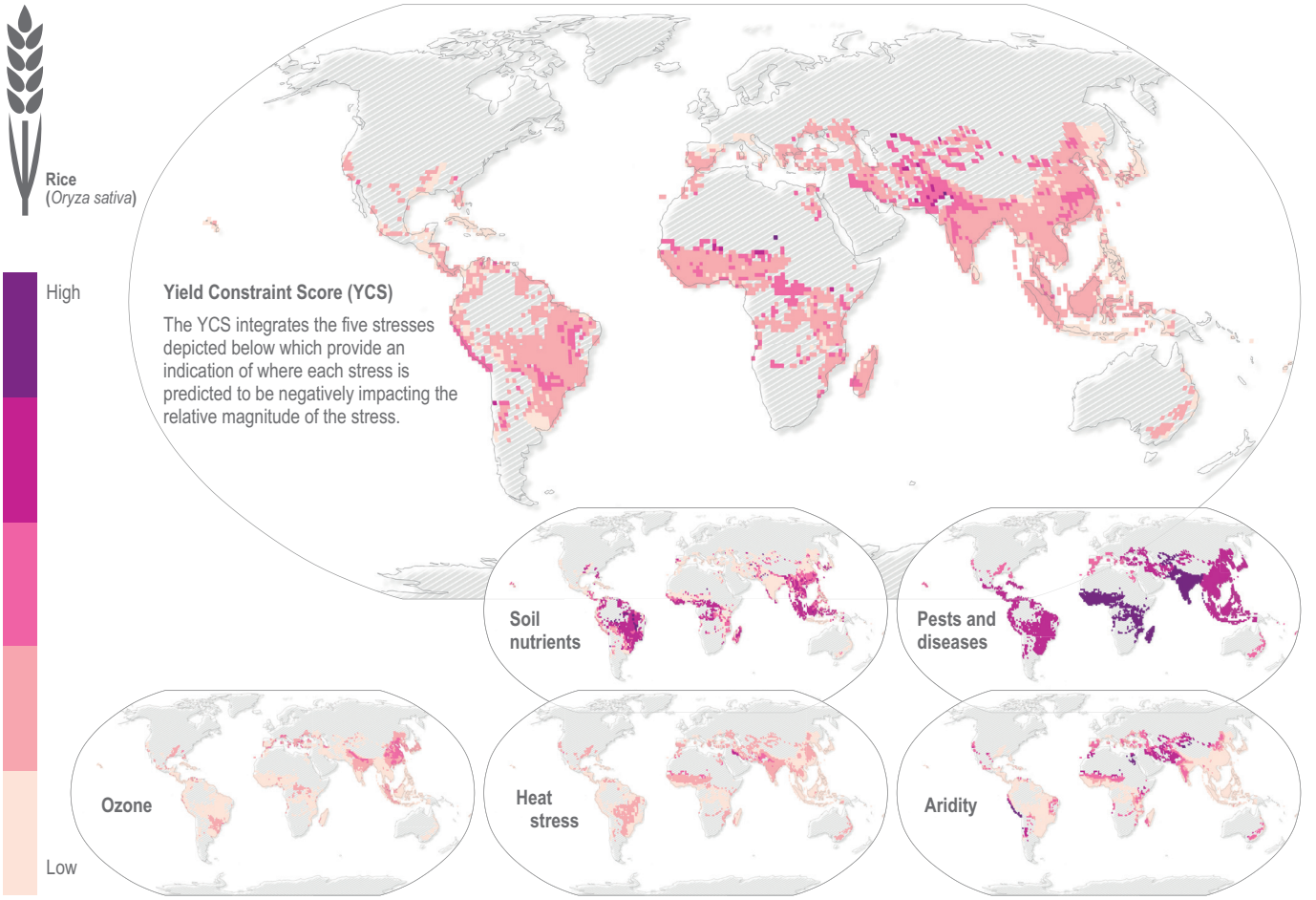

Figure AI.20 | Climatic and environmental stresses on global production of rice. Larger map depicts the combined effect of five stresses on yield represented as a Yield Constraint Score (YCS) on a five-category scale from low stress to high stress (Mills et al., 2018). Higher temperatures enhance not only ozone production but also ozone uptake by plants, thus exacerbating yield loss and quality damage. Data are available at Sharps et al. (2020). All data are presented for the 1 × 1° (latitude and longitude) grid squares. {5.4.1; Figure 5.4}

Climatic and environmental stresses on global production of maize

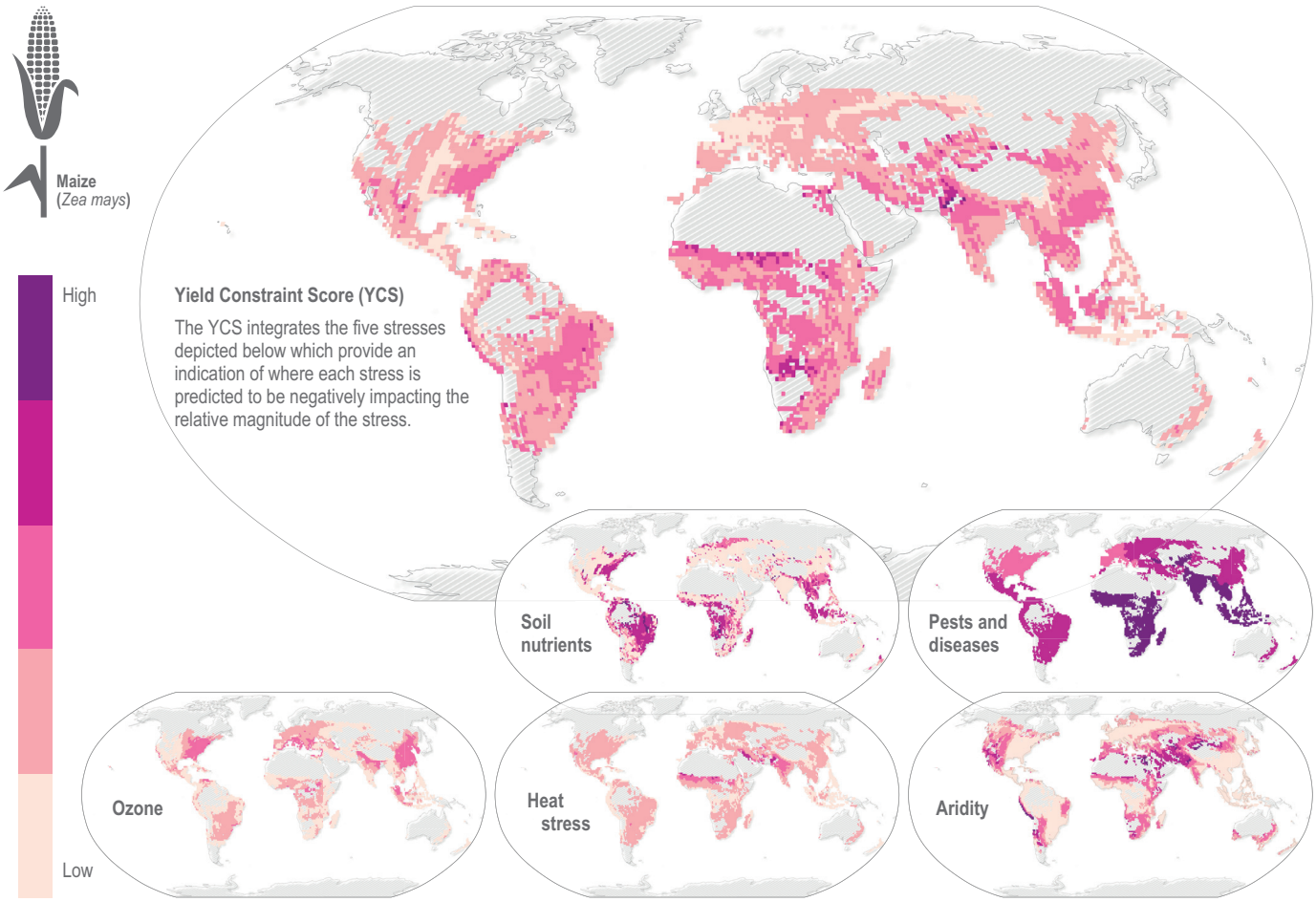

Figure AI.21 | Climatic and environmental stresses on global production of maize. Larger map depicts the combined effect of five stress on yield represented as a Yield Constraint Score (YCS) on a five-category scale from low stress to high stress (Mills et al., 2018). Higher temperatures enhance not only ozone production but also ozone uptake by plants, thus exacerbating yield loss and quality damage. Data are available at Sharps et al. (2020). All data are presented for the 1 × 1° (latitude and longitude) grid squares. {5.4.1; Figure 5.4}

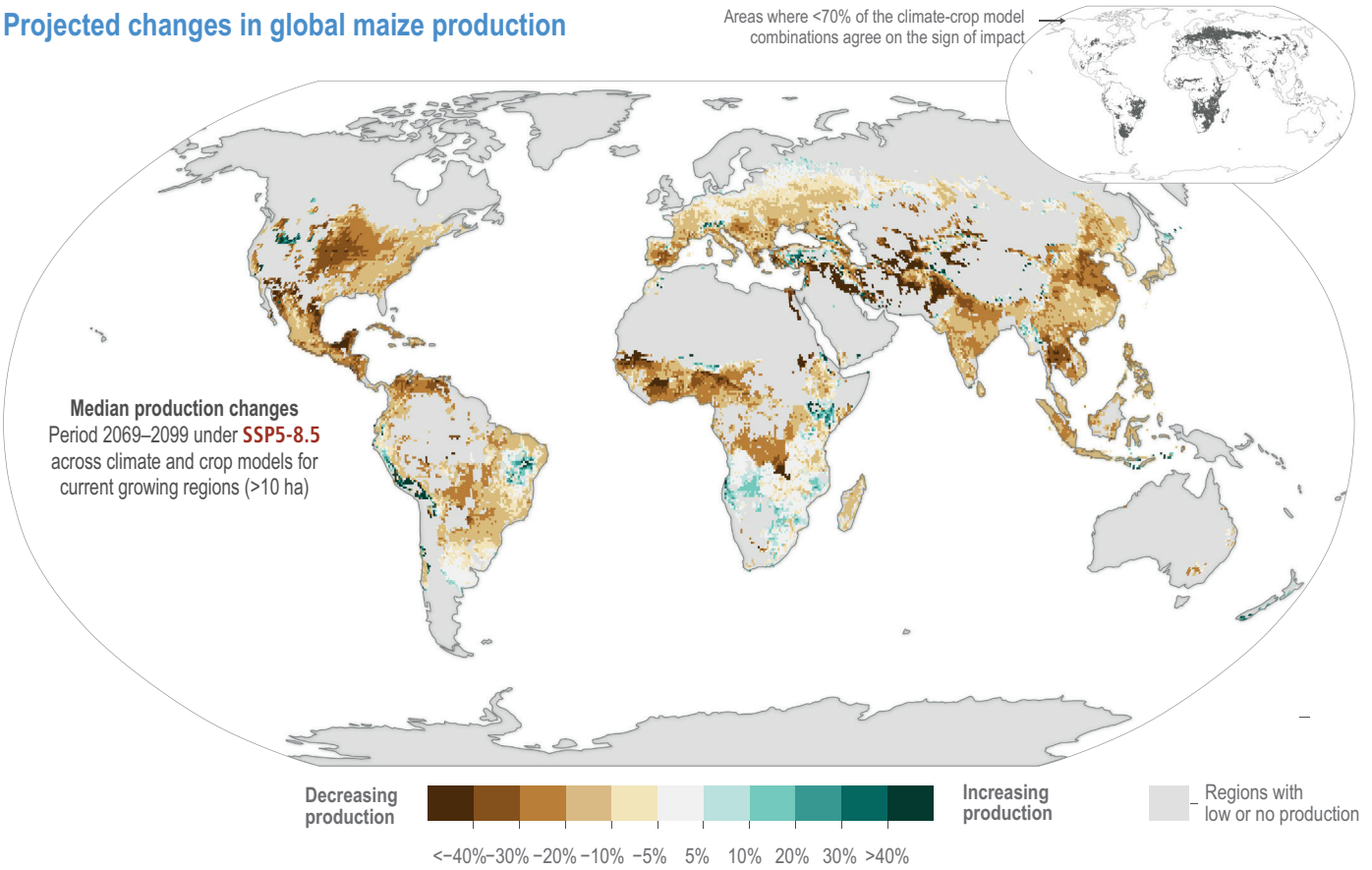

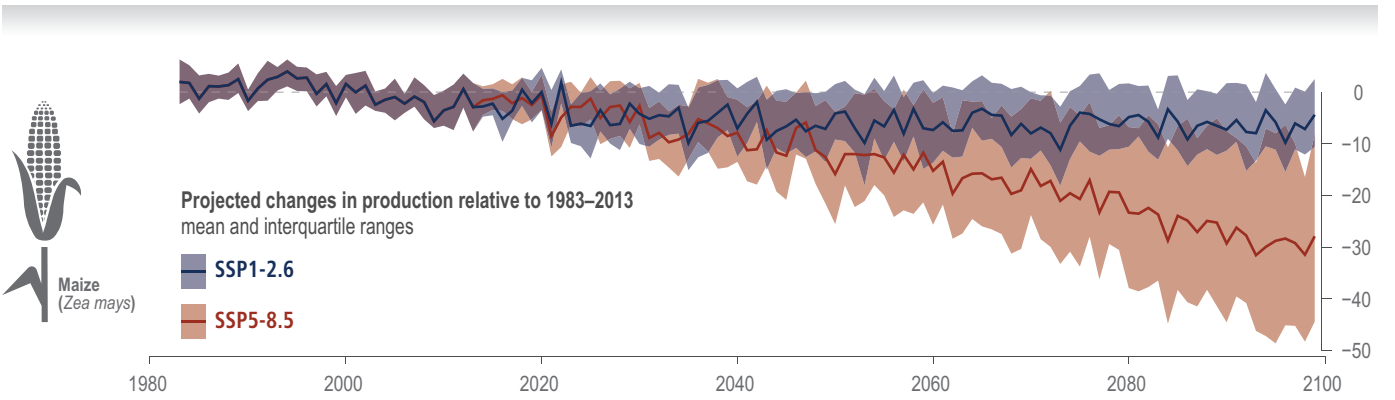

Figure AI.22 | Projected changes in global maize production. Map shows median yield changes (2069–2099) under SSP5-8.5 across climate and crop models for current growing regions (>10 ha). The time series in the lower graph is shown as relative changes to the 1983–2013 reference period under SSP1-2.6 and SSP5-8.5. Shaded ranges illustrate the interquartile range of all climate and crop model combinations (5 GCMs × 8 GGCMs). The solid line shows the median climate and crop model response (and a 30-year moving average). All data are shown for the default (CO_2) (Jägermeyr et al. 2021). {5.4.3.2}

https://doi.org/10.1017/9781009325844.028

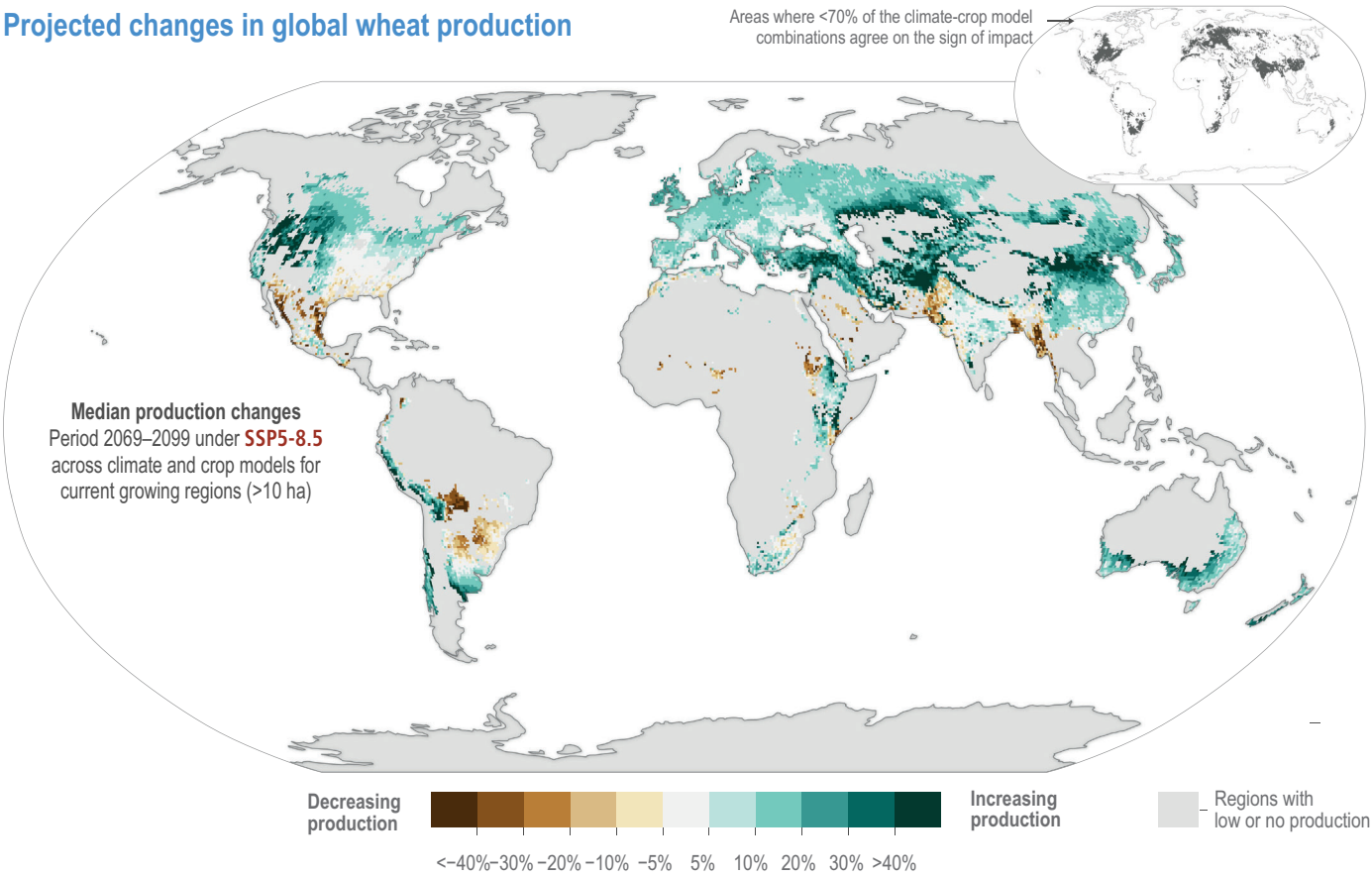

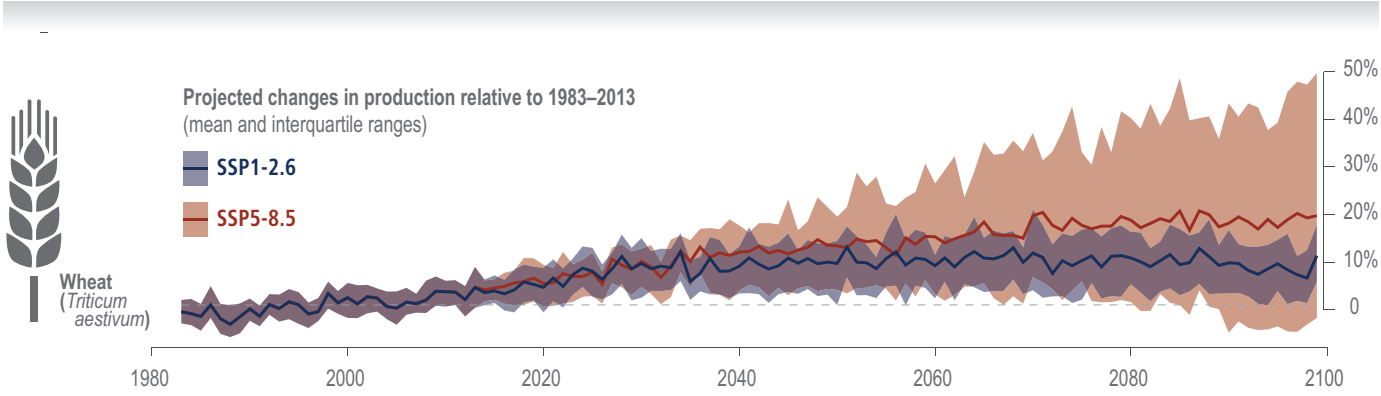

Figure AI.23 | Projected changes in global wheat production. Map shows median yield changes (2069–2099) under SSP5-8.5 across climate and crop models for current growing regions (>10 ha). The time series in the lower graph is shown as relative changes to the 1983–2013 reference period under SSP1-2.6 and SSP5-8.5. Shaded ranges illustrate the interquartile range of all climate and crop model combinations (5 GCMs × 8 GGCMs). The solid line shows the median climate and crop model response (and a 30-year moving average). All data are shown for the default (CO_2) (Jägermeyr et al. 2021). {5.4.3.2}

https://doi.org/10.1017/9781009325844.028

AI

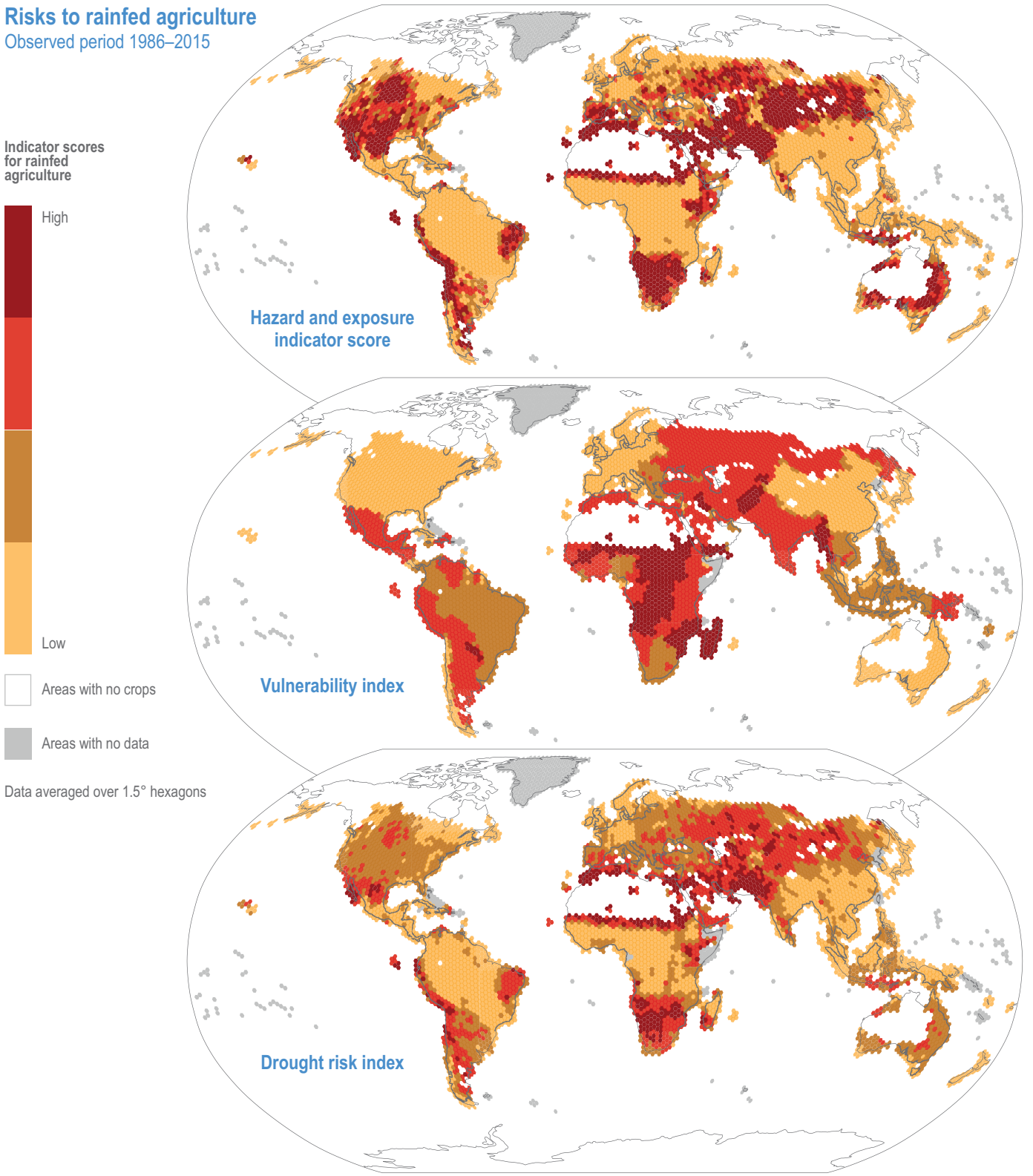

Figure AI.24 | Rain-fed agriculture: drought risks, hazards, exposure and vulnerability indicators. Hazard and exposure indicator score, vulnerability index and drought risk index for rain-fed agricultural systems between 1986 and 2015. Drought hazard indicator is defined as the ratio of actual crop evapotranspiration to potential crop evapotranspiration, calculated for 24 crops. Vulnerability index is the country-scale weighted average of a total of 64 indicators including social and ecological susceptibility indicators, and coping capacity. Risk index is calculated by multiplying hazard/exposure indicator score and vulnerability index (Meza et al., 2020). {Figure 5.5}

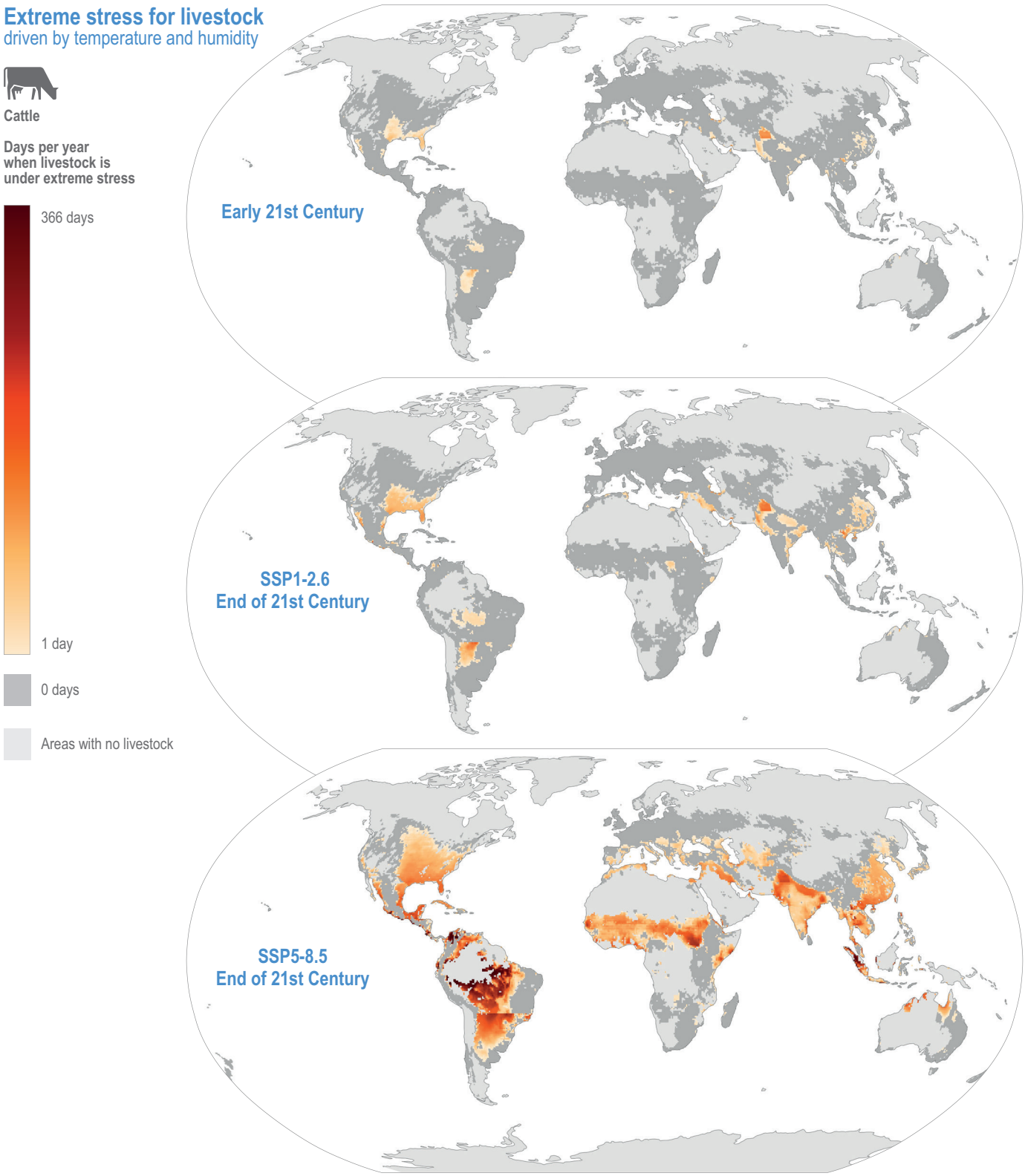

Figure AI.25a | Extreme stress for livestock driven by temperature and humidity. Change in the number of days per year above 'extreme stress' values from early 21st century (1991–2010) to end of century (2081–2100) estimated under SSP1-2.6 and SSP5-8.5 using the Temperature Humidity Index (THI). Mapped for species current global distribution (Gilbert et al., 2018) (grey areas, no change). (Thornton et al., 2021). {Figure 5.12}

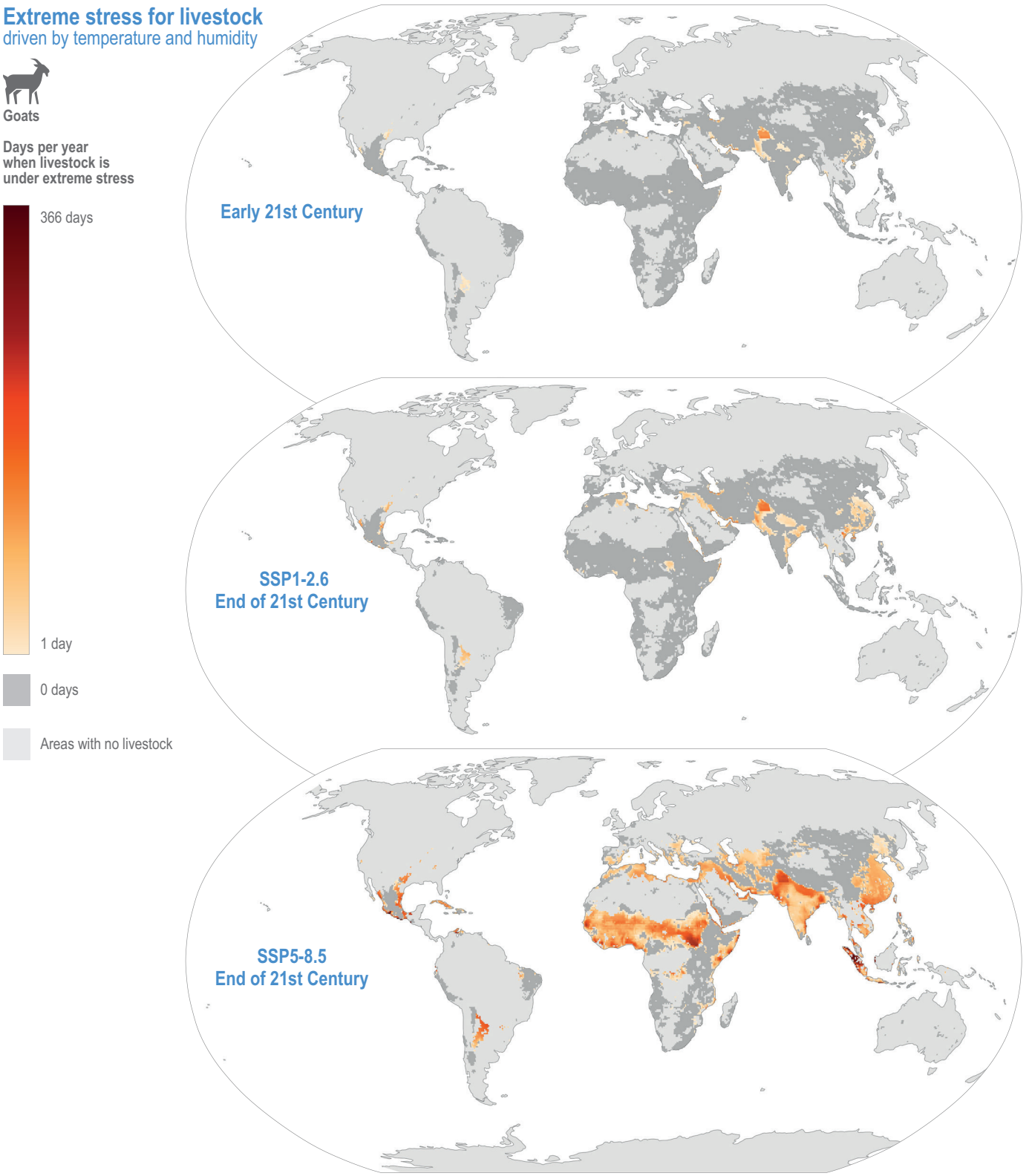

Figure AI.25b | Extreme stress for livestock driven by temperature and humidity. Change in the number of days per year above 'extreme stress' values from early 21st century (1991–2010) to end of century (2081–2100) estimated under SSP1-2.6 and SSP5-8.5 using the Temperature Humidity Index (THI). Mapped for species current global distribution (Gilbert et al., 2018) (grey areas, no change). (Thornton et al., 2021). {Figure 5.12}

https://doi.org/10.1017/9781009325844.028

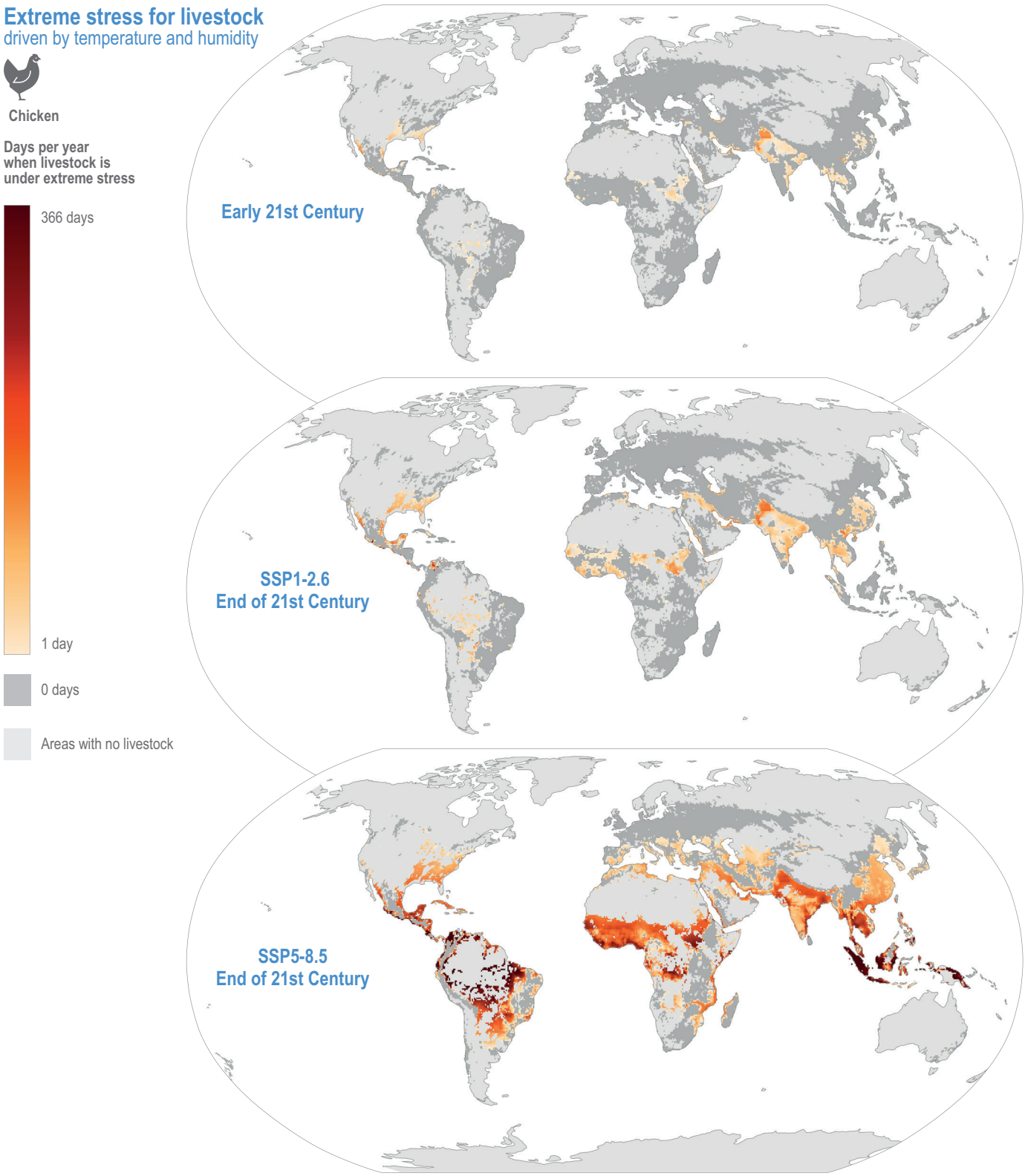

Figure AI.25c | Extreme stress for livestock driven by temperature and humidity. Change in the number of days per year above 'extreme stress' values from early 21st century (1991–2010) to end of century (2081–2100) estimated under SSP1-2.6 and SSP5-8.5 using the Temperature Humidity Index (THI). Mapped for species current global distribution (Gilbert et al., 2018) (grey areas, no change). (Thornton et al., 2021). {Figure 5.12}

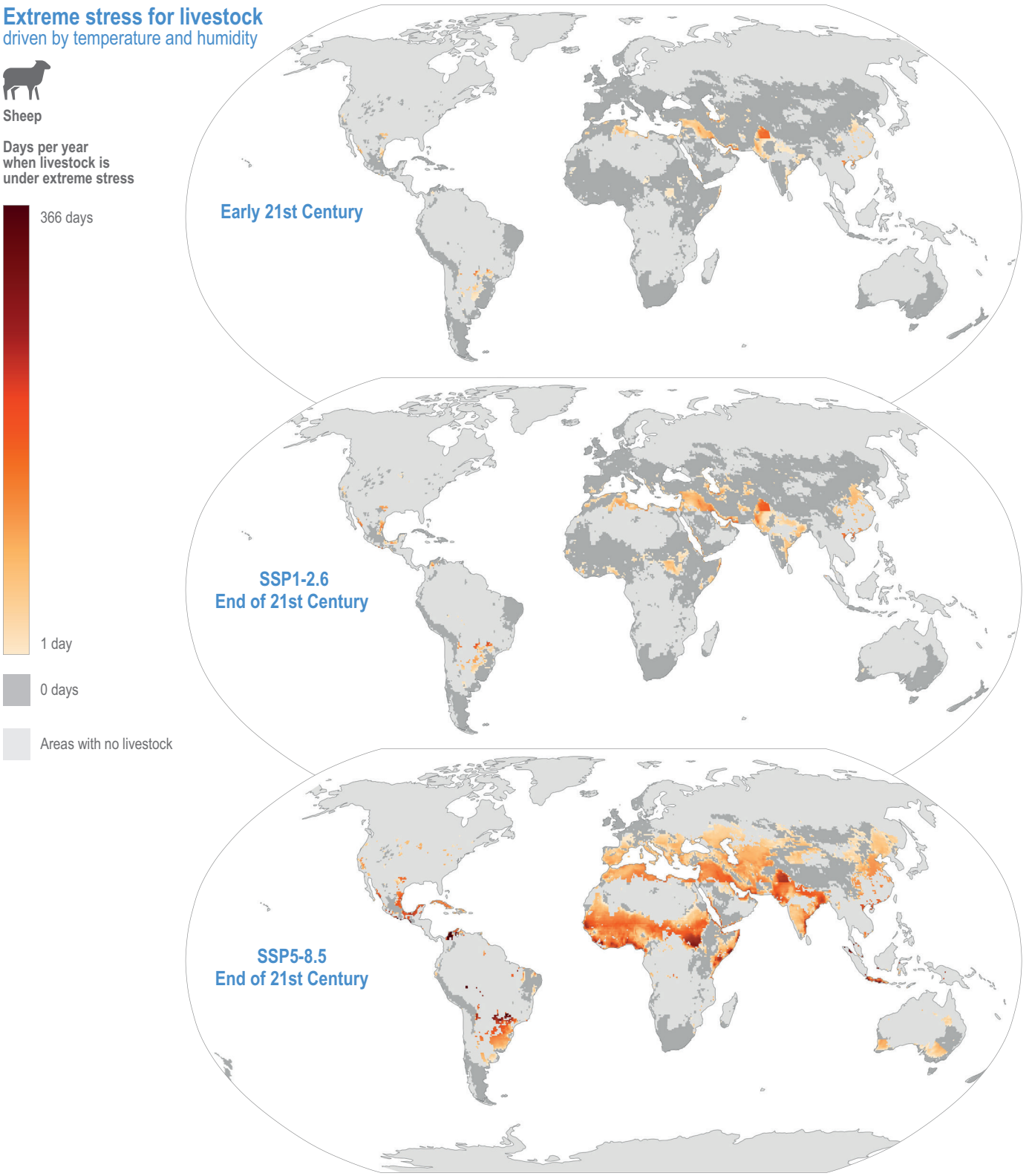

Figure AI.25d | Extreme stress for livestock driven by temperature and humidity. Change in the number of days per year above 'extreme stress' values from early 21st century (1991–2010) to end of century (2081–2100) estimated under SSP1-2.6 and SSP5-8.5 using the Temperature Humidity Index (THI). Mapped for species current global distribution (Gilbert et al., 2018) (grey areas, no change). (Thornton et al., 2021). {Figure 5.12}

https://doi.org/10.1017/9781009325844.028

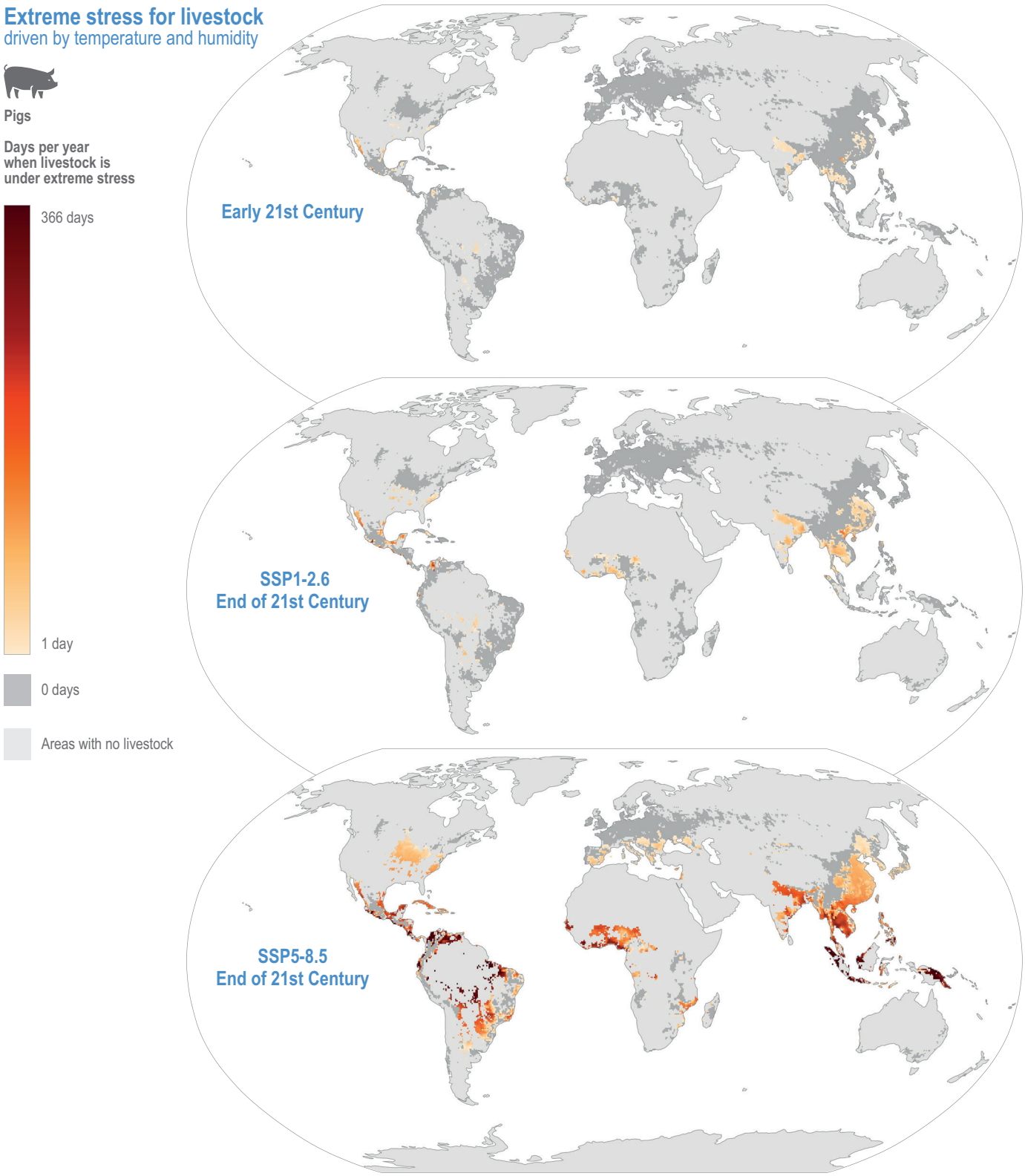

Figure AI.25e | Extreme stress for livestock driven by temperature and humidity. Change in the number of days per year above 'extreme stress' values from early 21st century (1991–2010) to end of century (2081–2100) estimated under SSP1-2.6 and SSP5-8.5 using the Temperature Humidity Index (THI). Mapped for species current global distribution (Gilbert et al., 2018) (grey areas, no change). (Thornton et al., 2021). {Figure 5.12}

https://doi.org/10.1017/9781009325844.028

AI

AI.2.1.3 Humans

Temperature and humidity-driven reduction in first-hour physical capacity for outdoor work

Lower insets and arrows point to the only locations across the globe where the first hour **loss of physical work capacity*** is 40% for the early century and end century SSP1-2.6 scenario. Other locations will have large capacity losses over the course of a work day. End century impacts will be much greater and more widespread under SSP5-8.5.

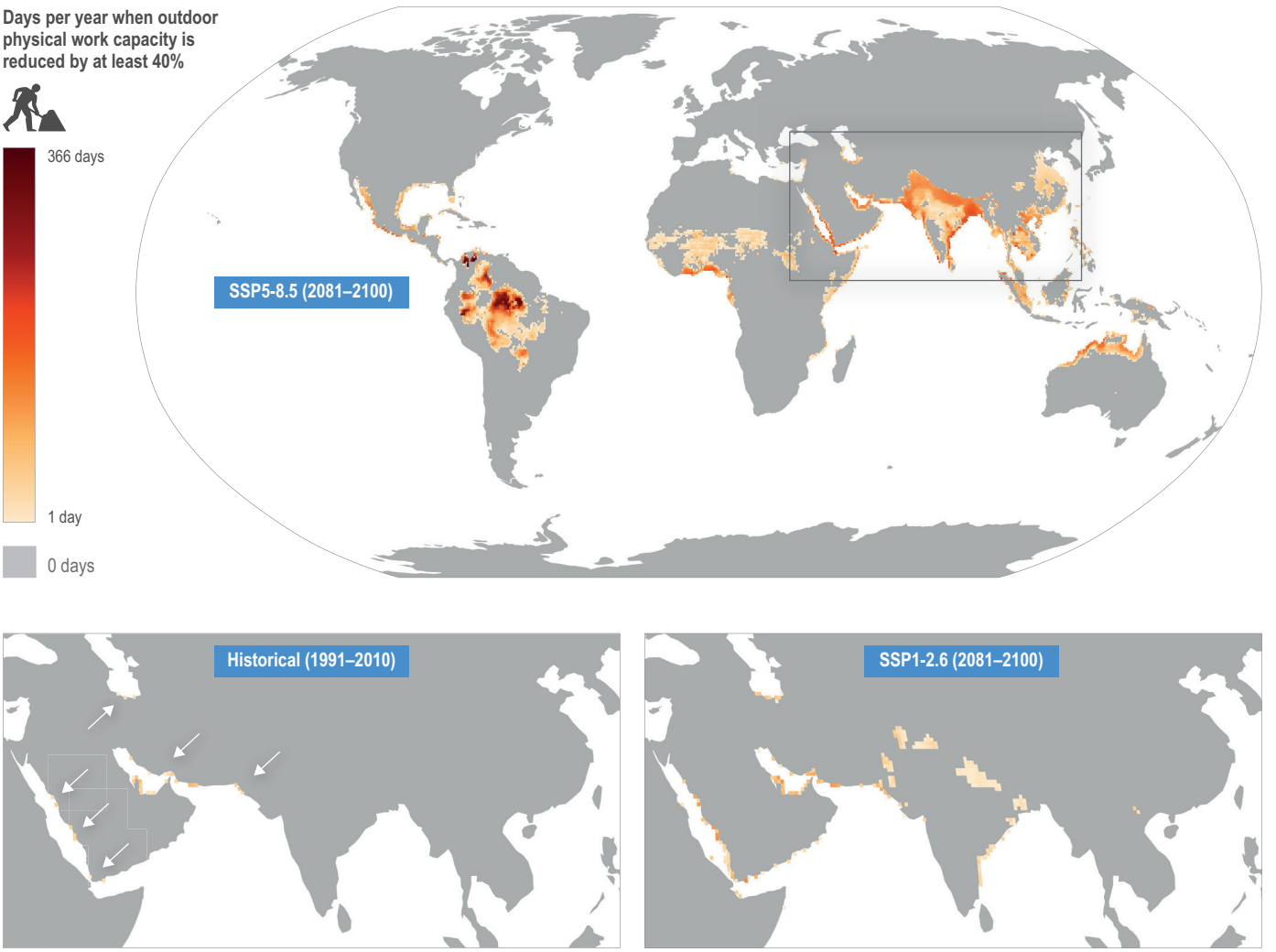

* The research for the representation of lost physical work capacity was undertaken in a controlled environment. The worker was on a treadmill operating at a constant speed for one hour in a room with controlled temperature and humidity. These conditions approximate work in a field with no wind (which would reduce heat effects) and no direct exposure to solar radiation (which would worsen heat effects). In addition, work capacity declines as hours in the field extend beyond one hour. Research is underway to take these additional factors into account.

Figure AI.26 | Temperature and humidity-driven reduction in physical work capacity for humans working outdoors. Projected increase in the number of days per year where physical work capacity is less than 60% based on average daily air temperature and relative humidity. Physical work capacity is defined as the maximum physical work output that can be reasonably expected from an individual performing moderate to heavy work in a 'cool' reference environment of 15°C. {Figure 5.18}

Mortality risk for humans and climate change

Projections shown are independent of regions's population density

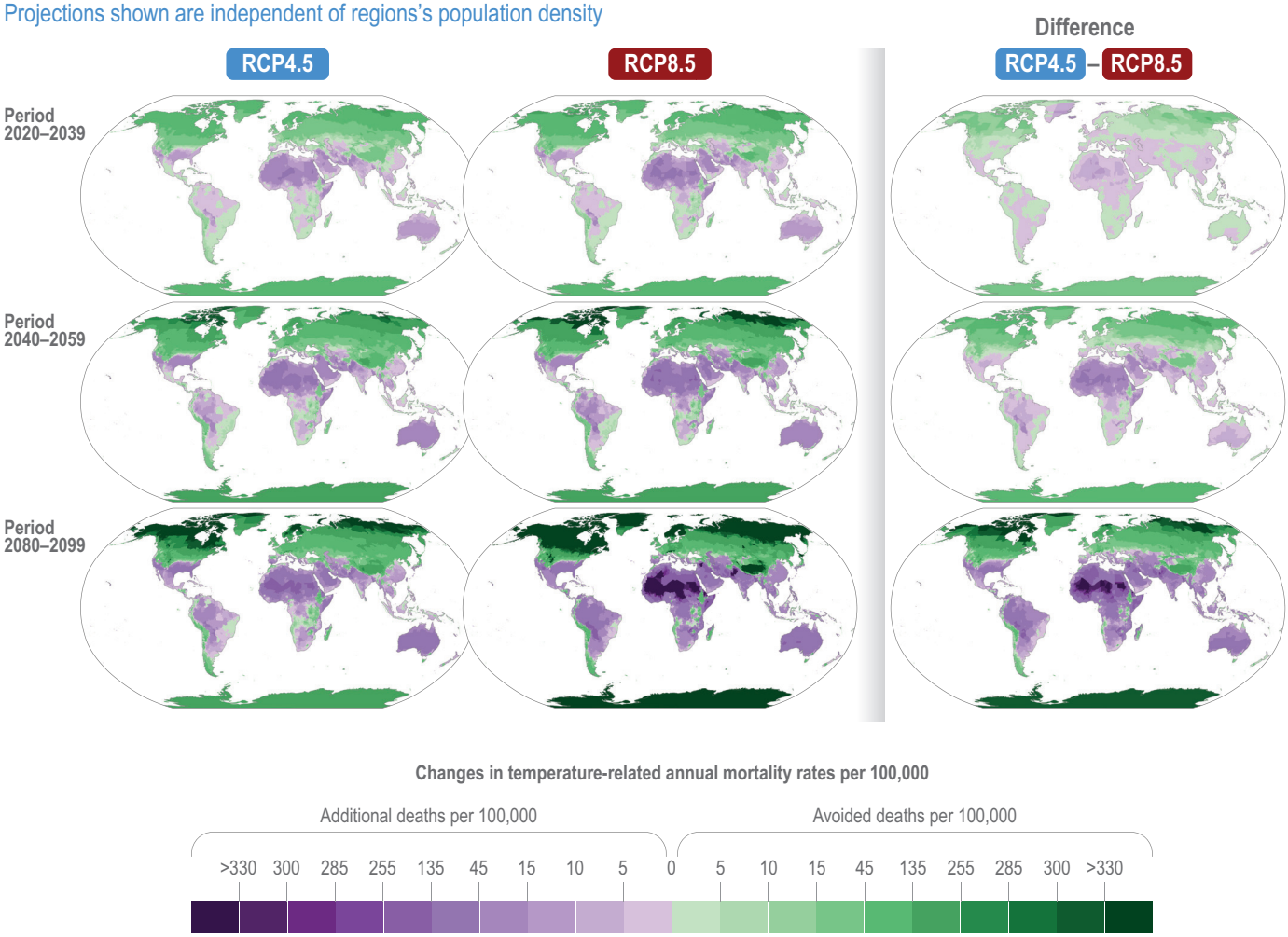

Figure AI.27 | Full mortality risk and climate change. Change in full risk mortality due to increases in temperatures. Estimates come from a model accounting for both the costs and the benefits of adaptation, and the map shows the climate model weighted mean estimate across Monte Carlo simulations conducted on 33 climate models (Carleton et al., 2018). {Figure 9.35, Section 9.10.1}

Projected geographical shift of the human temperature niche

For millennia, human populations have resided in the same narrow part of the climatic envelope available on the globe, characterized by a major mode around ≈11°C to 15°C mean annual temperature. Maps show current and projected geographical shift of the this temperature niche.

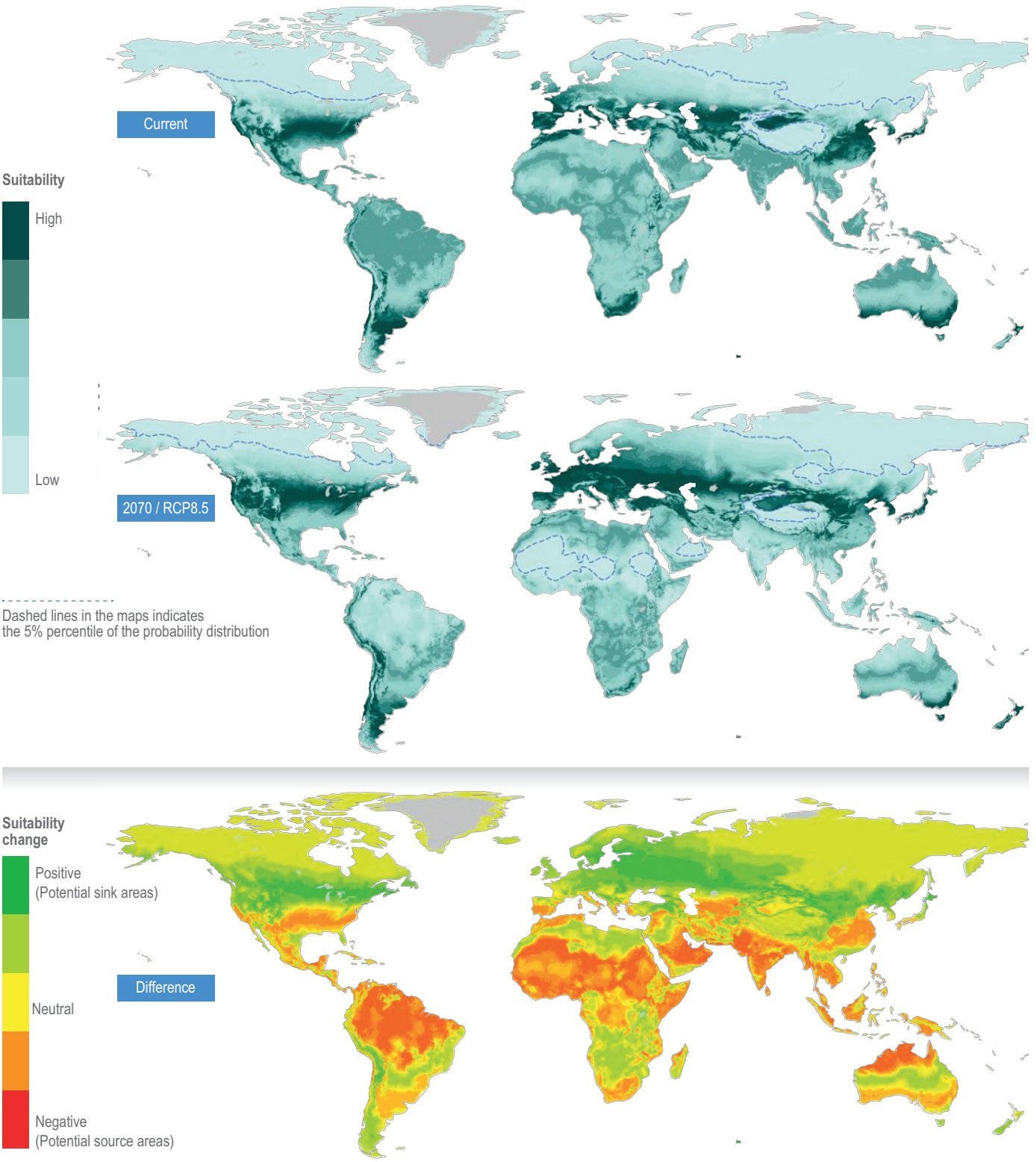

Figure AI.28 | Projected geographical shift of the human temperature niche. Geographical position of the human temperature niche projected on the current situation and the Representative Concentration Pathway RCP8.5 projected 2070 climate. These maps represent relative human distributions (summed to unity) for the imaginary situation that humans would be distributed over temperatures following the stylised double Gaussian model fitted to the modern data. Difference between the maps, visualising potential source and sink areas for the coming decades if humans were to be relocated in a way that would maintain this historically stable distribution with respect to temperature. (Xu et al., 2020) {Table 8.7; Section 8.4.5.6}

Global distribution of population exposed to hyperthermia from extreme heat and humidity

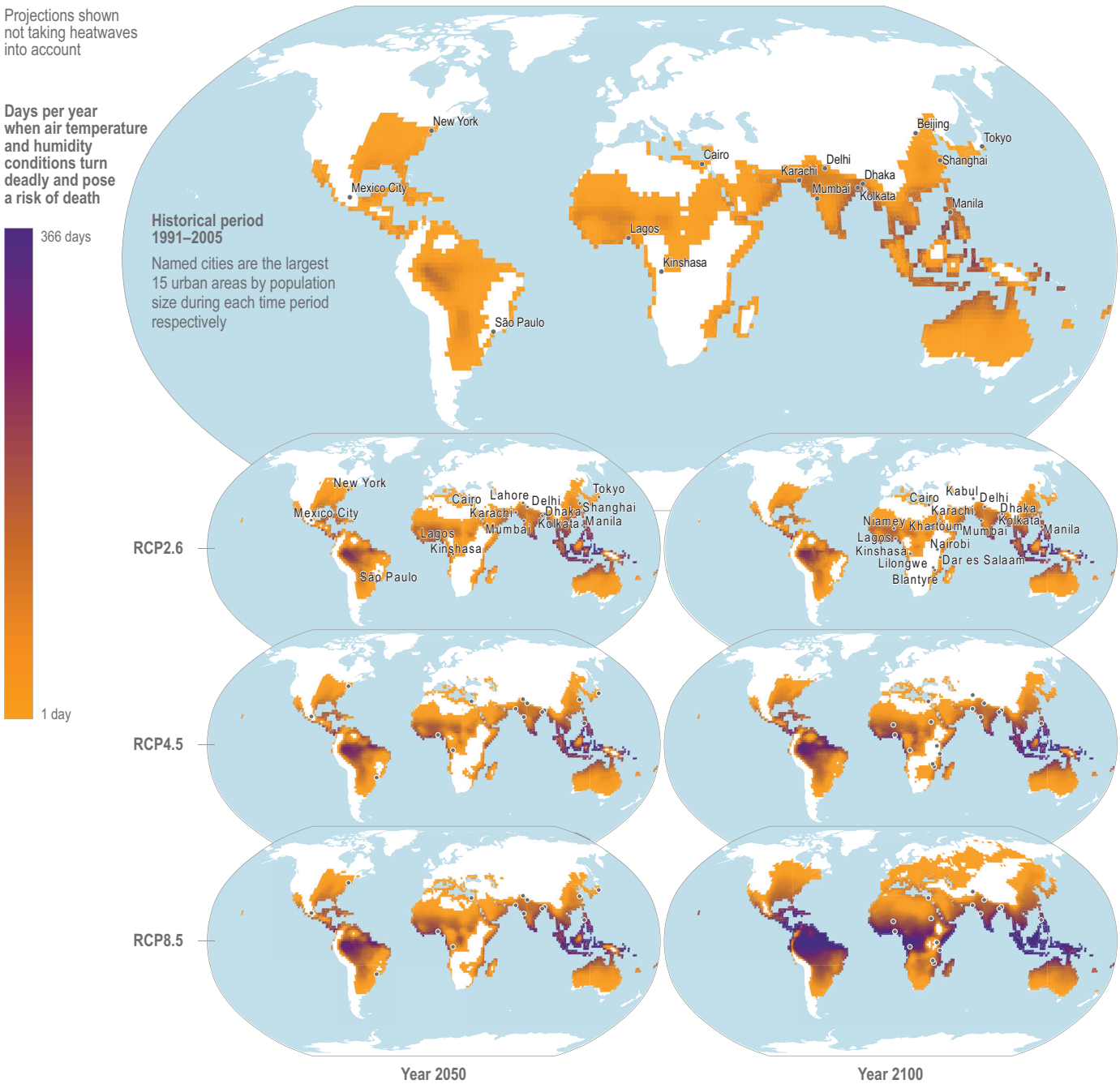

Figure AI.29 | Global population exposed to hyperthermia from extreme heat. Global distribution of population exposed to hyperthermia from extreme heat and humidity. Maps indicate the historical and projected number of days in a year in which conditions of air temperature and humidity surpass a common threshold beyond which conditions turned deadly and pose a risk of death (Mora et al., 2017). Largest fifteen urban areas by population size/number of citizens during 2020, 2050 and 2100 respectively, as projected by Hoornweg and Pope (2017). {Figure 6.3; Section 6.2.3.1}

https://doi.org/10.1017/9781009325844.028

AI

Present-day global distribution of camps for refugees and internally displaced people

Background of days with temperature exceeding 35°C in 2041–2060

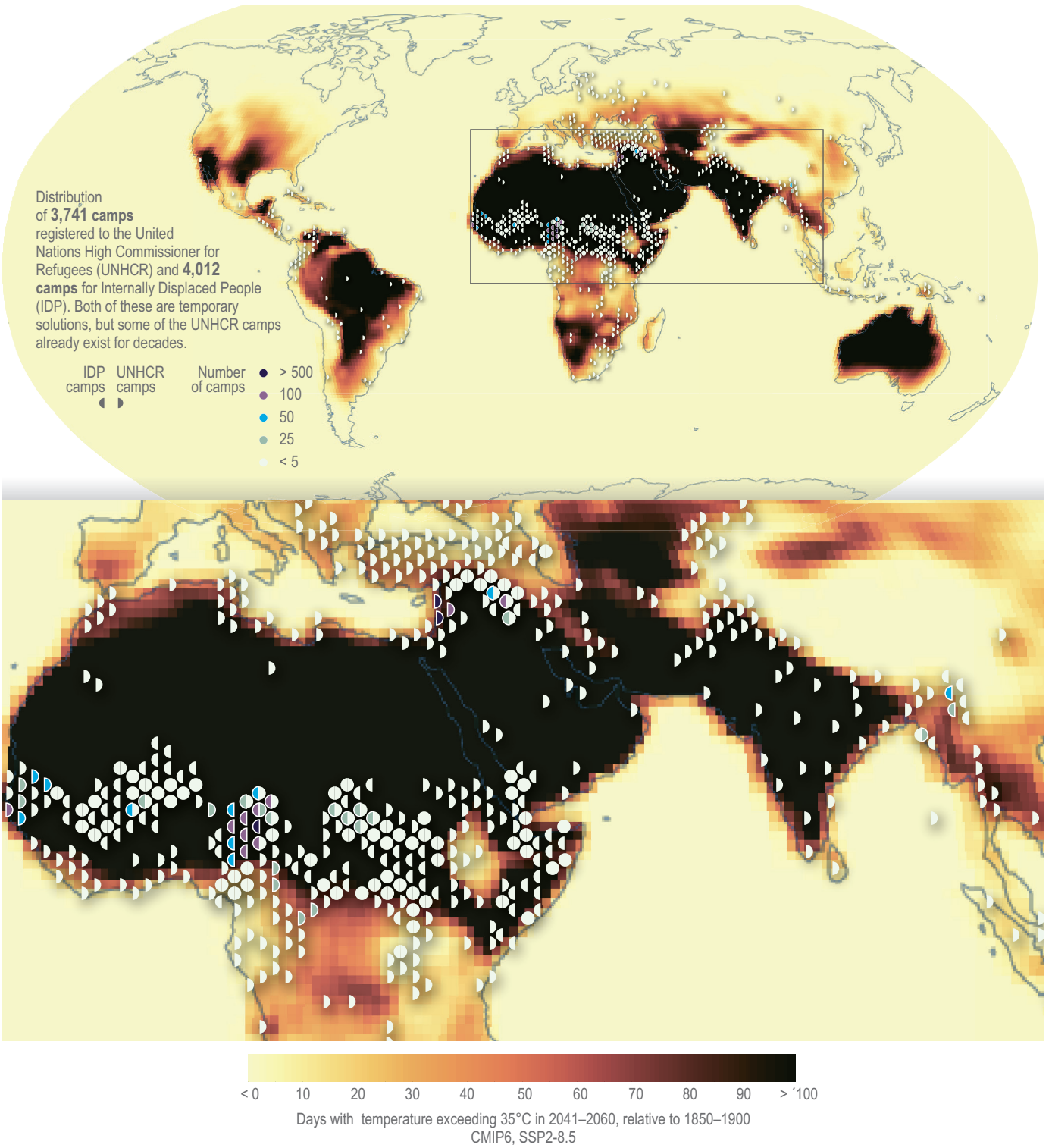

Figure AI.30 | Present day global distribution of camps for refugees and internally displaced people. The global distribution of the United Nations High Commissioner for Refugees (UNHCR) refugee and internally displaced people (IDP) settlements (as of 2018) overlaid with projected days with temperature exceeding 35°C in 2041–2060 relative to 1850–1900 under SSP2–8.5. {Figure Box 8.1.1; Box 8.1}

Estimated relative human dependence on marine ecosystems

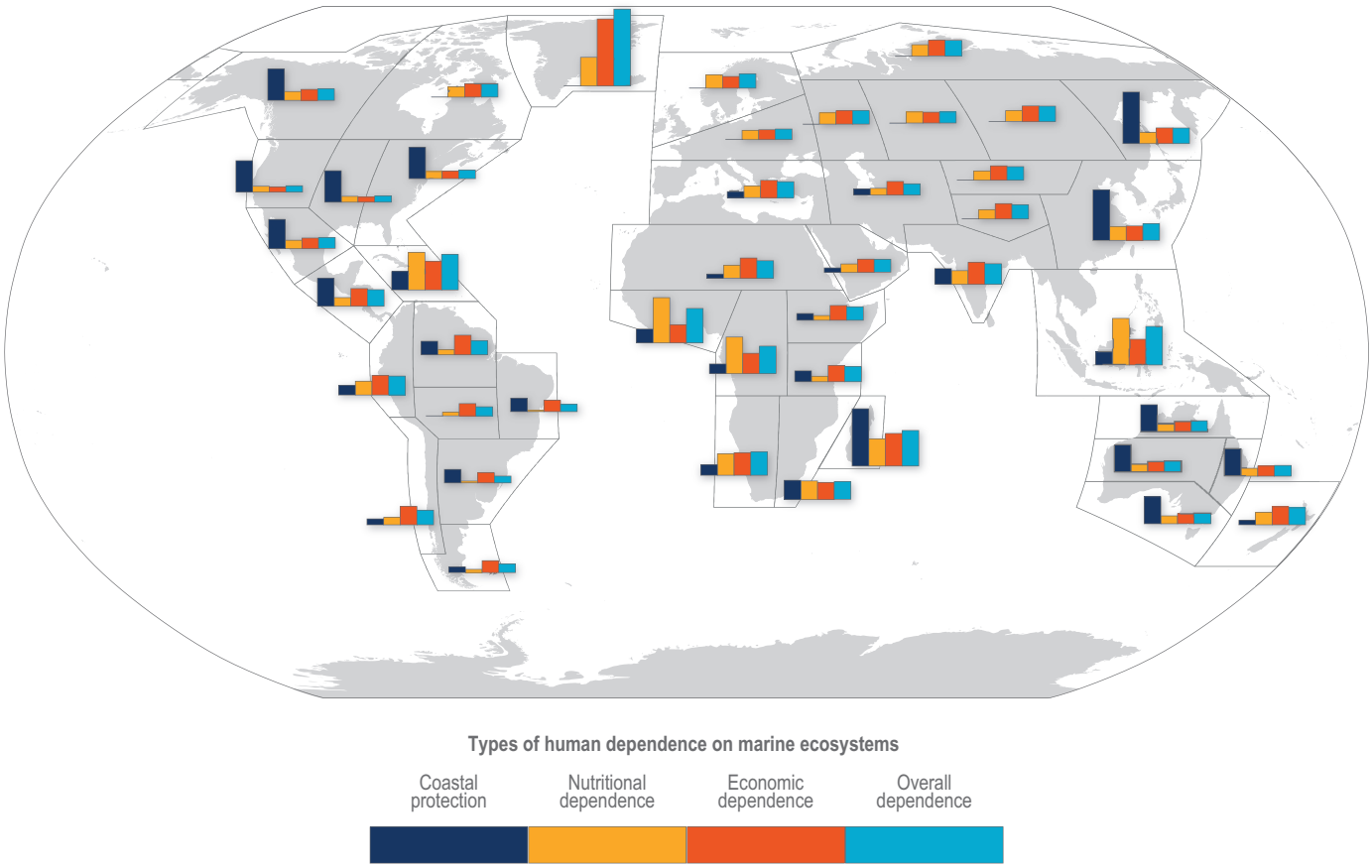

Figure AI.31 | Estimated relative human dependence on marine ecosystems. Relative human dependence on marine resources for coastal protection, nutrition, fisheries economic benefits and overall. Each bar represents an index value that semi-quantitatively integrates the magnitude, vulnerability to loss and substitutability of the benefit. Indices synthesise information on people's consumption of marine protein and nutritional status, gross domestic product, fishing revenues, unemployment, education, governance and coastal characteristics. Overall dependence is the mean of the three index values after standardisation from 0 to 1 (details are found in Table 1 and supplementary material of Selig et al., 2019). This index does not include the economic benefits from tourism or other ocean industries, and data limitations prevented including artisanal or recreational fisheries or the protective impact of saltmarshes (Selig et al., 2019). Values for reference regions established in the WGI AR6 Atlas (Gutiérrez et al., 2021) were computed as area-weighted means from original country-level data. {Figure 3.1}

https://doi.org/10.1017/9781009325844.028

AI

AI.2.1.4 Fish Stocks and Fisheries

Global vulnerabilities to current and projected climate change

(a) Projected changes in the number of extreme heat stress days for cattle from early to end of century.

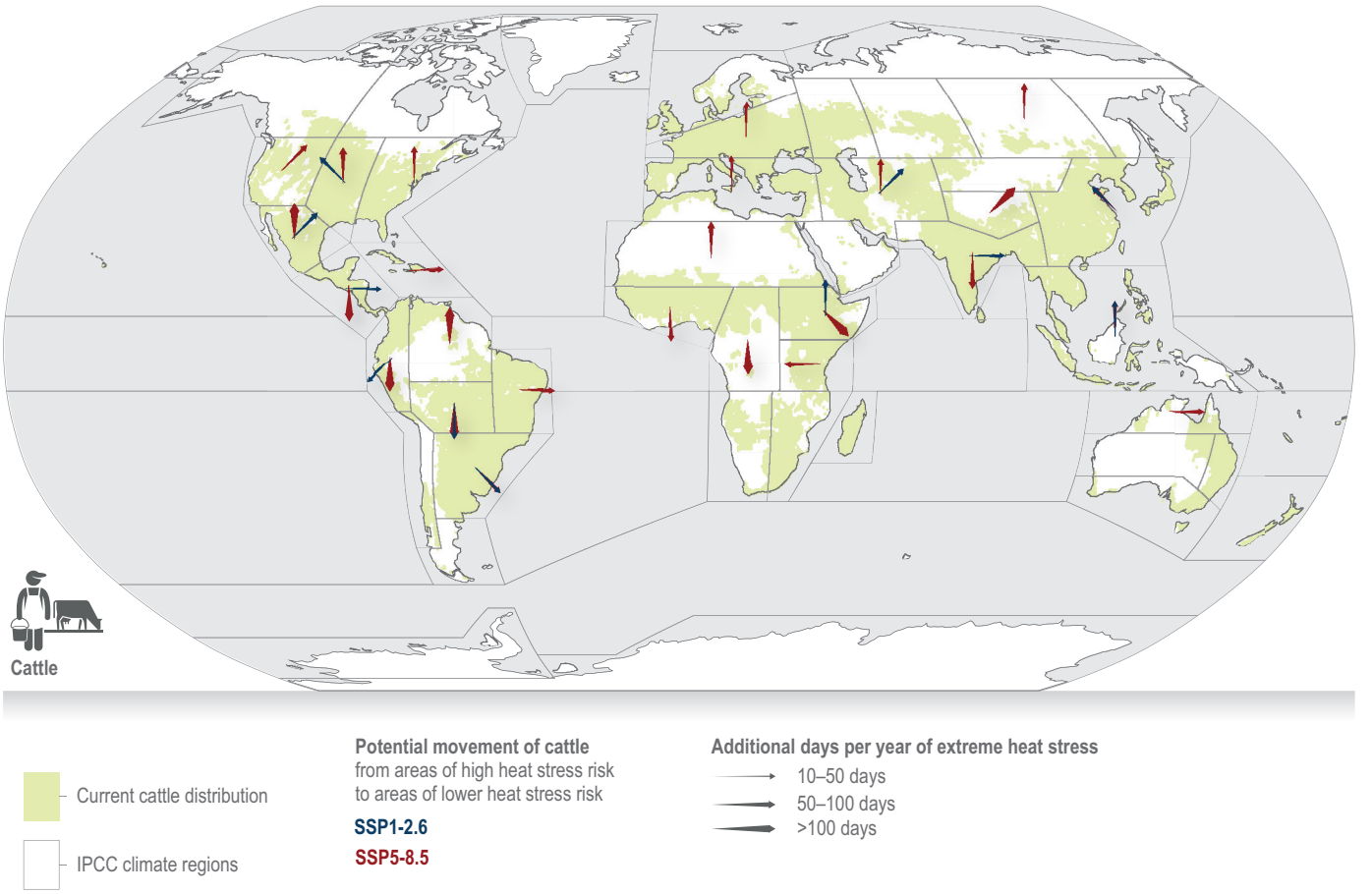

Figure AI.32a | Regional vulnerabilities to impacts of current and projected climate change on marine fishery and terrestrial livestock resources.

(a) Projected changes in the number of extreme heat stress days for cattle from early (1991–2010) to end of century (2081–2100) under SSP1-2.6 and SSP5-8.5, shown as arrows rooted in the most affected area in each IPCC sub-region pointing to the nearest area of reduced or no extreme heat stress. Arrows are shown only for sub-regions where >1 million additional animals are affected. Shaded areas are those with >5000 animals per 0.5° grid cell in the early 21st century (Thornton et al., 2021). {Figure MOVING PLATE.1 in Chapter 5}

Global vulnerabilities to current and projected climate change

(b) Ocean sensitivity for living marine resources within FAO regions and projected average fishing resource shifts in location

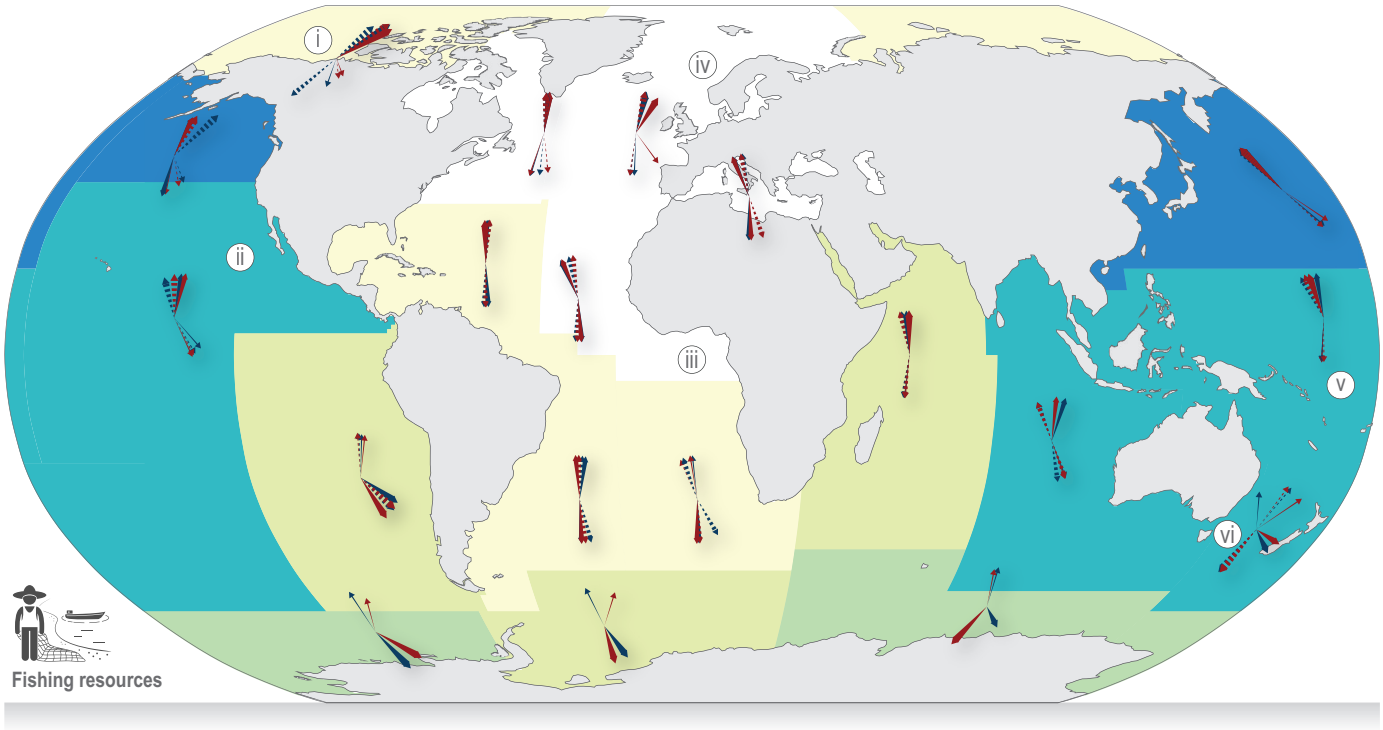

Figure AI.32b | Regional vulnerabilities to impacts of current and projected climate change on marine fishery and terrestrial livestock resources.

(b) Ocean areas are delineated into Food and Agricultural Organization of the United Nations (FAO) regions. Ocean sensitivity is calculated from aggregated sensitivities from Blasiak et al. (2017) S1 country data based on number of fishers, fisheries exports, proportions of economically active population working as fishers, total fisheries landings and nutritional dependence, which was subsequently reanalysed for each FAO region depicted here. Arrows denote projected average commercial and artisanal fishing resource shifts in location under Representative Concentration Pathways RCP2.6 and under RCP8.5 scenarios by 2100. Numbered circles highlight examples of vulnerabilities (Bell et al., 2018a), conflicts (Miller et al., 2013; Blasiak et al., 2017; Østhagen et al., 2020), or opportunities for marine resource usage (Robinson et al., 2015; Stuart-Smith et al., 2018; Meredith et al., 2019). {Figure MOVING PLATE.1 in Chapter 5}

https://doi.org/10.1017/9781009325844.028

Current fisheries adaptive capacity and risks related to human diets

(a) Documented fisheries adaptive capacity to climate change

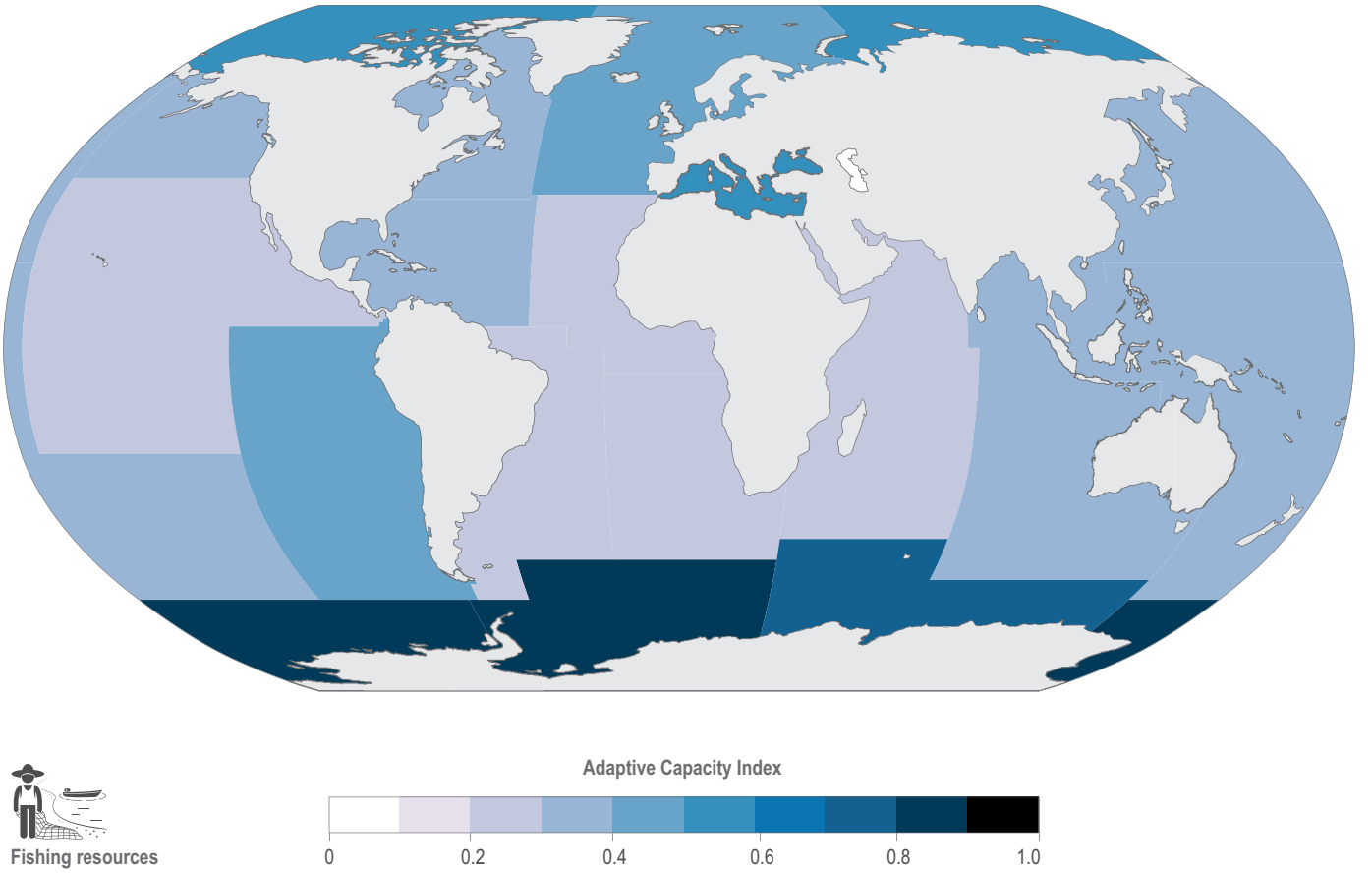

Figure AI.33a | Current fisheries adaptive capacity to climate change and regional dependence on seafood micronutrients in human diets.

(a) Fisheries management adaptive capacity is a function of the following: averaged gross domestic product (GDP) World Development Indicators for 2018 (World Bank, 2020); climate awareness assessments of 30 of the FAO (Food and Agricultural Organization of the United Nations) recognized most recent Regional Fisheries Management Organizations with direct fisheries linkages; governance effectiveness index based on six aggregate indicators (voice and accountability, political stability and absence of violence/terrorism, government effectiveness, regulatory quality, rule of law, control of corruption) from 2018 World Governance Indicator (World Bank, 2019) data; and heterogeneity of countries within each FAO zone (highly heterogeneous regions are less likely to establish sustainable and efficient fisheries management for the entire FAO zone). Adaptative capacity index ranges from 1 (high) to 0 (no adaptative capacity). Ocean areas are delineated into FAO regions. {Figure MOVING PLATE.3 in Chapter 5}

Current fisheries adaptive capacity and risks related to human diets

(b) Regional seafood-relevant micronutrient deficiency risk (Calcium, Iron, Zinc, Vitamin A) in human diets

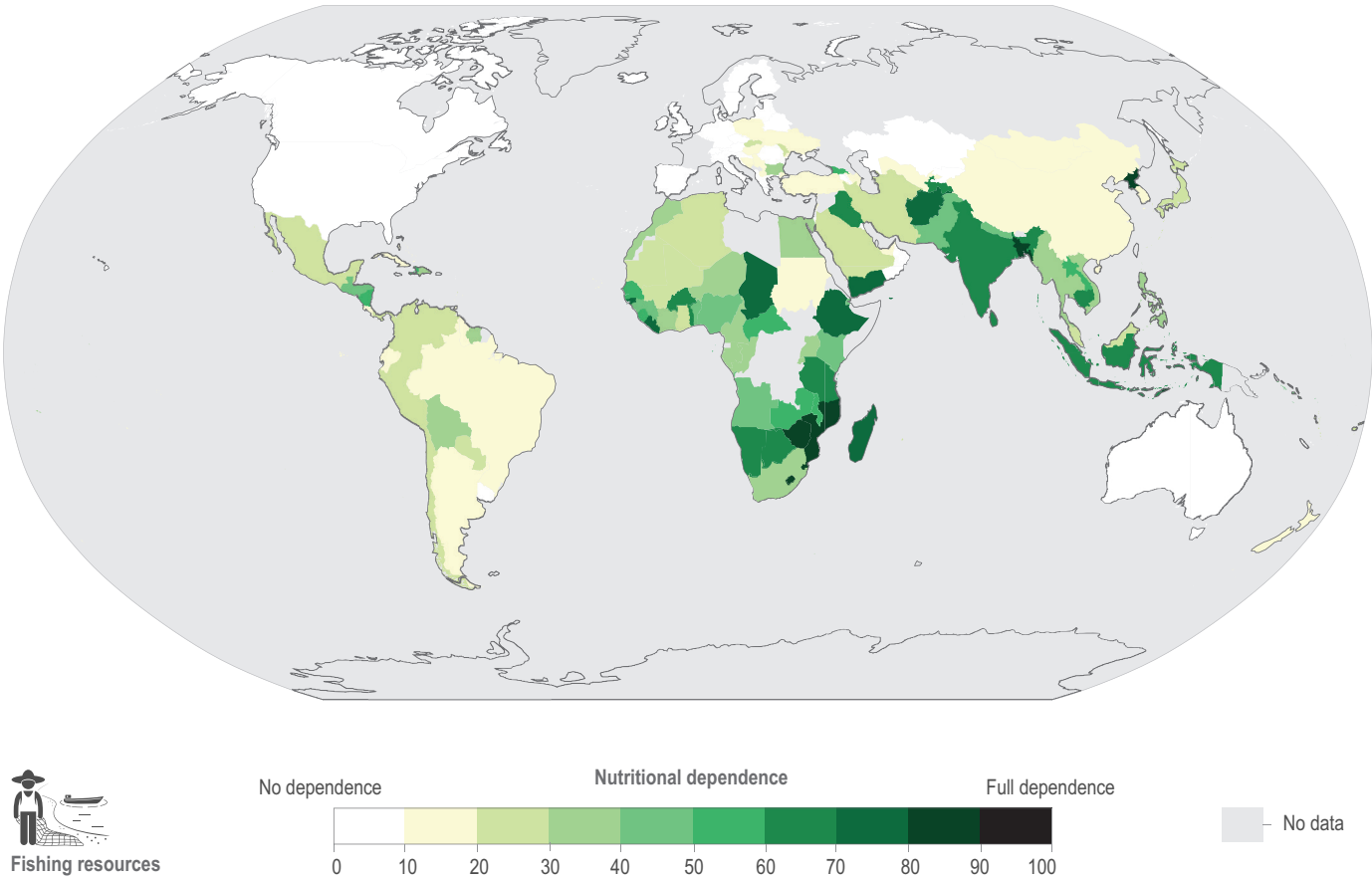

Figure AI.33b | Current fisheries adaptive capacity to climate change and regional dependence on seafood micronutrients in human diets.

(b) Nutritional dependence of regional human populations on micronutrient supply from marine fisheries. (Beal et al. 2017). {Figure MOVING PLATE.3 in Chapter 5}

Climate change risk to fisheries in Africa

(a) Inland/freshwater fisheries

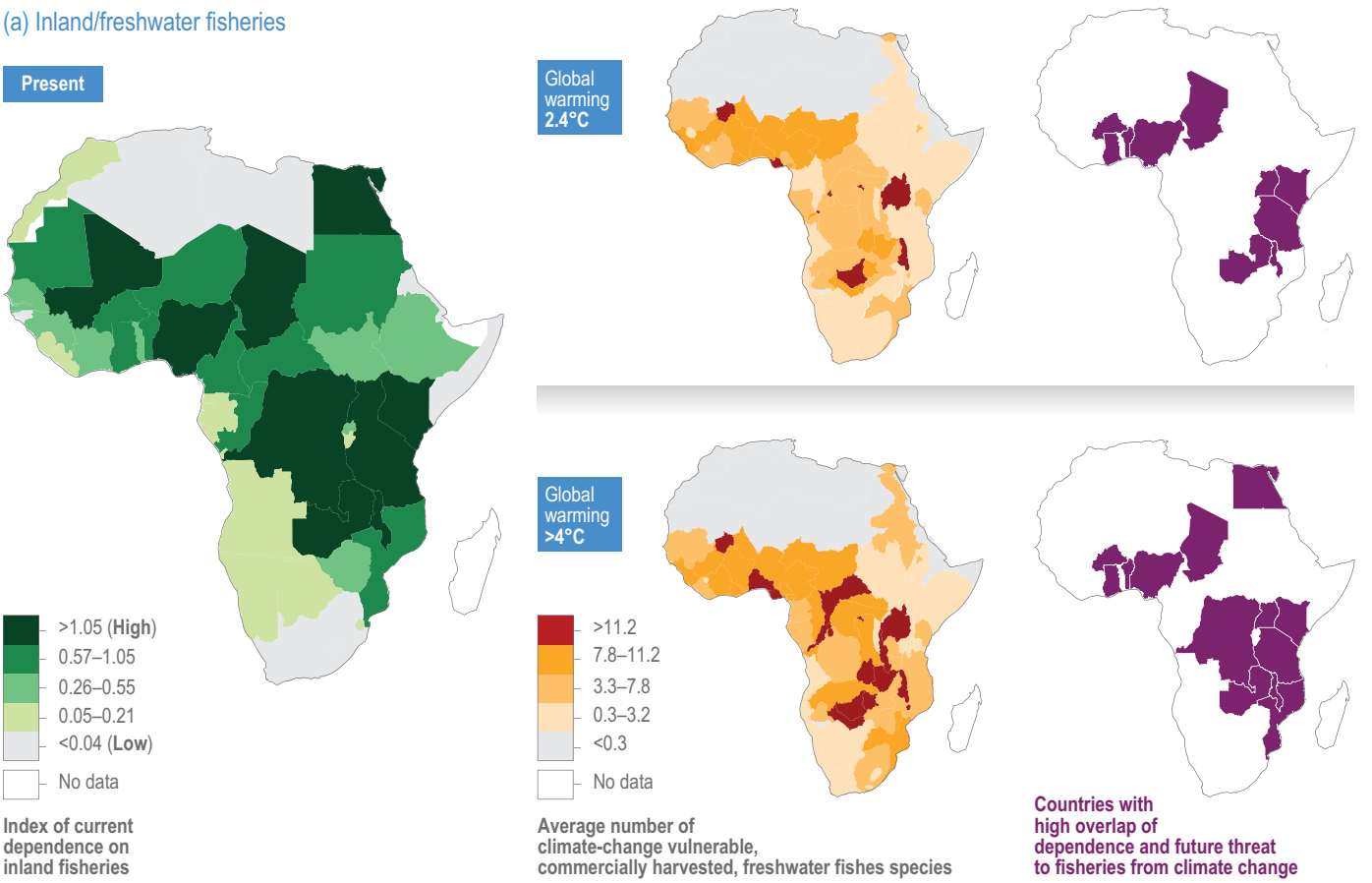

Figure AI.34a | Climate change risk to fisheries in Africa.

(a) Countries' reliance on inland fisheries was estimated by catch (total, tonnes) (FAO, 2018b; Fluet-Chouinard et al., 2018), per capita catch (kg per person per year) (FAO, 2018b), percent reliance on fish for micronutrients, and percent consumption per household (Golden et al., 2016). Z-scores of each metric were averaged for each country to create a composite index describing 'current dependence on freshwater fish' for each country with darker blue colours indicating higher dependence. Projected concentrations (numbers) of vulnerable freshwater fishery species averaged within freshwater ecoregions under >2°C global warming and >4°C global warming estimated from recent past (1961–1992) to the end of the 21st century (2071–2100) (Nyboer et al., 2019). Numbers of vulnerable fish species translate to an average of 55–68% vulnerable at >2°C and 77–97% vulnerable at <4°C global warming. Darker shades indicate higher concentrations of vulnerable fish species. Countries (in shades of green) that have an overlap between high dependence on freshwater fish and high concentrations of fishery species that are vulnerable to climate change under two warming scenarios. {Figures 9.26}

Climate change risk to fisheries in Africa

(b) Marine fisheries

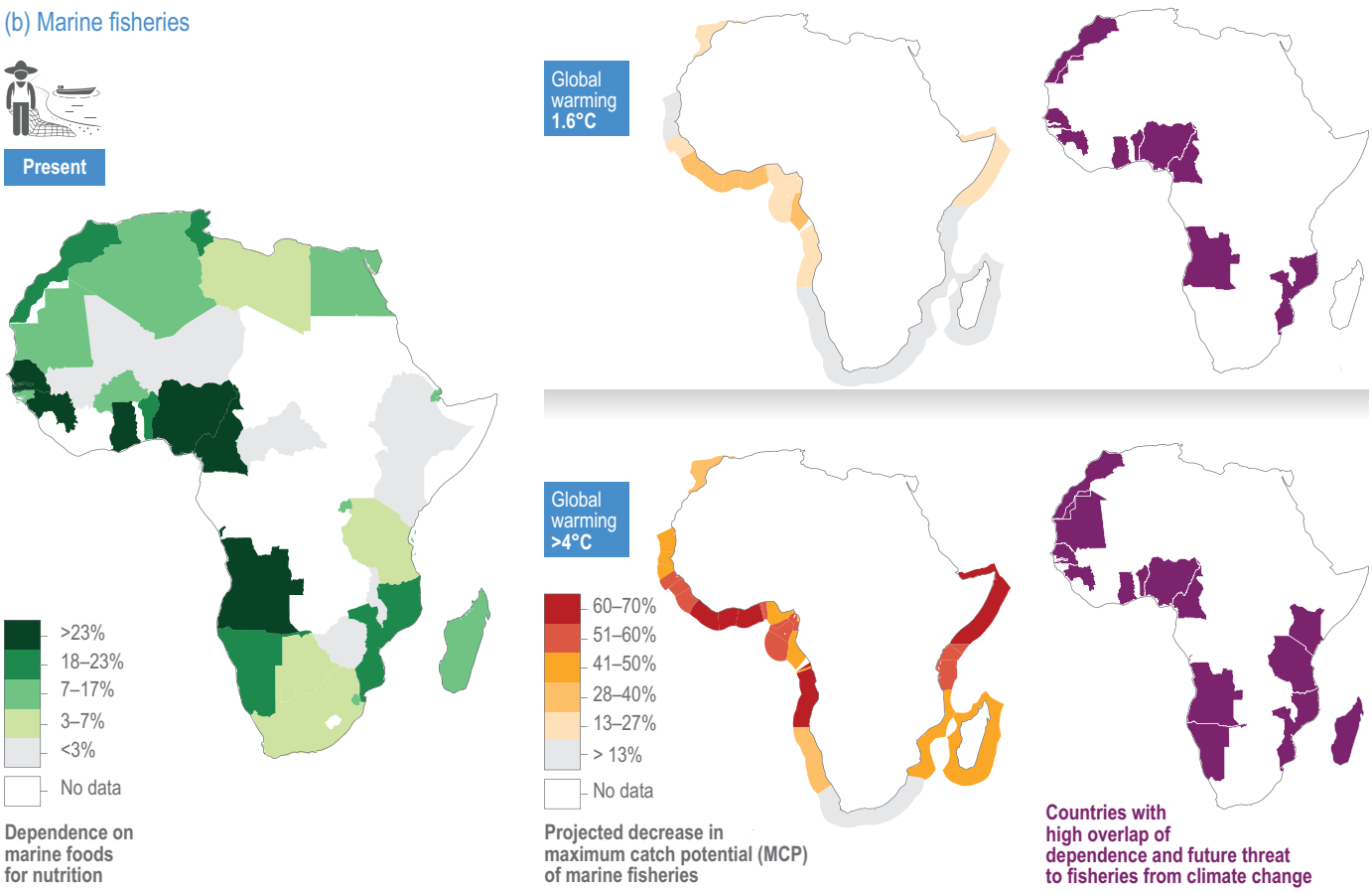

Figure AI.34b | Climate change risk to fisheries in Africa.

(b) Marine fisheries comparing countries' current percent dependence on marine foods for nutrition compared with projected change in maximum catch potential (MCP) from marine fisheries. The percentage of animal sources foods consumed that originate from a marine environment. Countries with higher dependence are indicated by darker shades (Golden et al., 2016). Projected percent change in MCP of marine fisheries under 1.6°C global warming and >4°C global warming from recent past (1986–2005) to end of 21st century (2081–2100) in countries' Exclusive Economic Zones (EEZs) (Cheung William et al., 2016). Darker shades indicate greater percent reduction (negative values). Countries (in shades of green) that have overlap between high nutritional dependence and high reduction in MCP under two warming scenarios. {Figure 9.25}

https://doi.org/10.1017/9781009325844.028

AI

AI.2.2 Water-related Challenges

Regional synthesis of assessed changes in water and consequent impacts

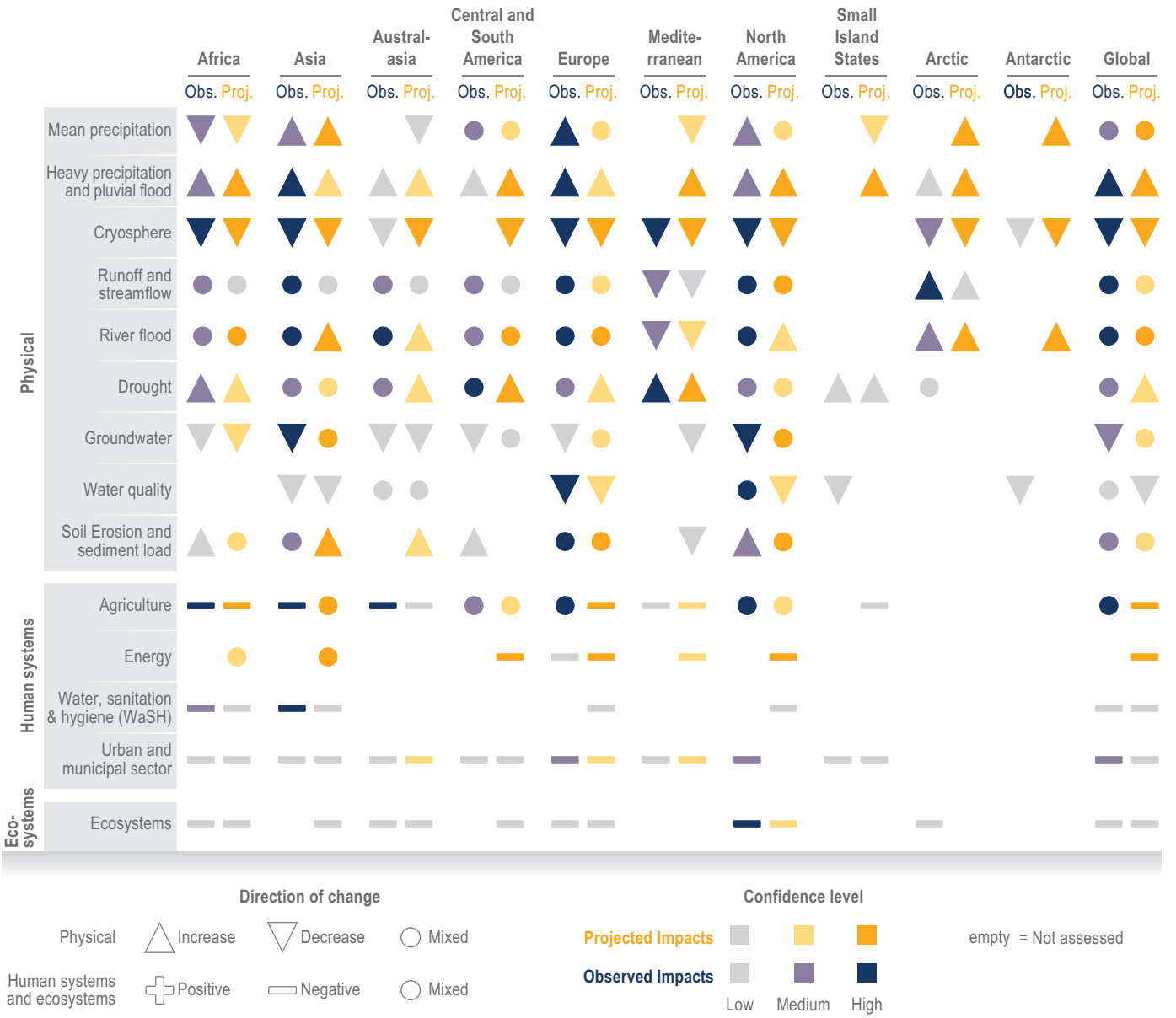

Figure AI.35 | Regional synthesis of changes in water and consequent impacts on ecosystems and human systems. For physical changes, increase/decrease refers to changes in the amount or frequency of the measured variable, and the level of confidence refers to confidence that the change has occurred. For impacts on ecosystems and human systems, plus or minus marks depicts whether an observed impact of hydrological change is positive (beneficial) or negative (adverse), respectively, to the given system, and the level of confidence refers to confidence in attributing an impact on that system to a climate-induced hydrological change. Circles indicate that within that region, both increase and decrease of physical changes are found, but are not necessarily equal, or beneficial and adverse assessed impacts on ecosystems and human systems. Empty fields indicate variables not assessed due to *limited evidence*. Agriculture refers to impacts on crop production. Energy refers to impacts on hydro- and thermoelectric power generation. {Figure 4.20}

https://doi.org/10.1017/9781009325844.028

AI.2.2.1 Drought

Current global drought risk

averages for period 1901–2010

(a) Drought hazard

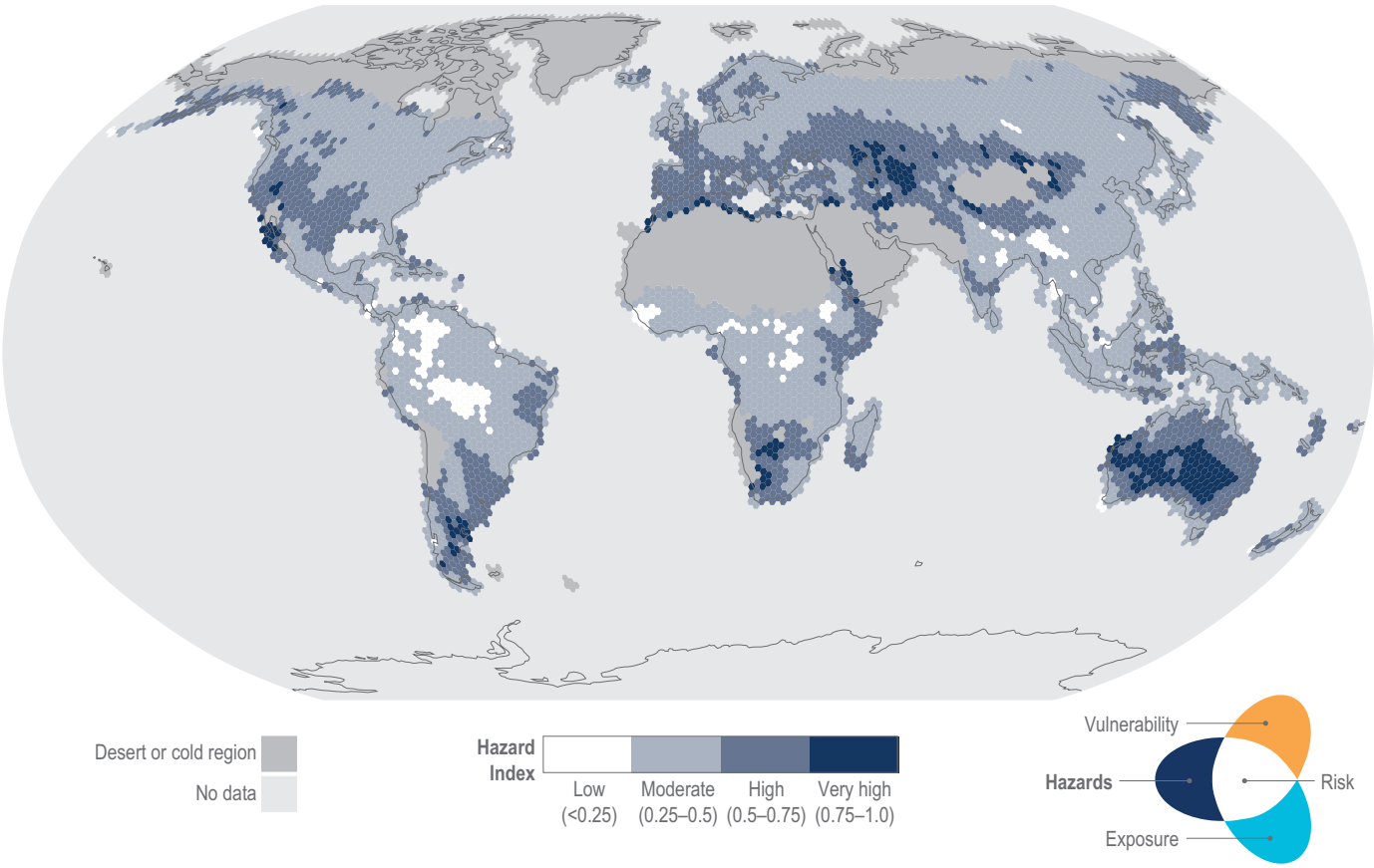

Figure AI.36a | Current global drought risk and its components.

(a) Drought hazard computed for the events between 1901 and 2010 by the probability of exceedance the median of global severe precipitation deficits, using precipitation data from the Global Precipitation Climatology Center (GPCC) for 1901–2010. {Figure 4.9}

https://doi.org/10.1017/9781009325844.028

Current global drought risk
averages for period 1901–2010

(b) Drought vulnerability

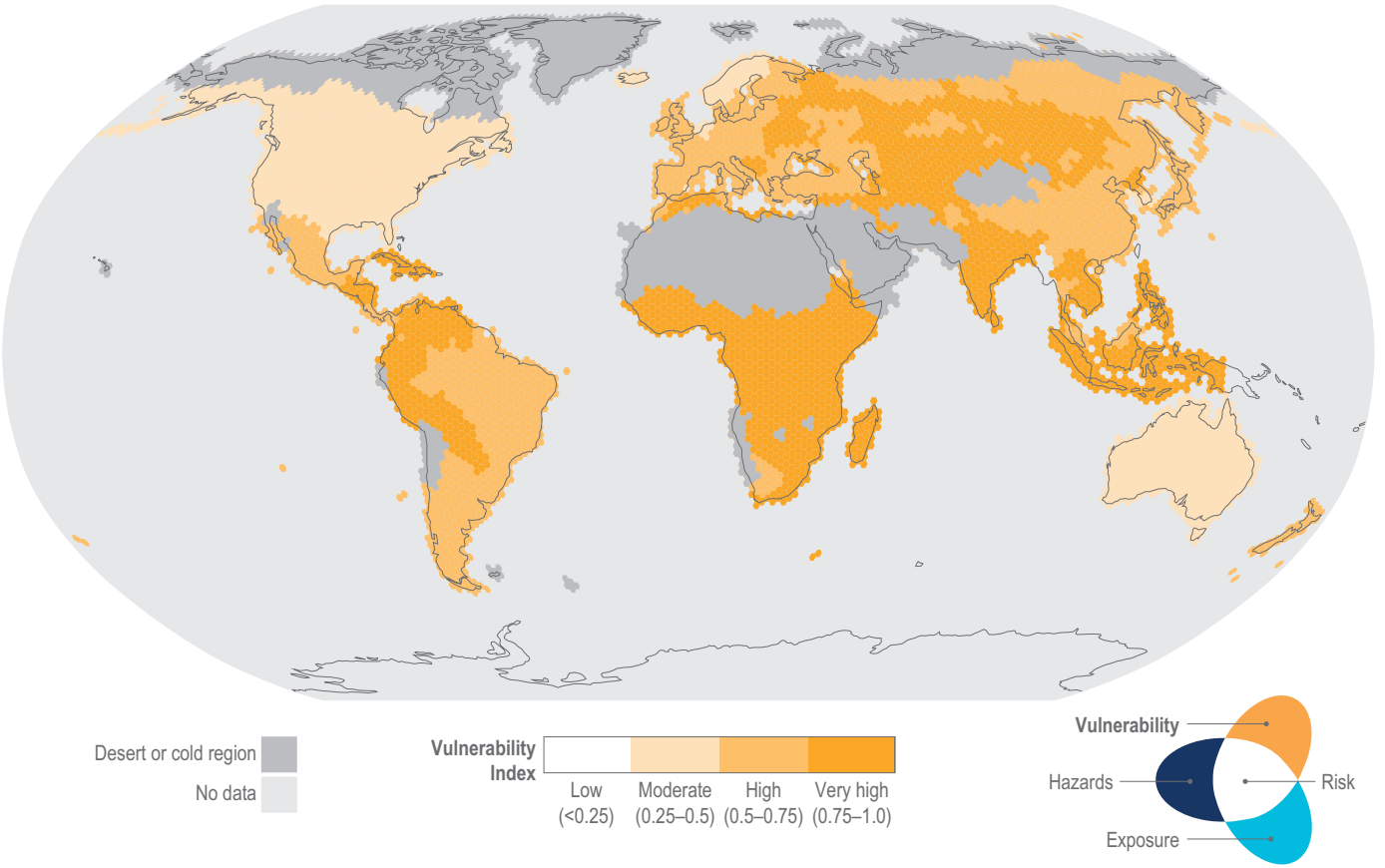

Figure AI.36b | Current global drought risk and its components.

(b) Drought vulnerability is derived from an arithmetic composite model combining social, economic and infrastructural factors proposed by UNISDR (2004). {Figure 4.9}

Current global drought risk
averages for period 1901–2010

(c) Drought exposure

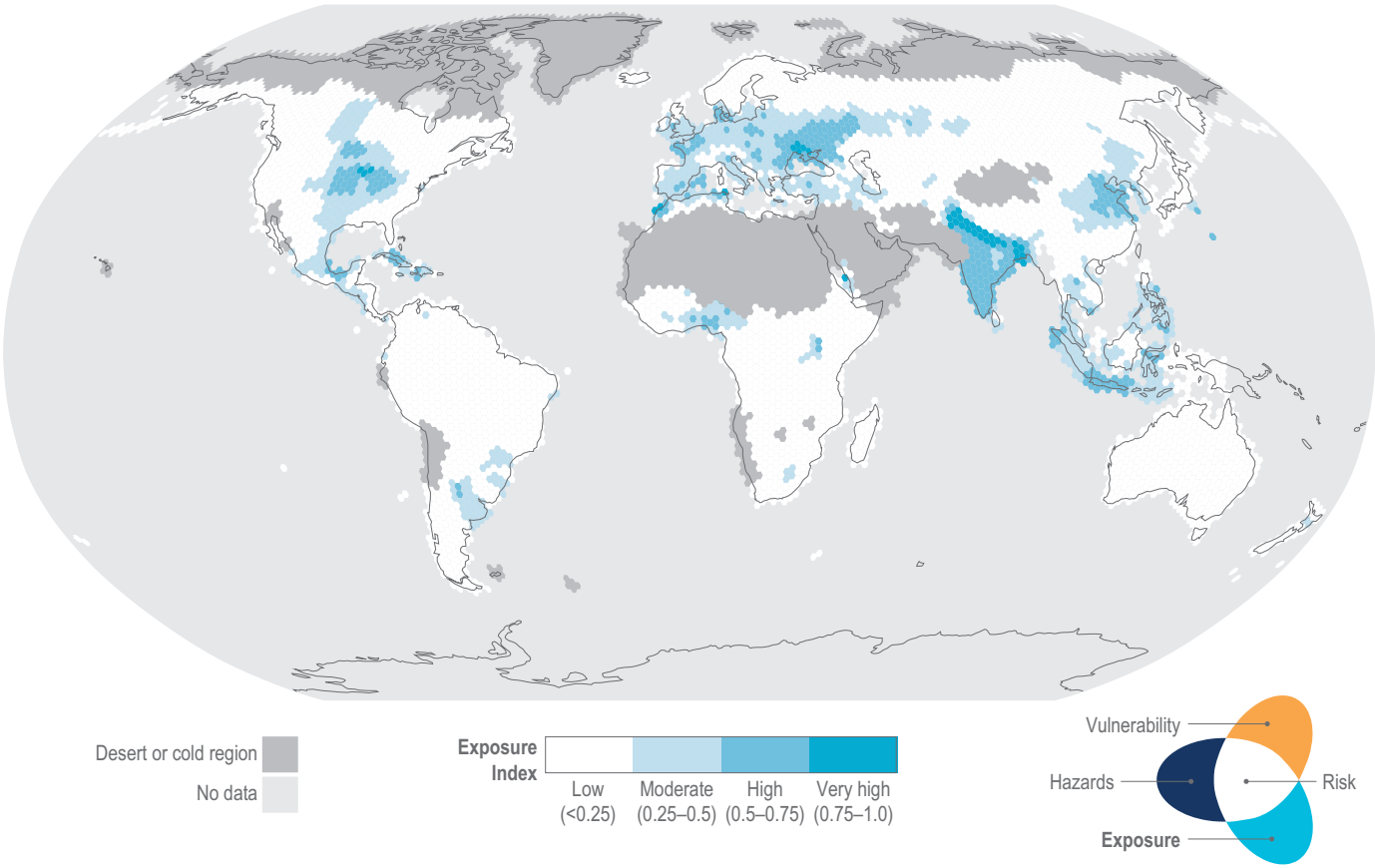

Figure AI.36c | Current global drought risk. Current global drought risk and its components.

(c) Drought exposure computed at the sub-national level with the non-compensatory Data Envelopment Analysis (DEA) model (Cook et al., 2014). {Figure 4.9}

Current global drought risk
averages for period 1901–2010

(d) Drought risk

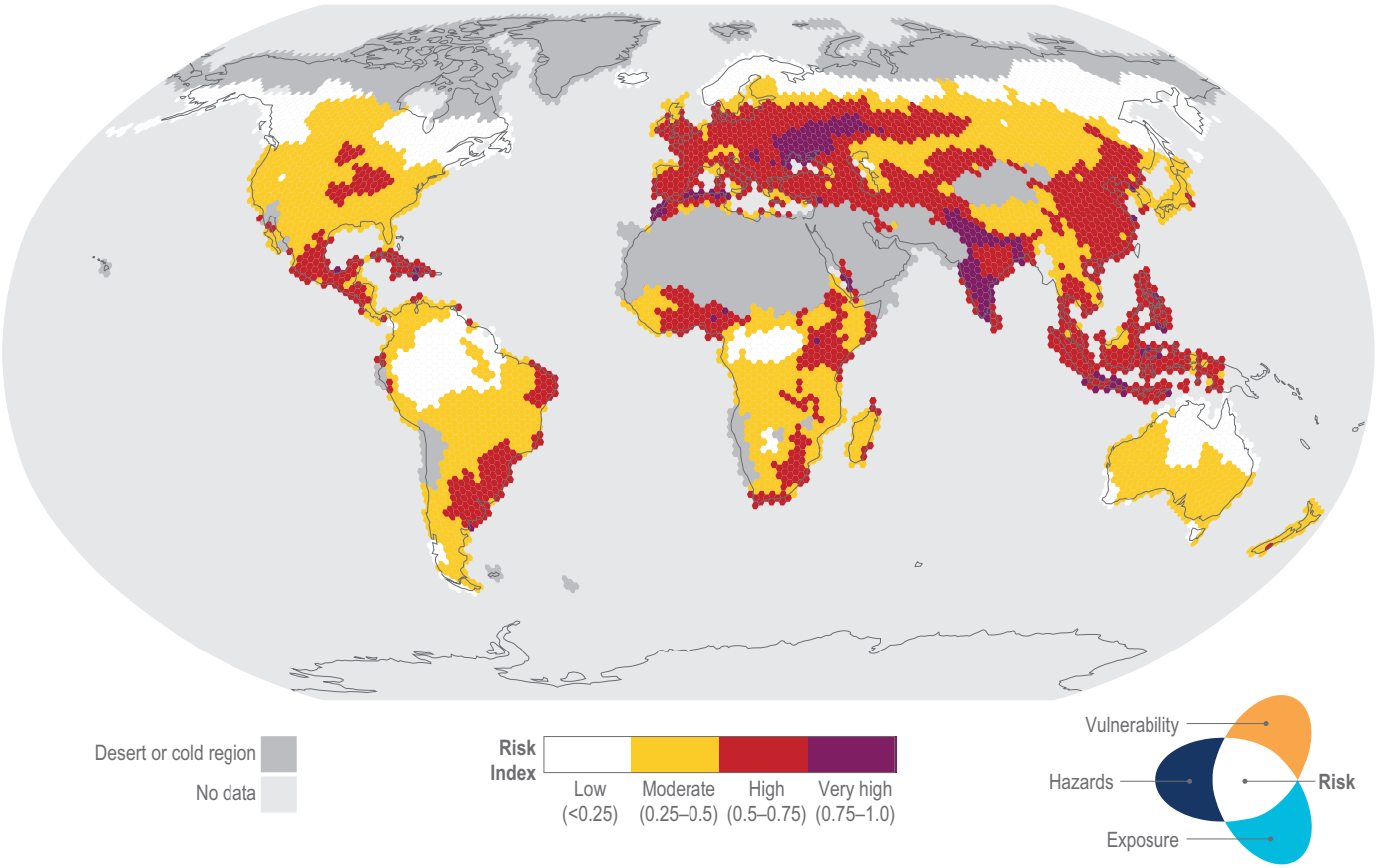

Figure AI.36d | Current global drought risk and its components.

(d) Drought risk based on the components of hazard, vulnerability and exposure, scored on a scale of 0 (lowest risk) to 1 (highest risk) with the lowest and highest hazard, exposure and vulnerability (Carrão et al., 2016). {Figure 4.9}

https://doi.org/10.1017/9781009325844.028

Importance of mountain water resources for lowland areas and populations

(a) Importance of mountain regions for lowland water resources (2041–2050, SSP2-RCP6.0)

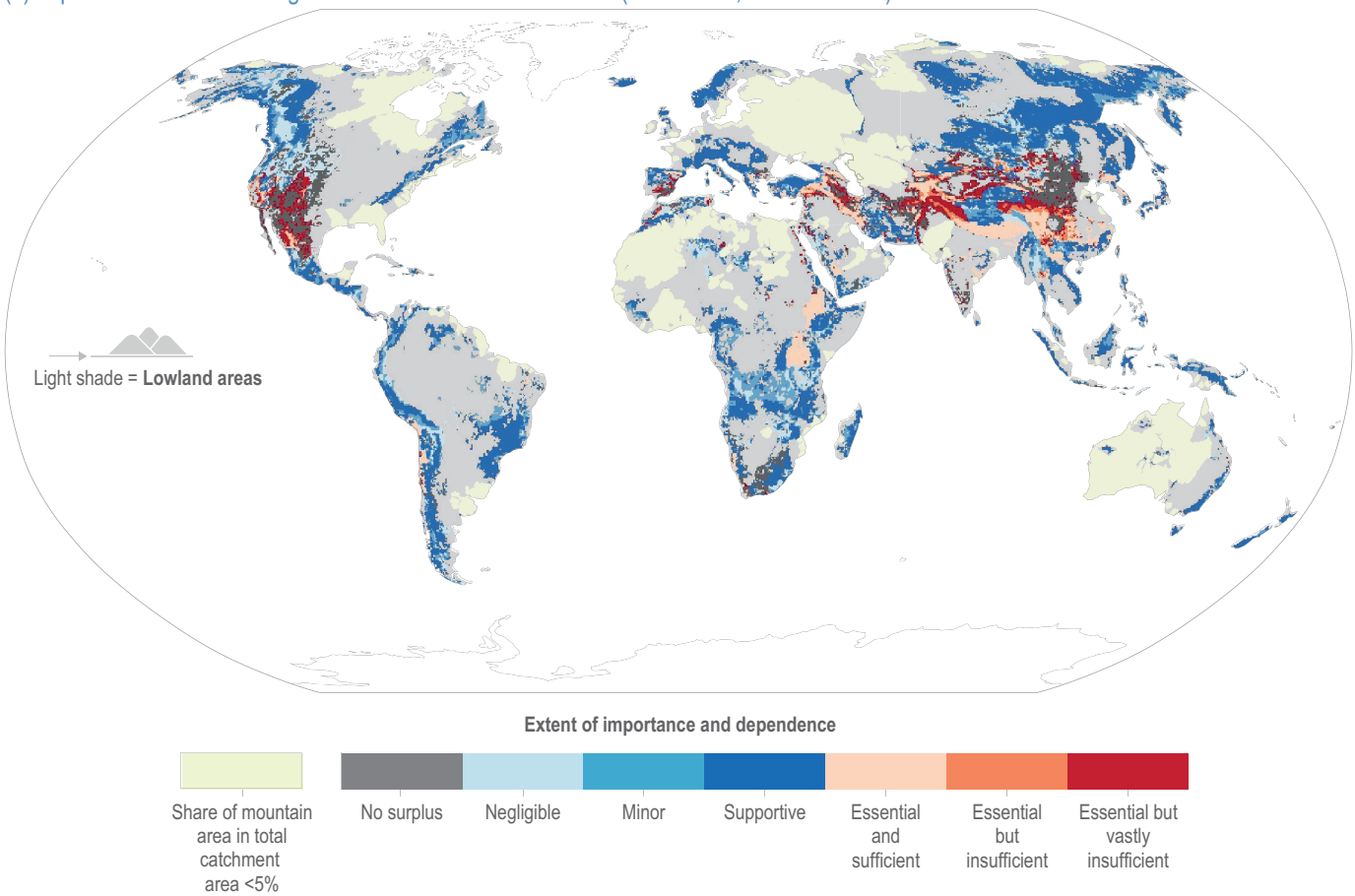

Figure AI.37a | Dependence of land surface areas and population on mountain water resources 1961–2050. Results are shown as decadal averages for lowland population in each category of dependence on mountain water, from no surplus and negligible to essential.

(a) Global mountain regions and their differentiated importance for lowland water resources.

https://doi.org/10.1017/9781009325844.028

Importance of mountain water resources for lowland areas and populations

(b) Lowland population dependence on mountain water resources (2041–2050, SSP2-RCP6.0)

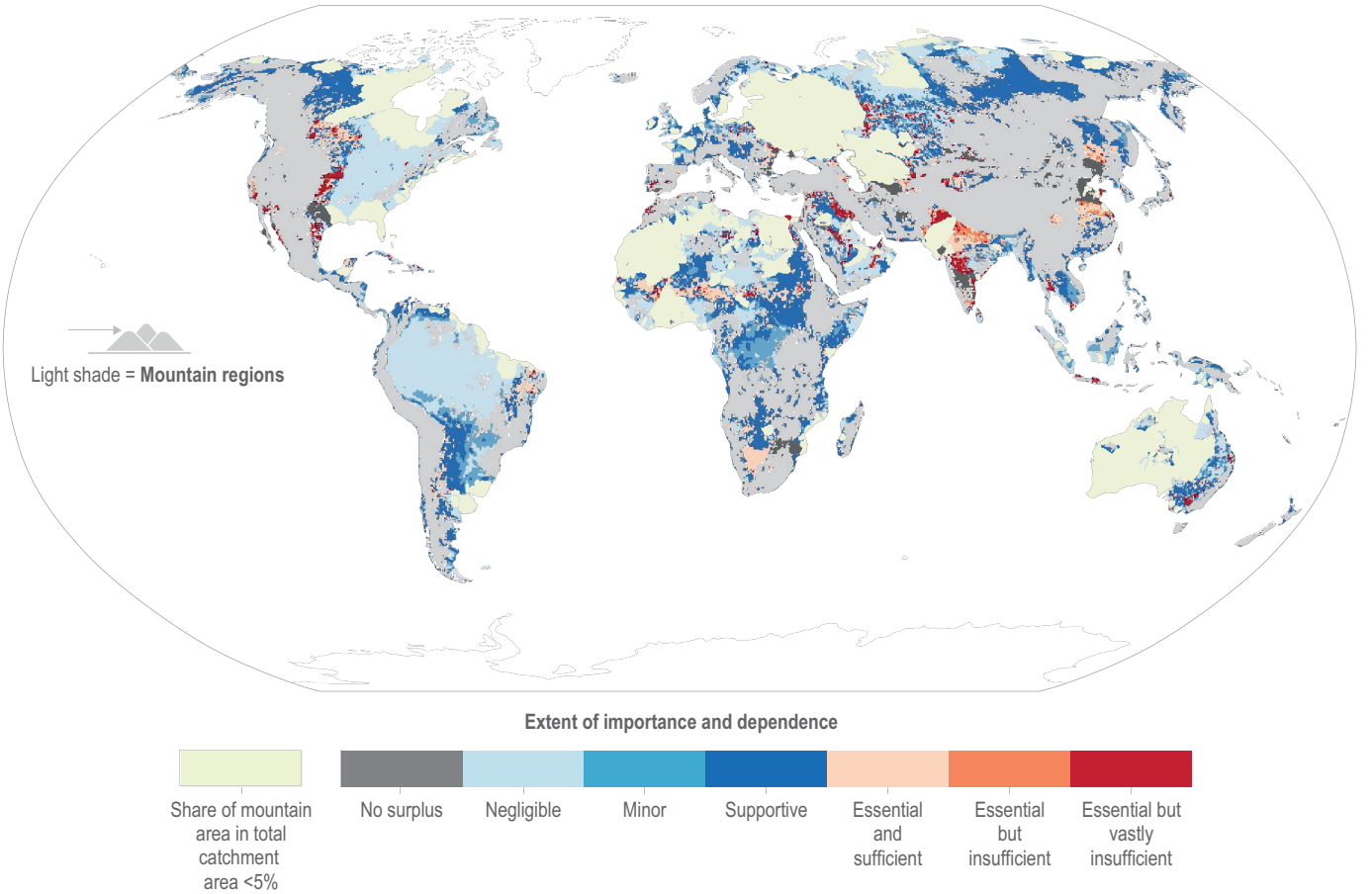

(c) Lowland population dependence on mountain water resources over time

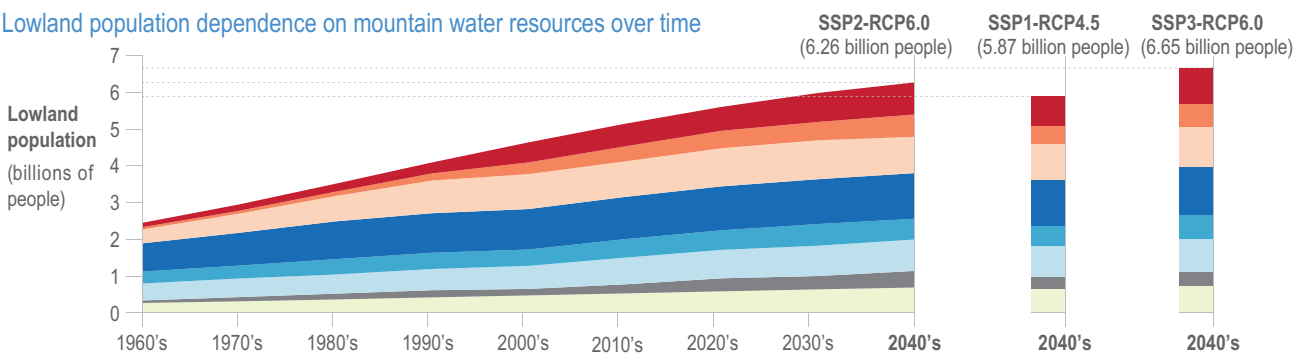

Figure AI.37b | Dependence of land surface areas and population on mountain water resources 1961–2050.

(b) Lowland population and their differentiated dependence on mountain water resources, both for the scenario combination SSP2-6.0 and for the time period 2041–2050.

(c) Number of lowland population and their differentiated dependence on mountain water resources from the 1960s to the 2040s for three different scenario combinations (based on Viviroli et al., 2020). {Figure CCP5.2}

Risks to livelihoods and the economy from changing mountain water resources

between 1.5°C and 2°C global warming level in AR6 WGI reference regions

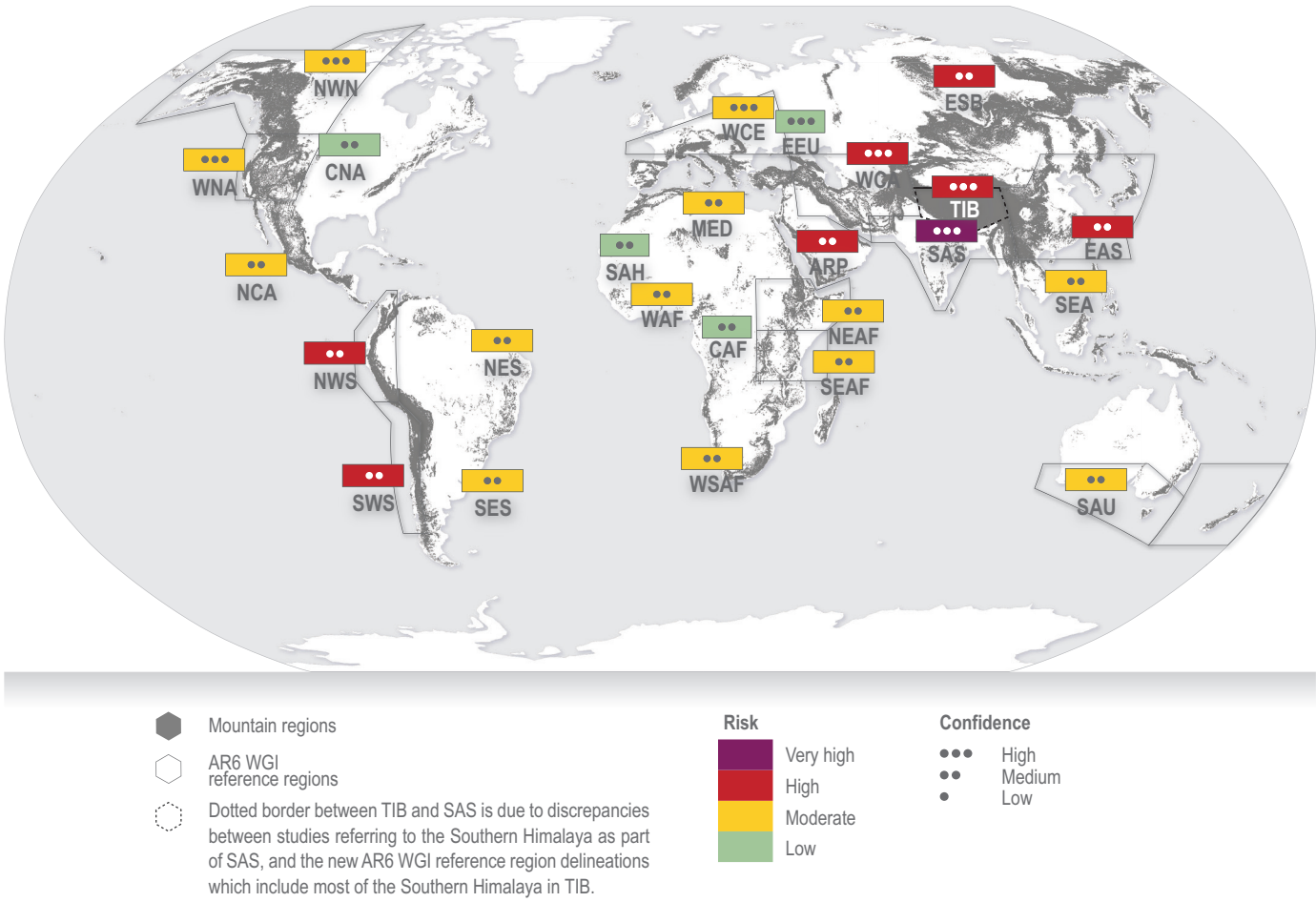

Figure AI.38 | Risk to livelihoods and the economy from changing mountain water resources. The majority of studies assessed focus on impacts up to mid-century (2030–2060) and for Representative Concentration Pathways RCP2.6, RCP4.5 and RCP6.0, which was converted into the corresponding warming level range 1.5–2.0°C global warming level (GWL) (see Cross-Chapter Box CLIMATE in Chapter 1). Methodological details are provided in Section SMCCP5.4, Figure SMCCP5.1, Table SMCCP5.16 and SMCCP5.18. Due to the *limited evidence* available to determine risks against high GWLs, and the relatively high uncertainties associated with future irrigation trends for the second half of the century (see, e.g., Viviroli et al., 2020), assessment of risks associated with GWLs greater than 2.0°C GWL was not conducted. {Figure CCP5.6}

AI

AI.2.2.2 Flooding

Extreme sea level events

Due to projected global mean sea level (GMSL) rise, local sea levels that historically occurred once per century (**historical centennial events, HCEs**) are projected to become at least annual events at most locations during the 21st century. The height of a HCE varies widely, and depending on the level of exposure can already cause severe impacts. Impacts can continue to increase with rising frequency of HCEs.

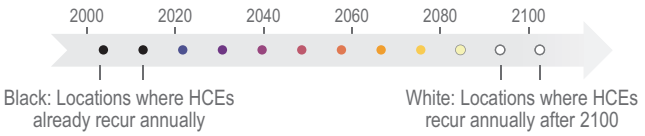

(a) Year when HCEs are projected to recur once per year on average

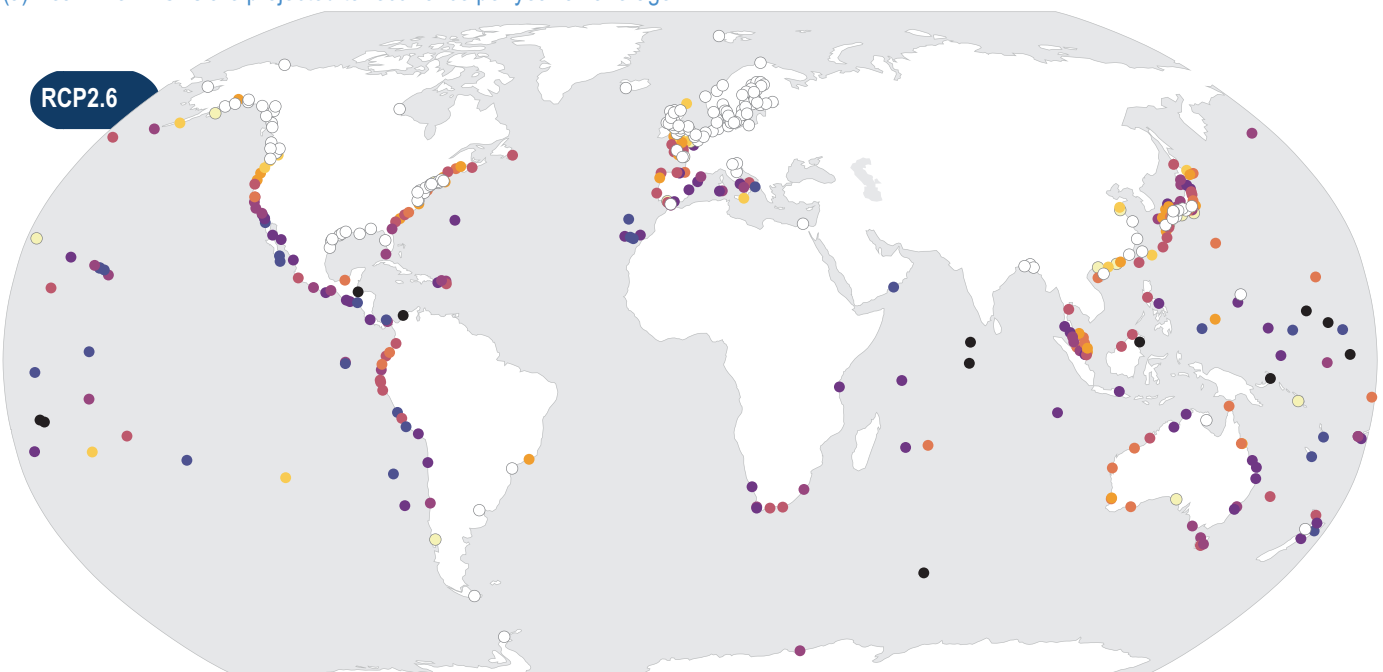

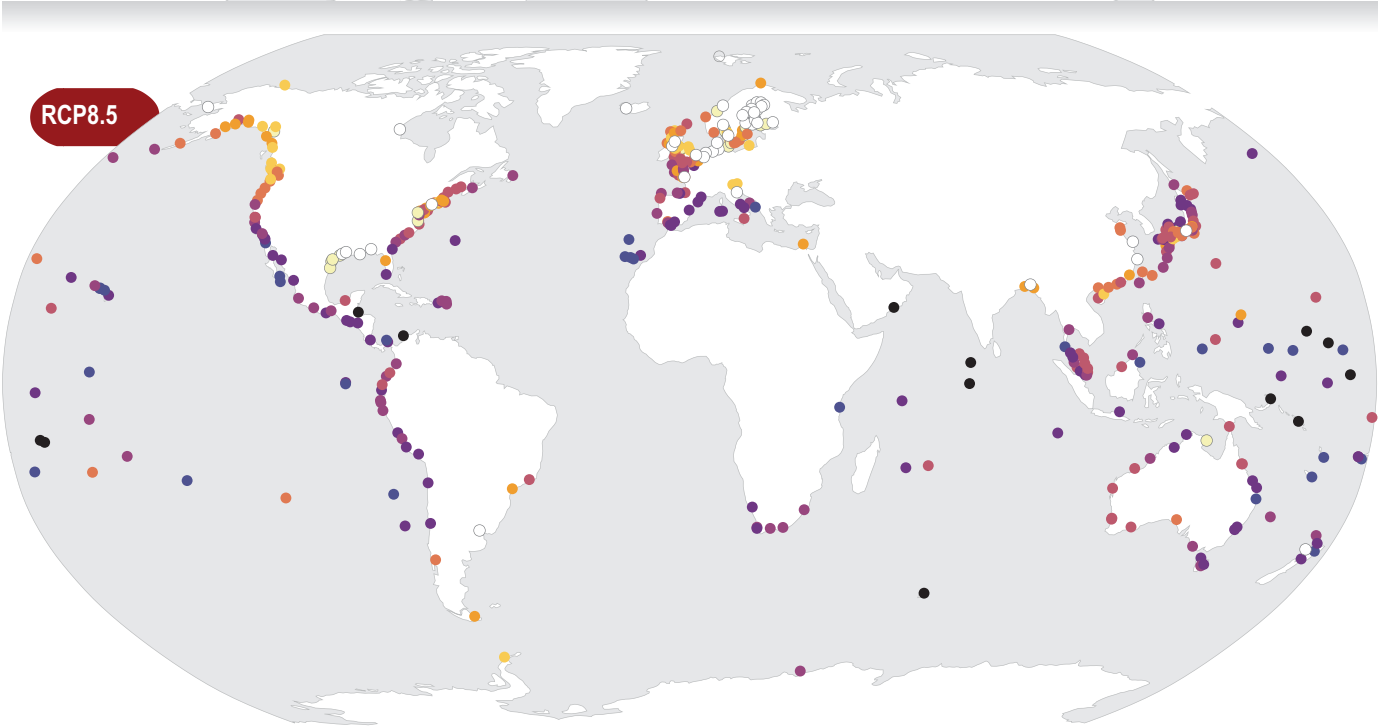

Figure AI.39a | The effect of regional sea level rise on extreme sea level events at coastal locations.

(a) The year in which historical centennial events (HCEs) are expected to recur once per year on average under Representative Concentration Pathways RCP8.5 and RCP2.6, at the 439 individual coastal locations where the observational record is sufficient. The absence of a circle indicates an inability to perform an assessment due to a lack of data but does not indicate absence of exposure and risk. The darker the circle, the earlier this transition is expected. The likely range is ±10 years for locations where this transition is expected before 2100. White circles (33% of locations under RCP2.6 and 10% under RCP8.5) indicate that HCEs are not expected to recur once per year before 2100.

Extreme sea level events

(b) Difference between RCP8.5 and RCP2.6

The difference map shows locations where the HCE becomes annual at least 10 years later under RCP2.6 than under RCP8.5.

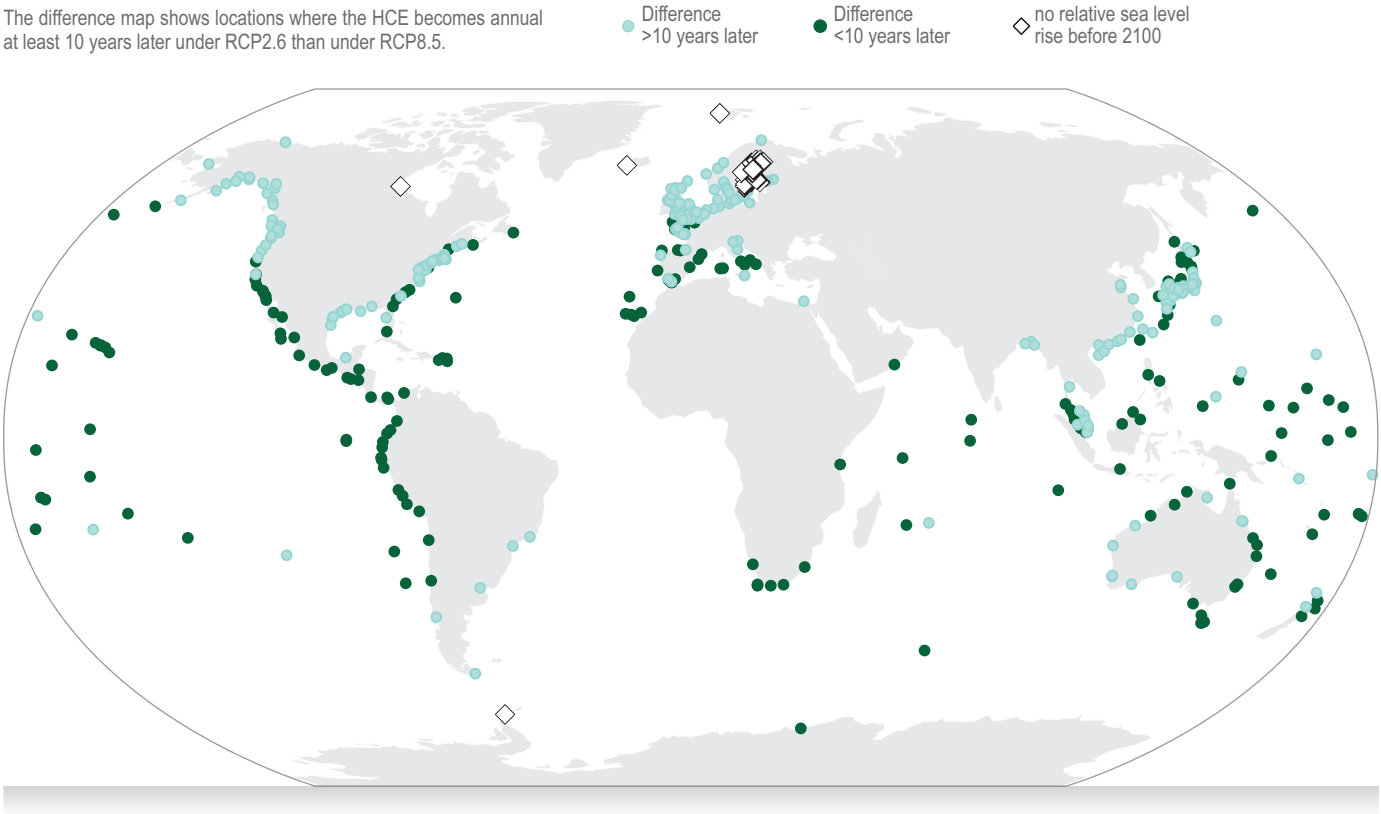

(c) Schematic effect of regional sea level rise on projected extreme sea level events (not to scale)

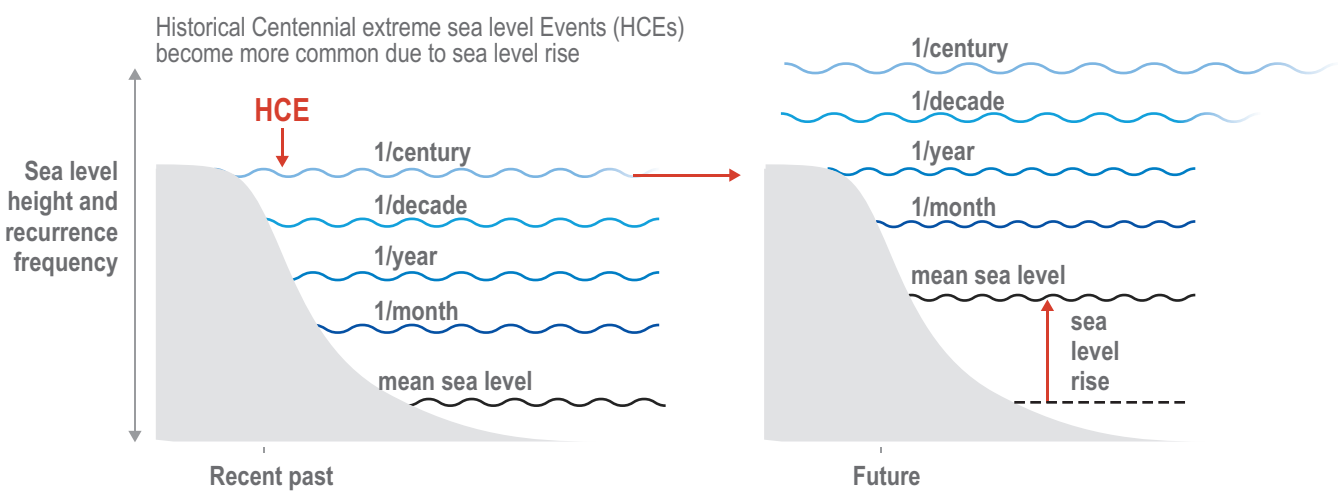

Figure AI.39b | The effect of regional sea level rise on extreme sea level events at coastal locations.

(b) An indication at which locations this transition of HCEs to annual events is projected to occur more than 10 years later under RCP2.6 compared with RCP8.5. As the scenarios lead to small differences by 2050 in many locations, results are not shown here for RCP4.5.

(c) Schematic illustration of extreme sea level events and their average recurrence in the recent past (1986–2005) and the future. As a consequence of mean sea level rise, local sea levels that historically occurred once per century HCEs are projected to recur more frequently in the future. {4.2.3, Figures 4.10, 4.12}

Relative trends in projected regional shoreline change (advance/retreat relative to 2010)

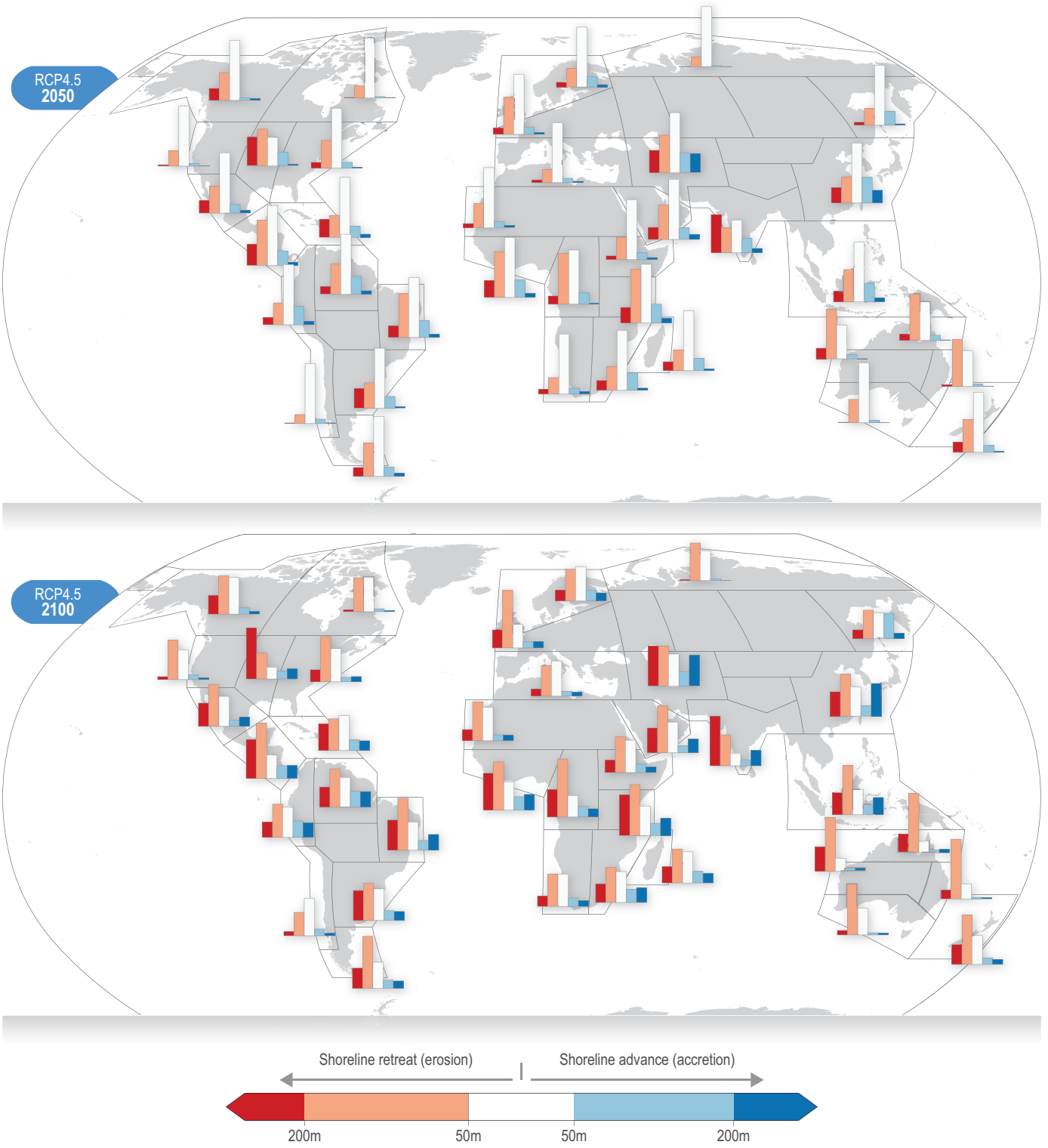

Figure AI.40a | Relative trends in projected regional shoreline change. Advance/retreat relative to 2010. Frequency distributions of median projected change by 2050 and 2100 under RCP4.5. Projections account for both long-term shoreline dynamics and sea level rise and assume no impediment to inland transgression of sandy beaches. Data for Small Island States are aggregated and plotted in the Caribbean. Data from Vousdoukas et al. (2020b). Values for reference regions established in the WGI AR6 Atlas (Gutiérrez et al., 2021) were computed as area-weighted means from original country-level data. For model assumptions and associated debate, see Vousdoukas et al. (2020a) and Cooper et al. (2020a). {Figure 3.14}

Relative trends in projected regional shoreline change (advance/retreat relative to 2010)

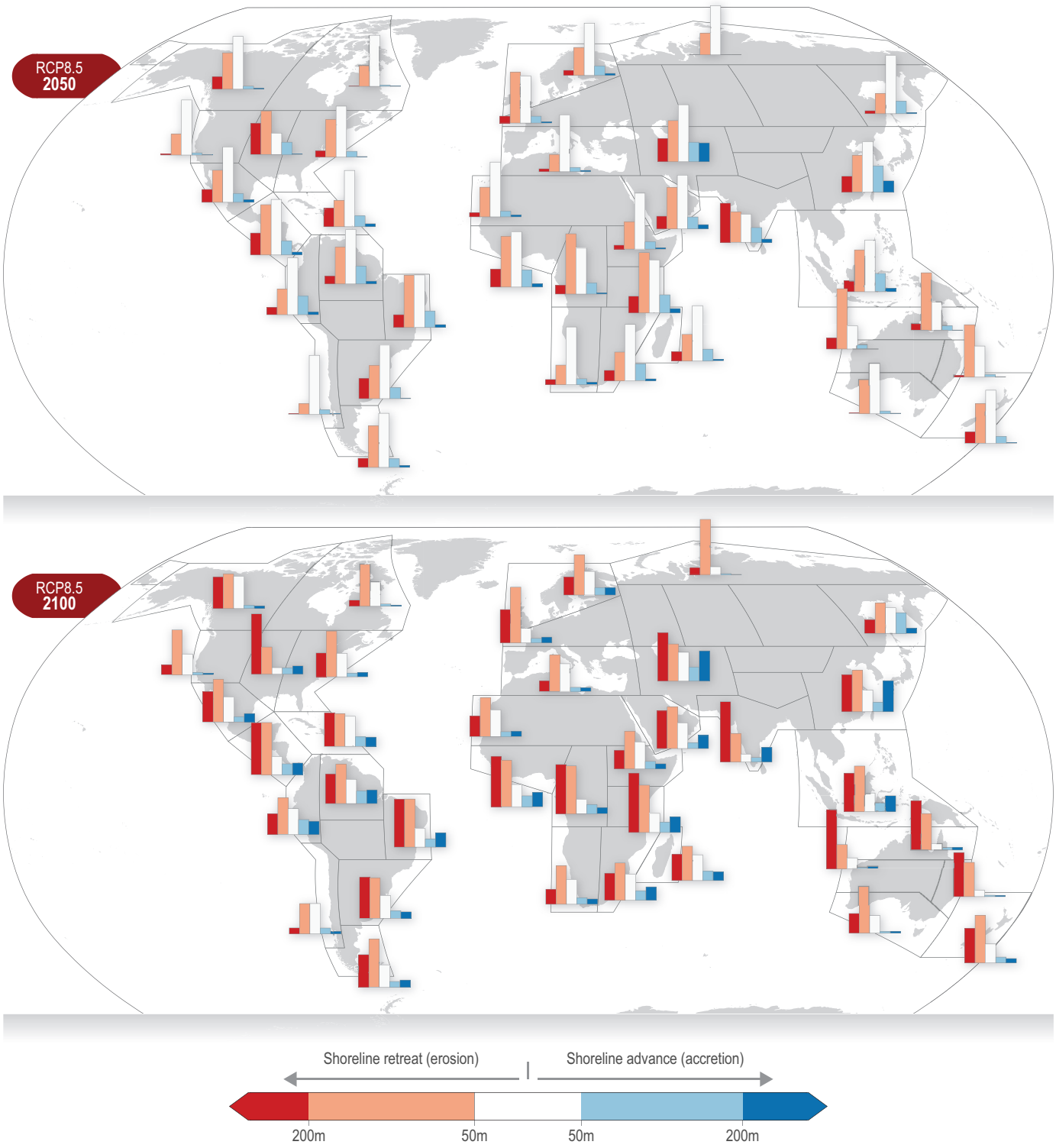

Figure AI.40b | Relative trends in projected regional shoreline change. Advance/retreat relative to 2010. Frequency distributions of median projected change by 2050 and 2100 under RCP8.5. Projections account for both long-term shoreline dynamics and sea level rise and assume no impediment to inland transgression of sandy beaches. Data for Small Island States are aggregated and plotted in the Caribbean. Data from Vousdoukas et al. (2020b). Values for reference regions established in the WGI AR6 Atlas (Gutiérrez et al., 2021) were computed as area-weighted means from original country-level data. For model assumptions and associated debate, see Vousdoukas et al. (2020a) and Cooper et al. (2020a). {Figure 3.14}

https://doi.org/10.1017/9781009325844.028

Population living in small islands that may be exposed to coastal inundation by 2100 under RCP4.5

For selected islands, each dot represents the corresponding percentage of the population occupying **vulnerable land**, that may be exposed to coastal inundation either by permanently falling below mean higher high water (MHHW), or temporarily falling below the local annual flood height.

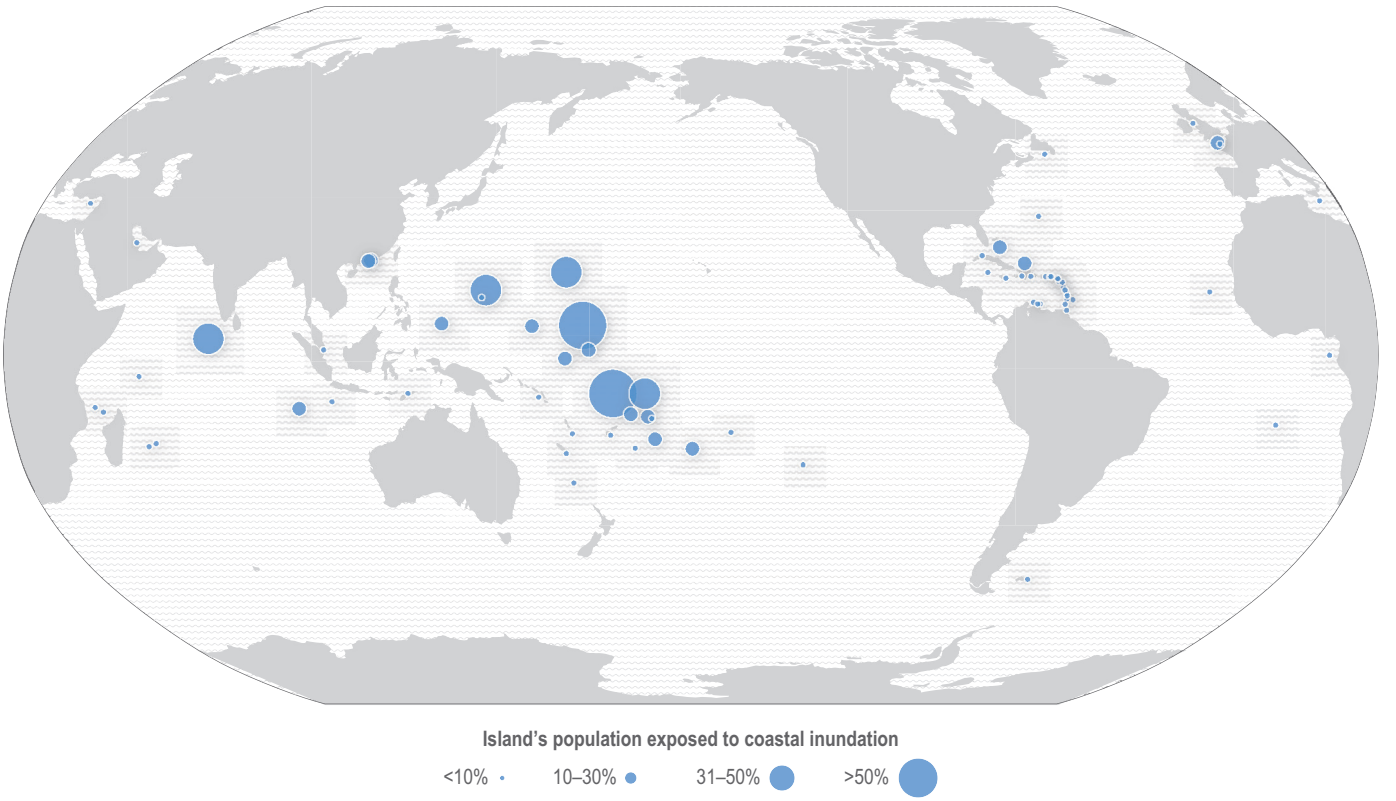

Figure AI.41 | Population living in small islands that may be exposed to coastal inundation. Projected percentage of current population in selected small islands occupying vulnerable land (the number of people on land that may be exposed to coastal inundation—either by permanently falling below mean higher high water, or temporarily falling below the local annual flood height (adapted from Kulp et al., 2019, using the CoastalDEM_Perm_p50 model). Positions on the map are based on the capital city or largest town. {Figure 15.3}

Projected number of people at risk of a 100-year coastal flood

Calculated for sea level rise and population change, based on current protection levels

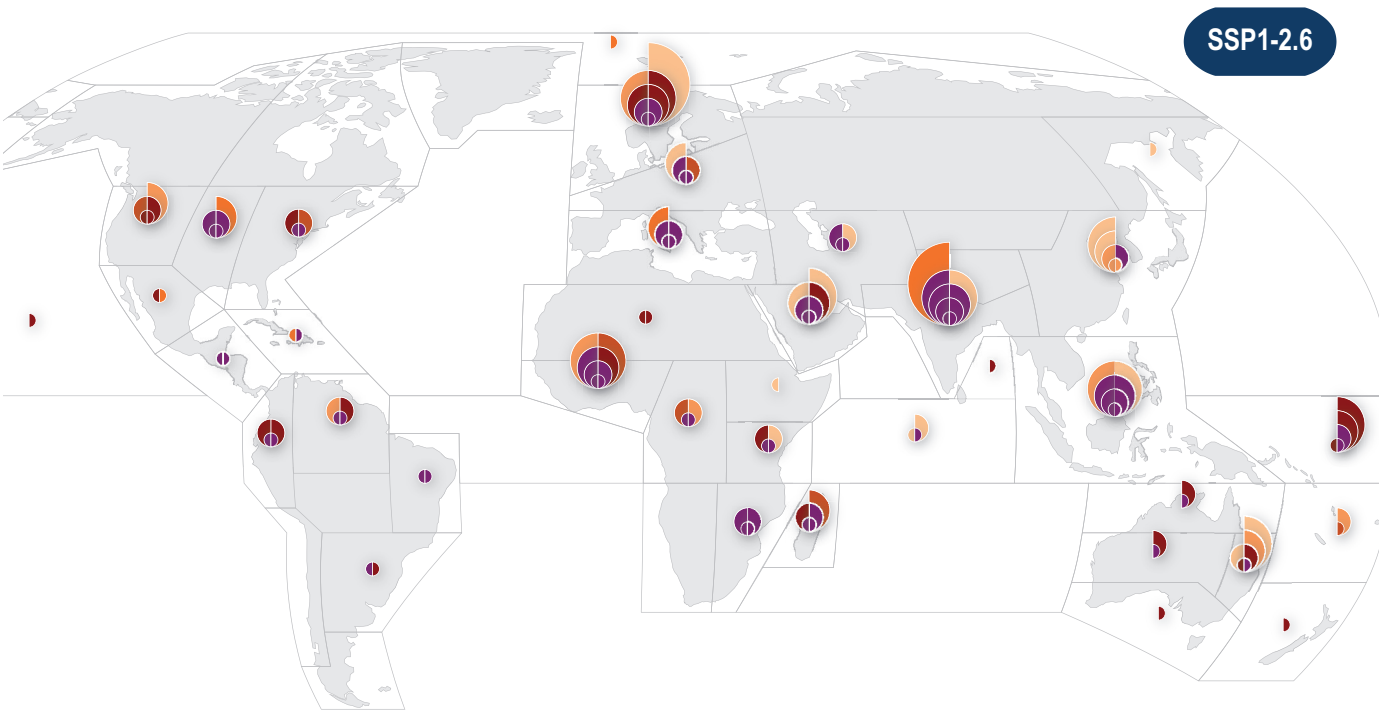

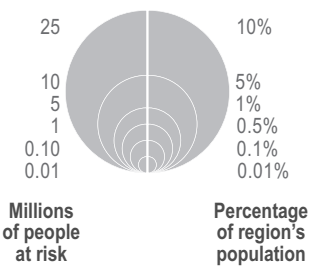

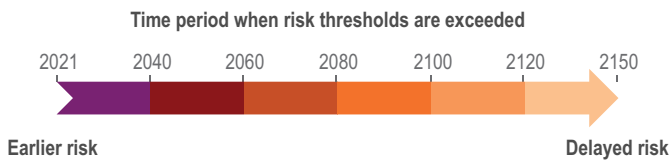

In following pages. SSP2-4.5 SSP5-8.5

Projected number of people at risk of a 100-year coastal flood

Calculated for sea level rise and population change, based on current protection levels

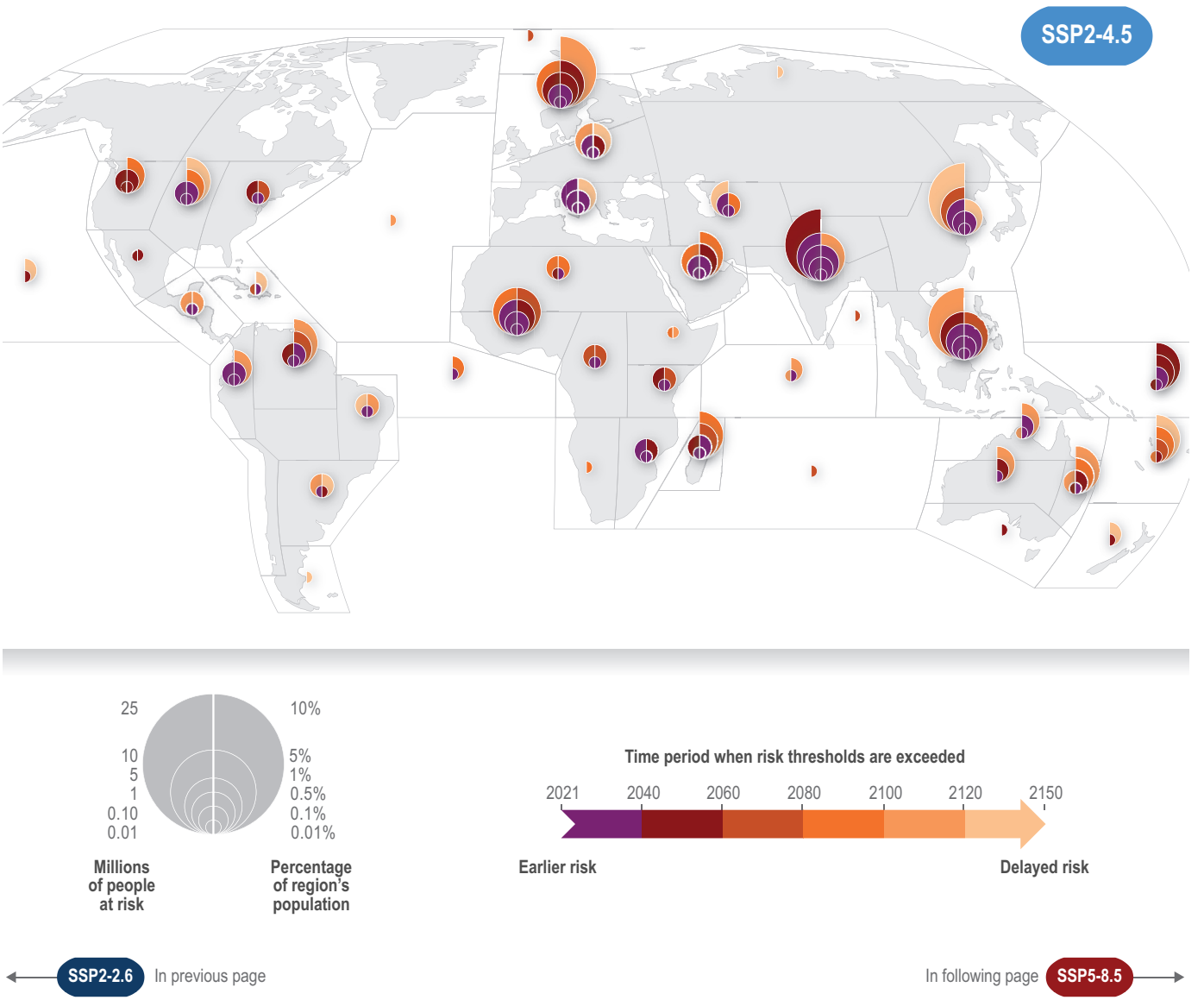

SSP2-2.6 In previous page

In following page SSP5-8.5

Projected number of people at risk of a 100-year coastal flood

Calculated for sea level rise and population change, based on current protection levels

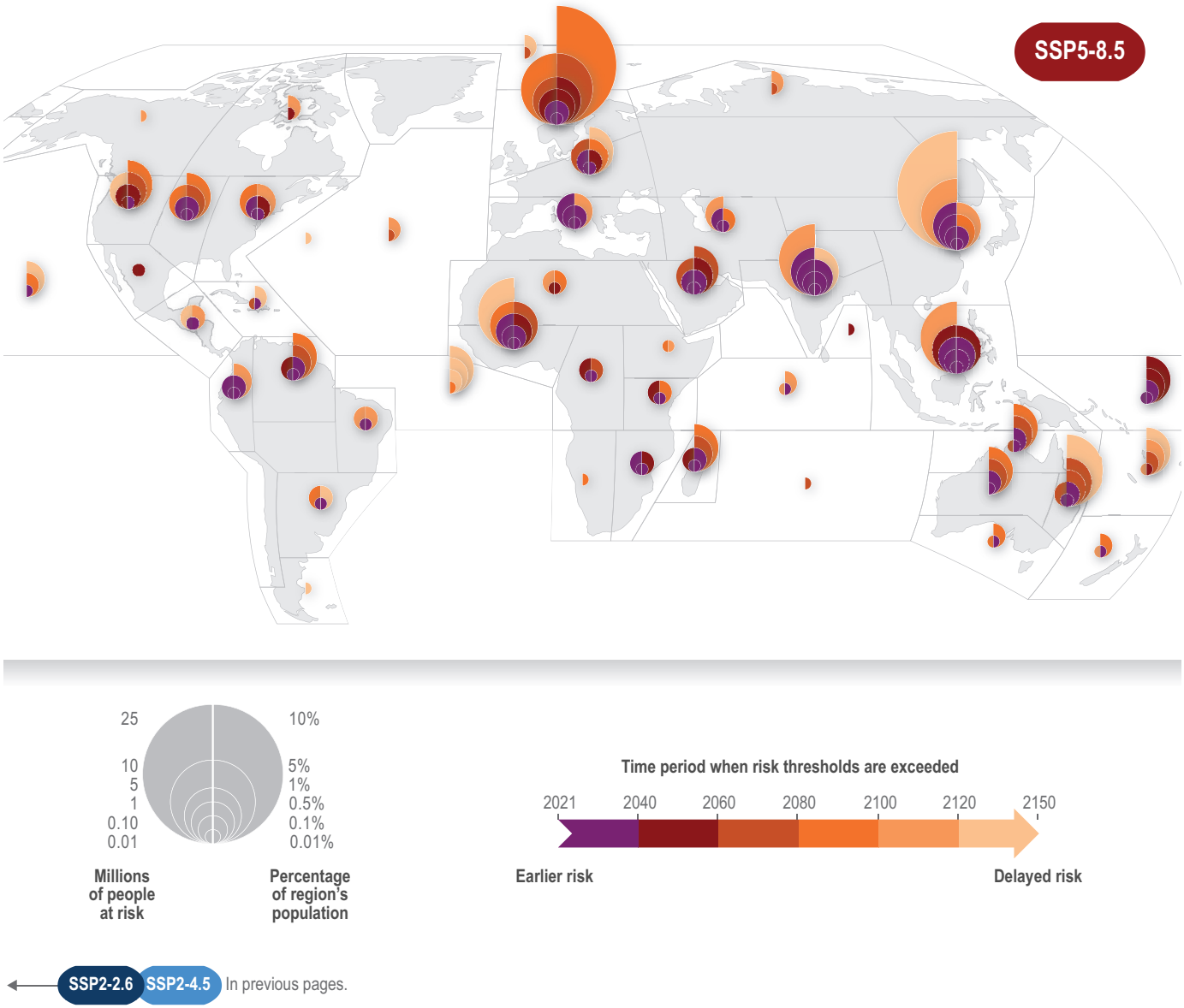

Figure AI.42 | Projected number of people at risk of a 100-year coastal flood. The size of the circle represents the number of people at risk per reference regions established in the WGI AR6 Atlas (Gutiérrez et al., 2021) and the colours show the timing of risk based on projected sea level rise (Haasnoot et al., 2021) under three different Shared Socioeconomic Pathways (SSPs). Darker colours indicate earlier in setting risks. The left side of the circles shows absolute population at risk and the right side the share of the population in percentage. {Figure CCP2.3}

https://doi.org/10.1017/9781009325844.028

AI

Selected regions at risk of potential sea level rise

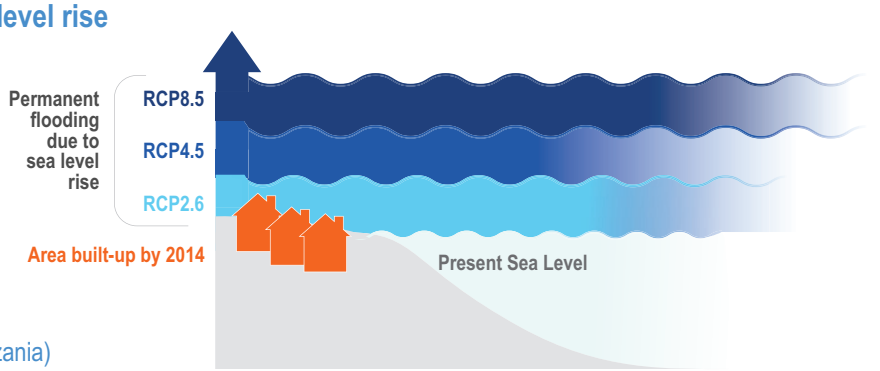

(a) Dar es Salaam, Bagamoyo and Stonetown (Tanzania)

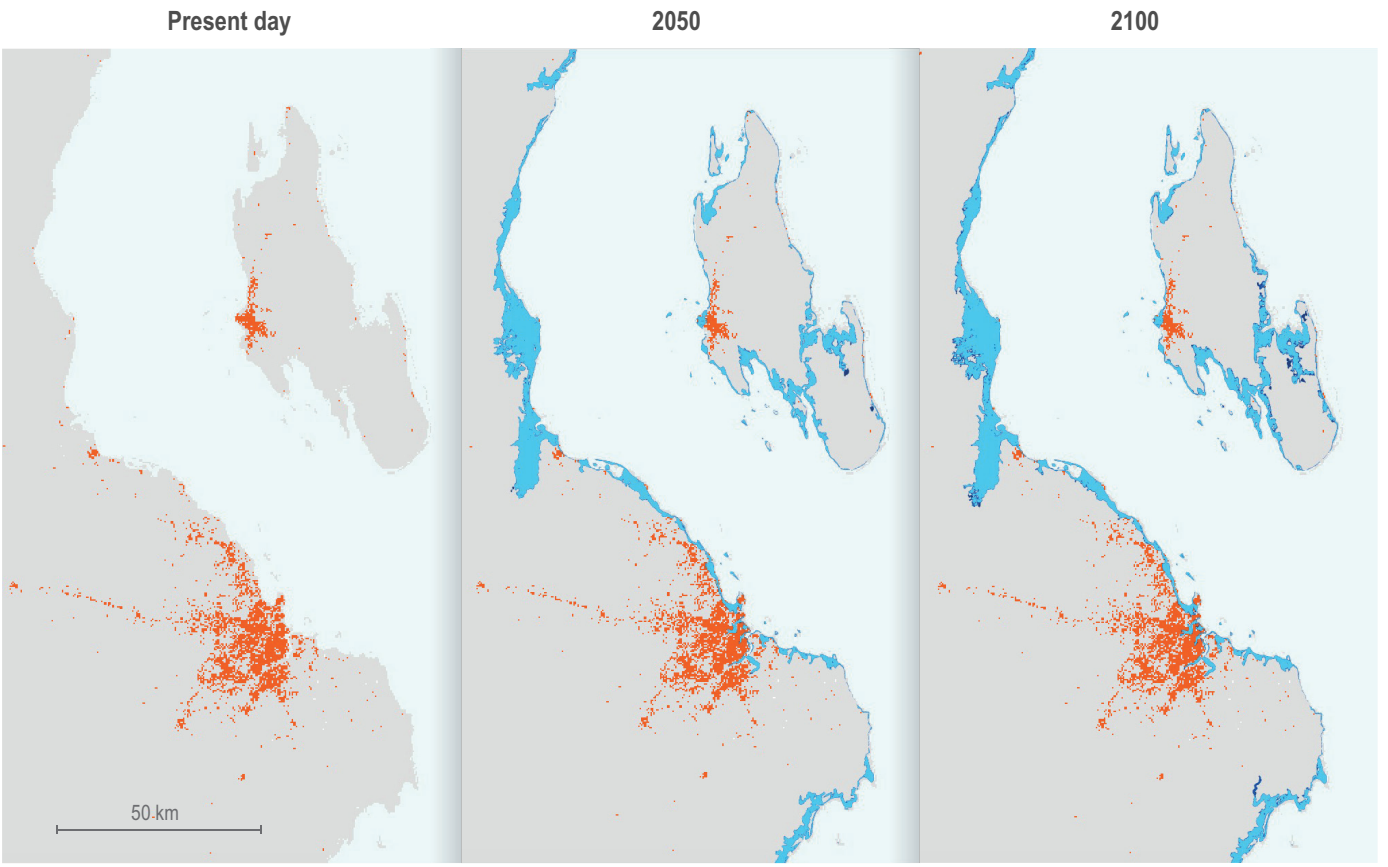

Figure AI.43 | Selected African cities exposed to sea level rise. Selected African cities exposed to sea level rise include

(a) Dar es Salaam, Bagamoyo and Stone Town in Tanzania (East Africa) in this page and

(b) Lagos in Nigeria and Cotonou and Porto-Novo in Benin (West Africa), and

(c) Cairo and Alexandria in Egypt (North Africa) in the following two pages. Orange shows built-up areas in 2014. Shades of blue show permanent flooding due to sea level rise by 2050 and 2100 under low (RCP2.6), medium (RCP4.5) and high (RCP8.5) greenhouse gas emissions scenarios. Darker colours for higher emissions scenarios show areas projected to be flooded in addition to those for lower emissions scenarios. The figure assumes failure of coastal defences in 2050 and 2100. Some areas are already below current sea level rise and coastal defences need to be upgraded as sea level rises (e.g., in Egypt), others are just above mean sea levels and they do not necessarily have high protection levels, so these defences need to be built (e.g., Dar Es Salam and Lagos). Blue shading shows permanent inundation surfaces predicted by coastal digital elevation model (DEM) and Shuttle Radar Topography Mission (SRTM) given the 95th percentile K14/RCP2.6, RCP4.5 and RCP8.5, for present day, 2050 and 2100 sea level projection for permanent inundation (inundation without a storm surge event) and RL10 (10-year return level storm) (Kulp and Strauss, 2019). Low-lying areas isolated from the ocean are removed from the inundation surface using connected components analysis. Current water bodies are derived from the SRTM water body dataset. Orange areas represent the extent of coastal human settlements in 2014 (Corbane et al., 2018). See Figure CCP4.7 for projections including subsidence and worst-case scenario projections for 2100. {Figure 9.29}

https://doi.org/10.1017/9781009325844.028

Selected regions at risk of potential sea level rise

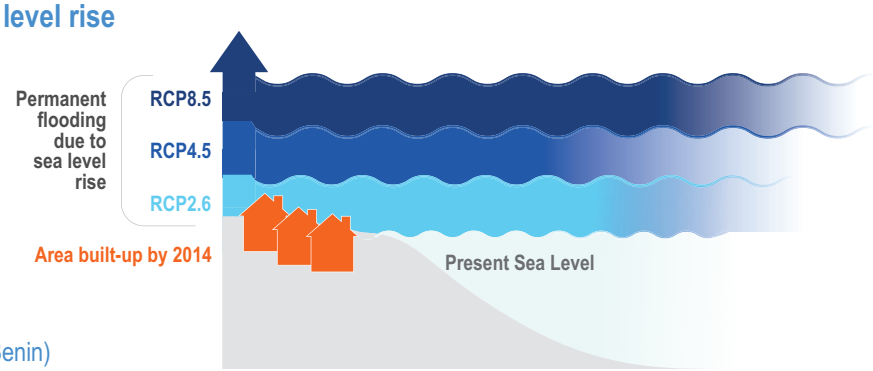

(b) Lagos (Nigeria) and Cotonou and Porto-Novo (Benin)

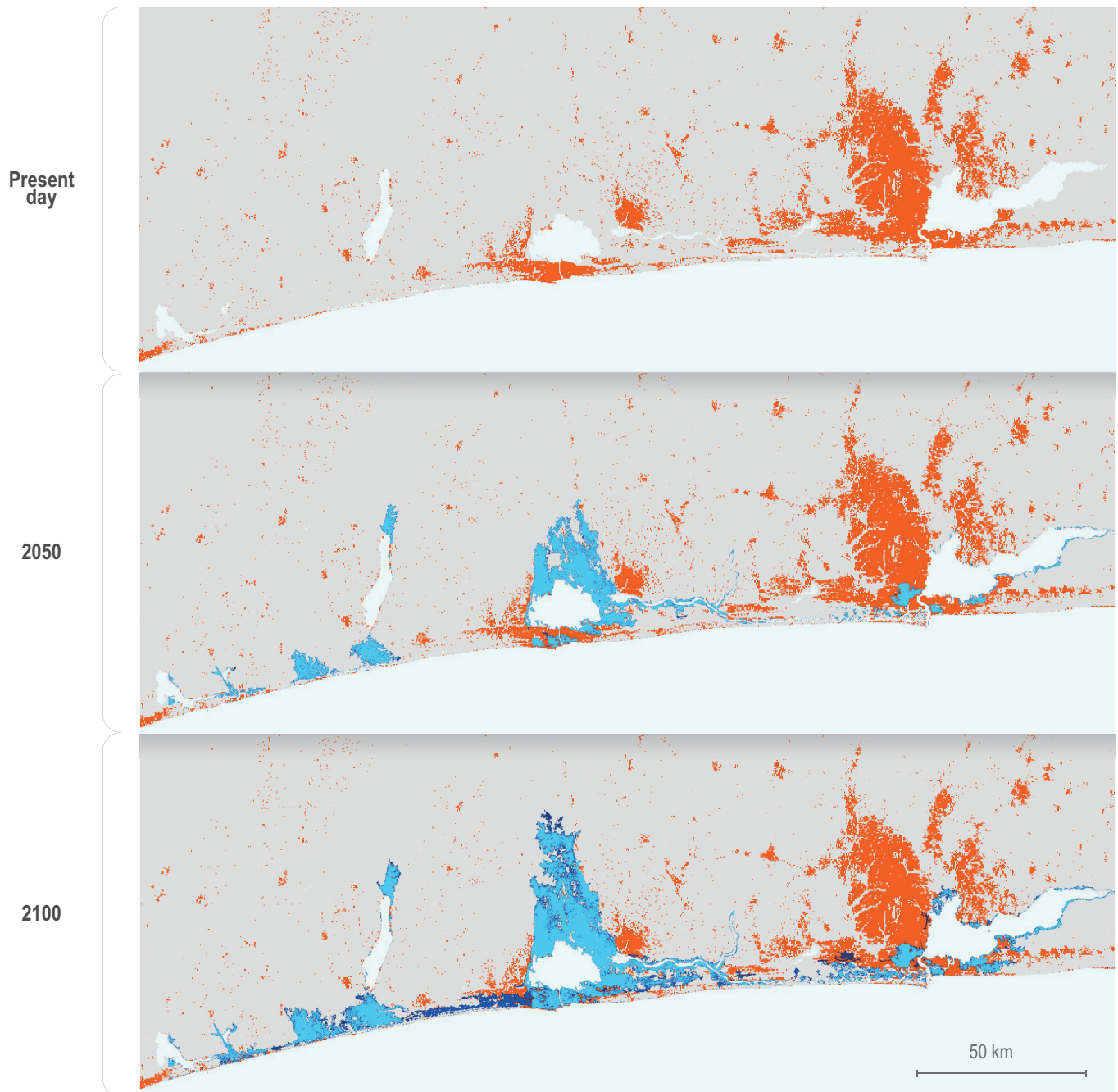

Selected regions at risk of potential sea level rise

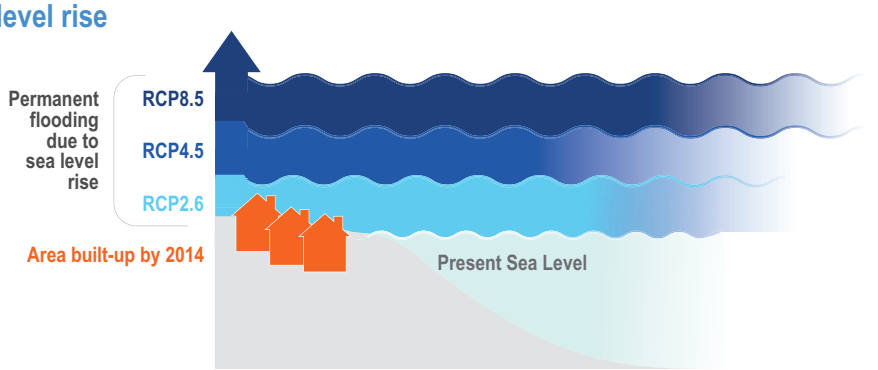

(c) Cairo and Alexandria (Egypt)

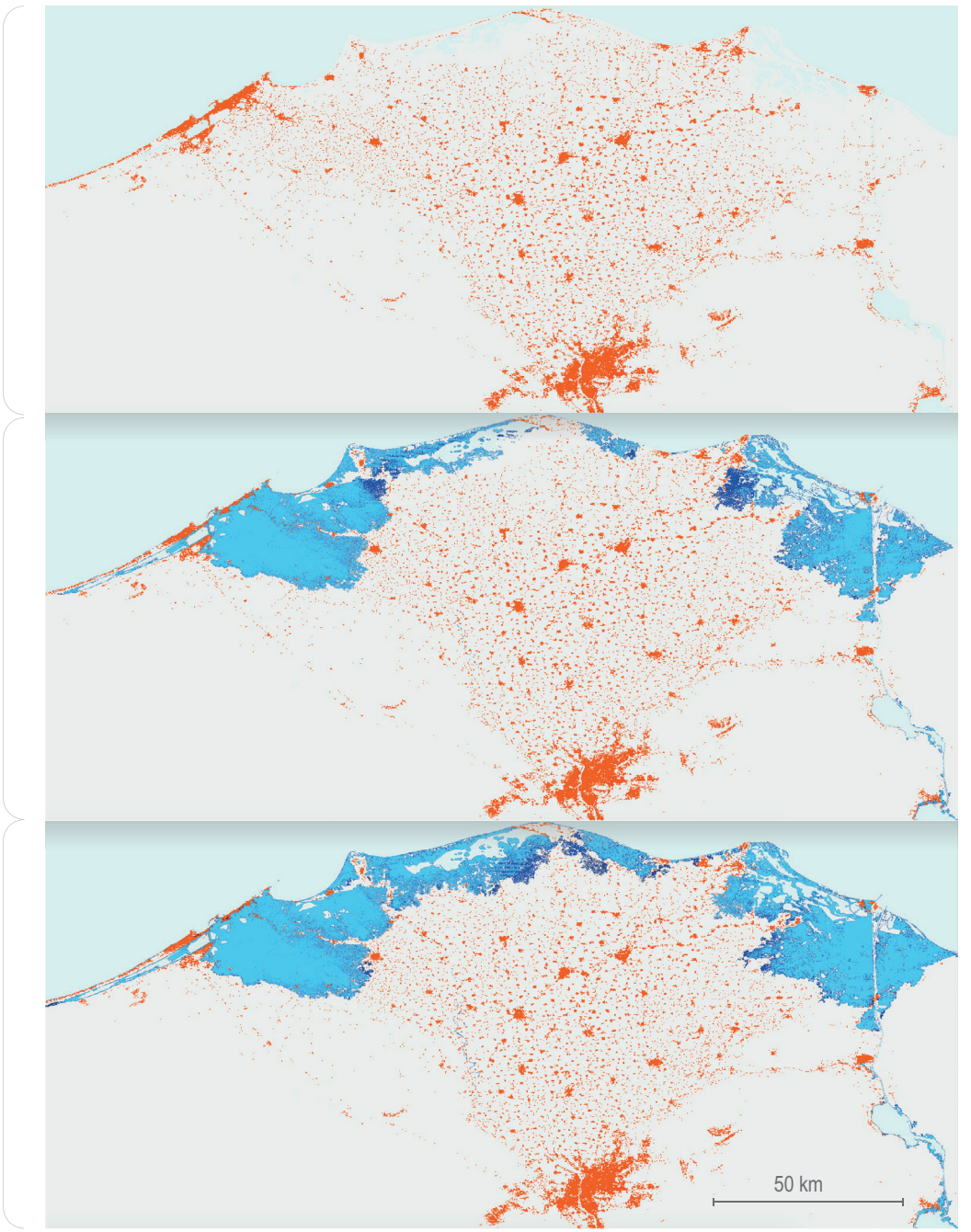

Risk of historical and projected river flooding

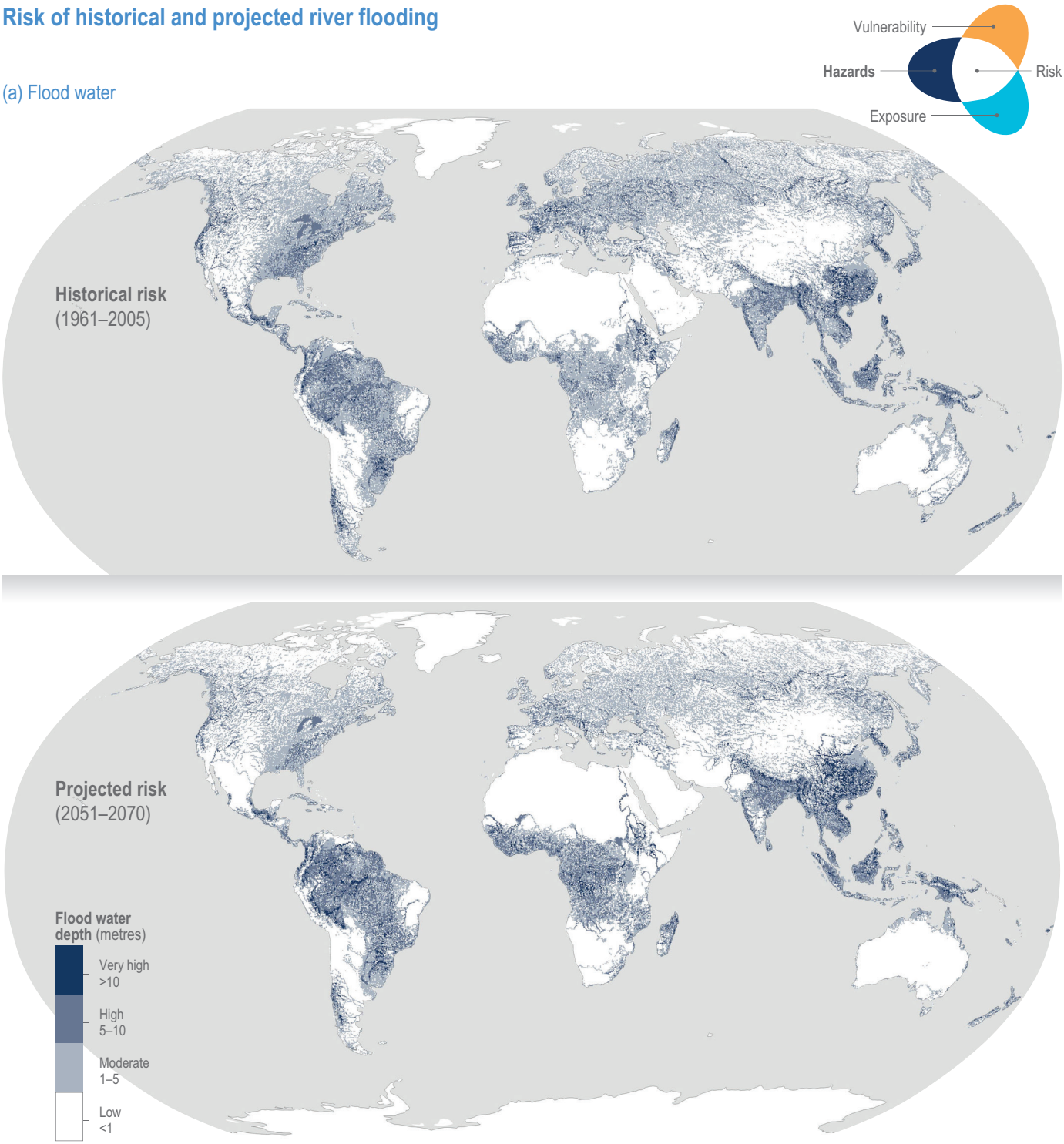

Figure AI.44a | Risk of historical and projected river flooding.

(a) Hazard. Modelled mean global fluvial flood water depth (Tanoue et al., 2016, 2021) based on a land surface model and a river and inundation model driven by reanalysis climate forcing of 5 Coupled Model Intercomparison Project 5 (CMIP5) global climatic models (GCMs). The annual maximum daily river water was allocated along elevations, and inundation depth was calculated for each year and averaged for the target period. {Figure 4.8}

Risk of historical and projected river flooding

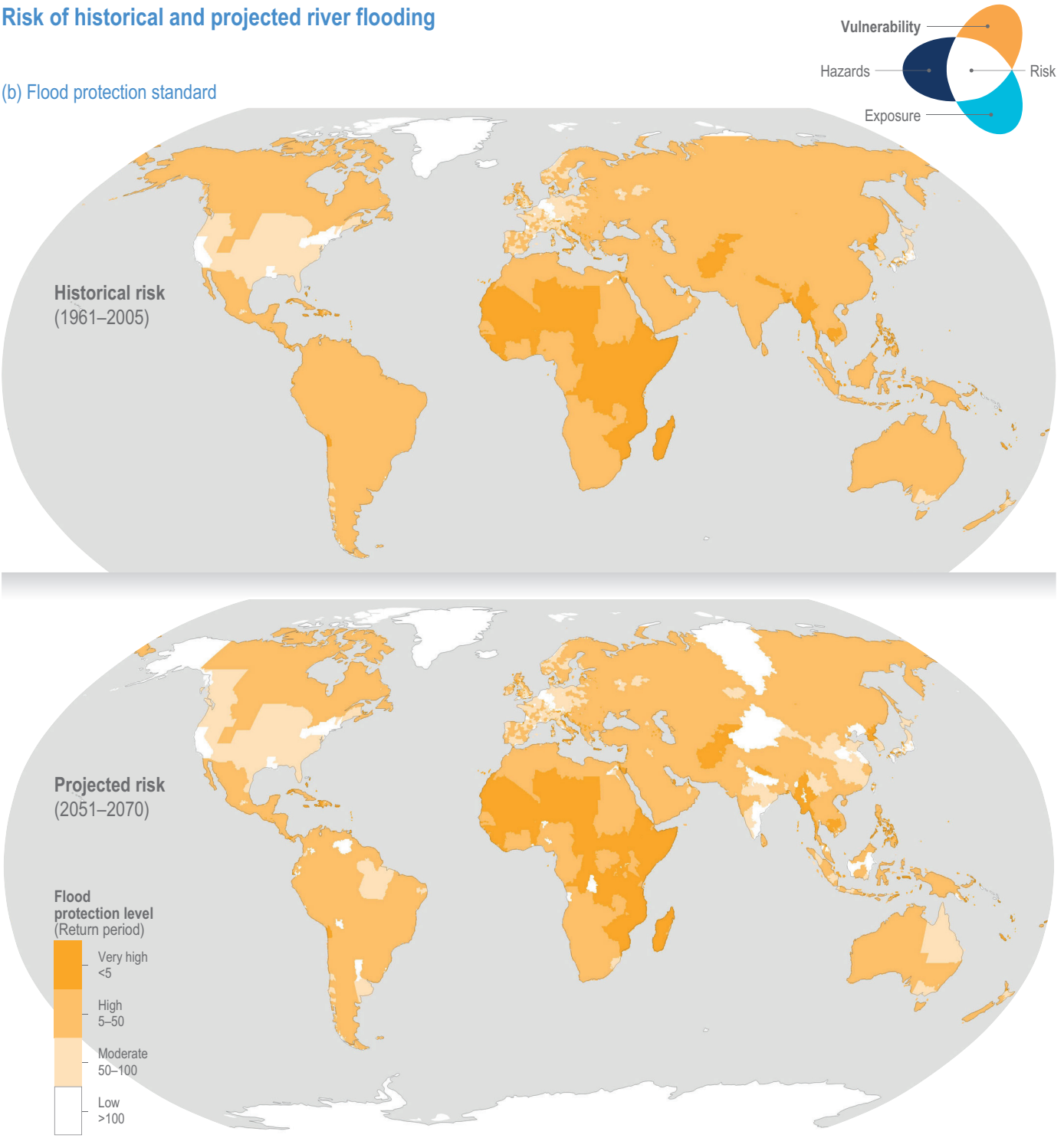

Figure AI.44b | Risk of historical and projected river flooding.

(b) Vulnerability. Local flood protection standard (return period) at sub-country scale (Scussolini et al., 2016) based on published reports and documents, websites and personal communications with experts. Note that the vulnerability of this map reflects local flood protection such as complex infrastructure and does not fully reflect the other source of vulnerabilities, including exposure. {Figure 4.8}

Risk of historical and projected river flooding

(c) Population distribution

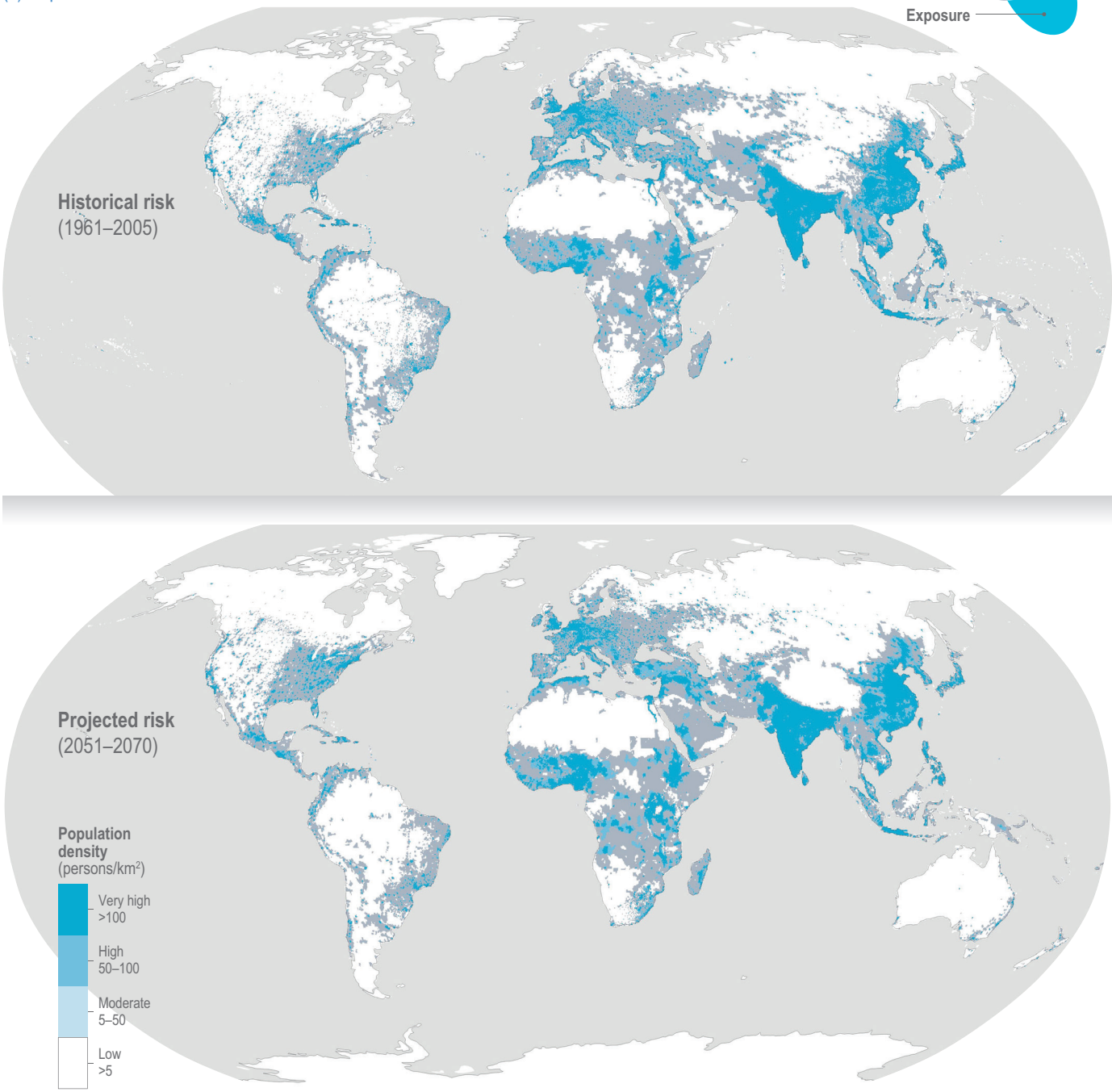

Figure AI.44c | Risk of historical and projected river flooding.

(c) Exposure. Population distribution per 30 arc second grid cell (Klein Goldewijk et al., 2010, 2011). {Figure 4.8}

Risk of historical and projected river flooding

(d) Population exposed to river flooding

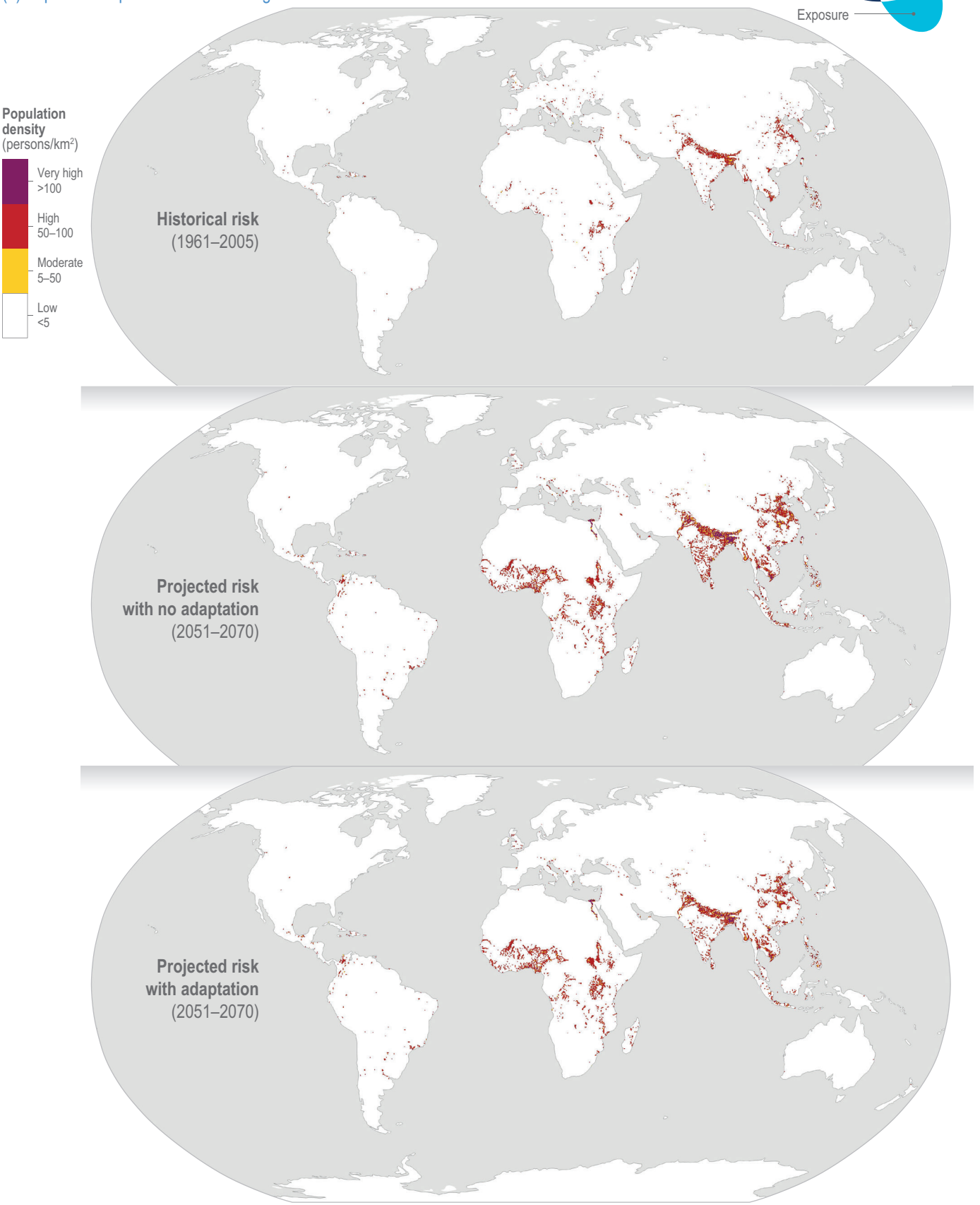

Figure AI.44d | Risk of historical and projected river flooding.

(d) Risk as population exposed to flood (number of people where inundation occurs) per 30 arc-second grid cell. Population under inundation depth >0 m as in panel **(a)** was counted when the return period of annual maximum daily river water exceeds the flood protection standard as in panel **(b)**. {Figure 4.8}

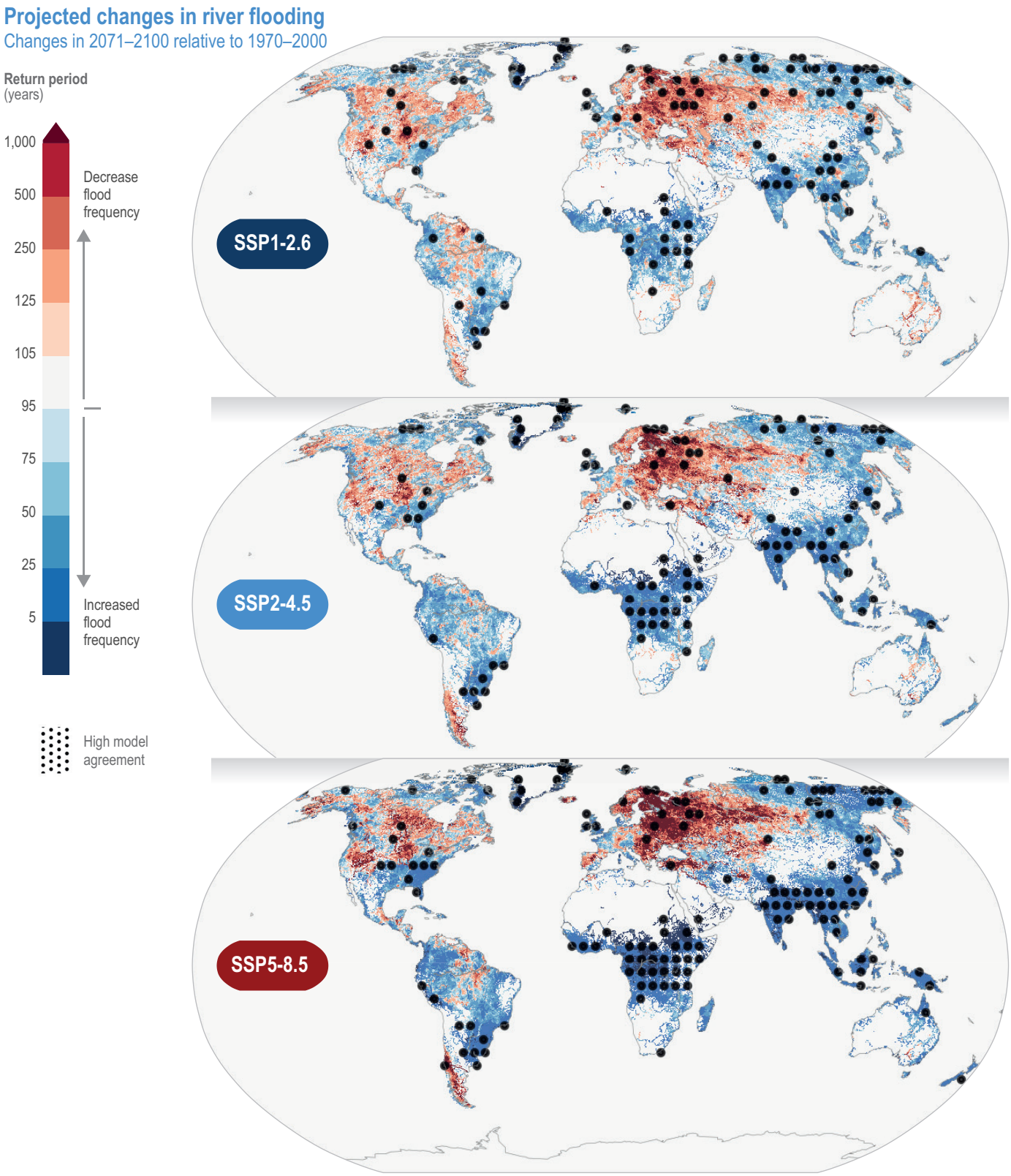

Figure AI.45a | Projected changes in river flooding. Multi-model median return period (years) for the 20th century 100-year river flood, based on a global river and inundation model, CaMa-Flood, driven by runoff output of 9 Coupled Model Intercomparison Project 6 (CMIP6) Models in the SSP1-2.6, SSP2-4.5 and SSP5-8.5 scenarios. All changes are estimated in 2071–2100 relative to 1970–2000. A dot indicates regions with high model consistency (more than 7 models out of 9 show the same direction of change). {Figure 4.17}

https://doi.org/10.1017/9781009325844.028

Projected changes in river flooding

Global and regional potential exposure of the population

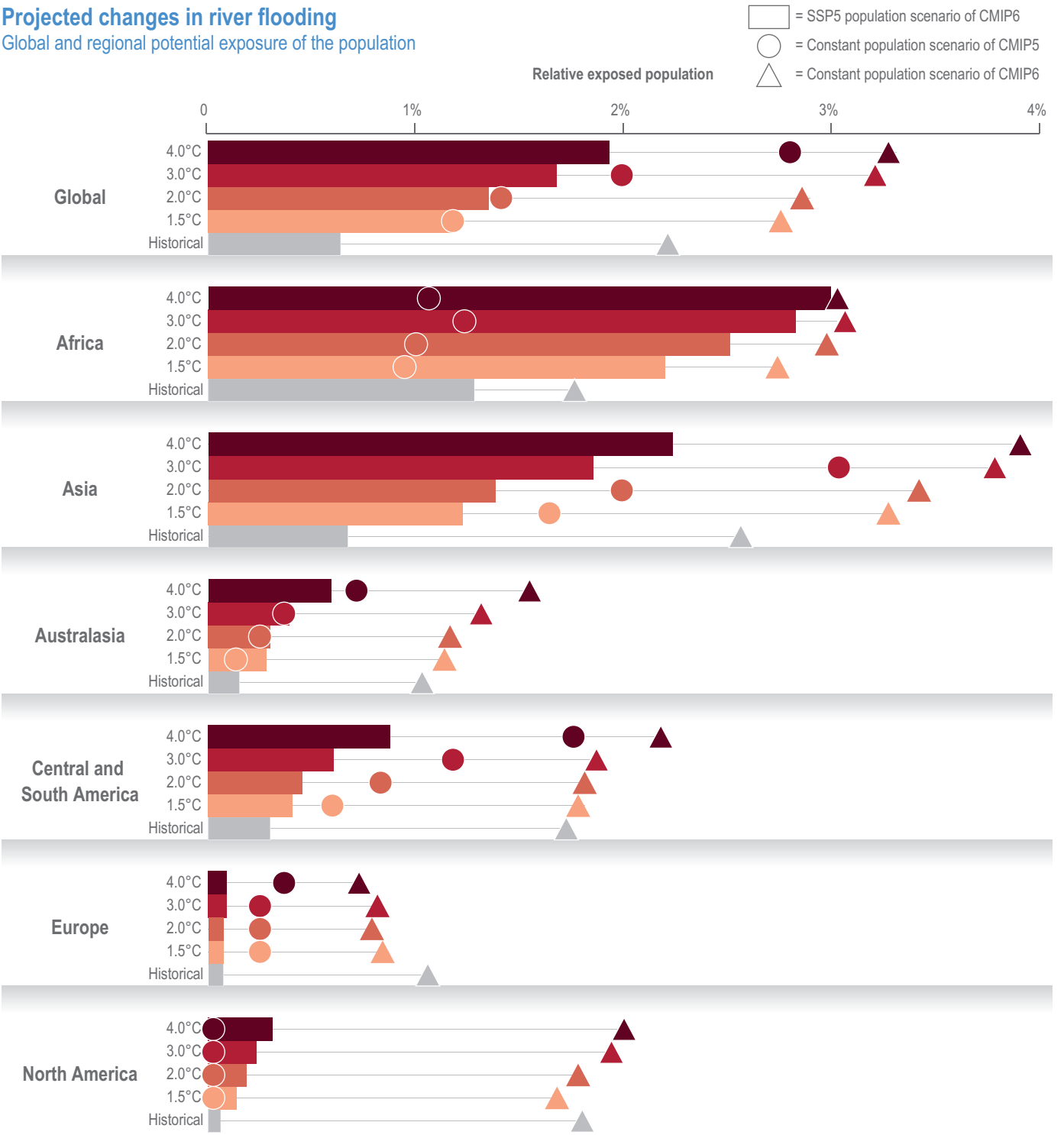

Figure AI.45b | Projected changes in river flooding. Global or regional potential exposure (% of the total population affected by flooding) under different warming levels with constant population scenario of CMIP5 (Alfieri et al., 2017) and with population scenario of SSP5 of CMIP6 (Hirabayashi et al., 2021b). Inundation is calculated when the magnitude of flood exceeds current flood protection (Scussolini et al., 2016). Note that number of GCMs used to calculate global warming level of 4.0°C is less than that for other global warming levels, as the global mean temperature of some GCMs did not exceed 4°C. {Figure 4.17}

https://doi.org/10.1017/9781009325844.028

AI.2.3 Global to Regional Risks (Including Economic) and Adaptive Capacities

Burning ember diagrams of regional and global risk assessments

https://doi.org/10.1017/9781009325844.028

https://doi.org/10.1017/9781009325844.028

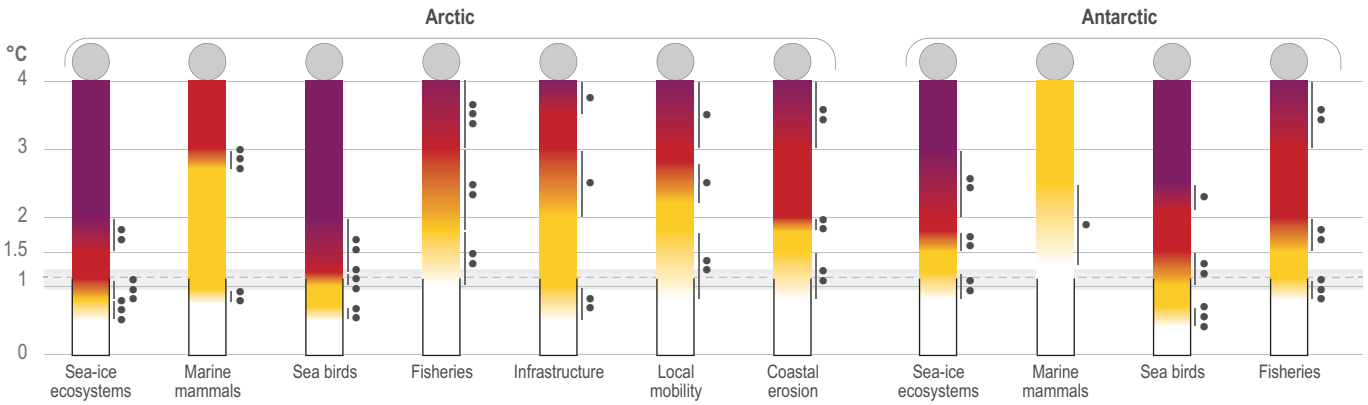

(d) Ecosystem risk assessments

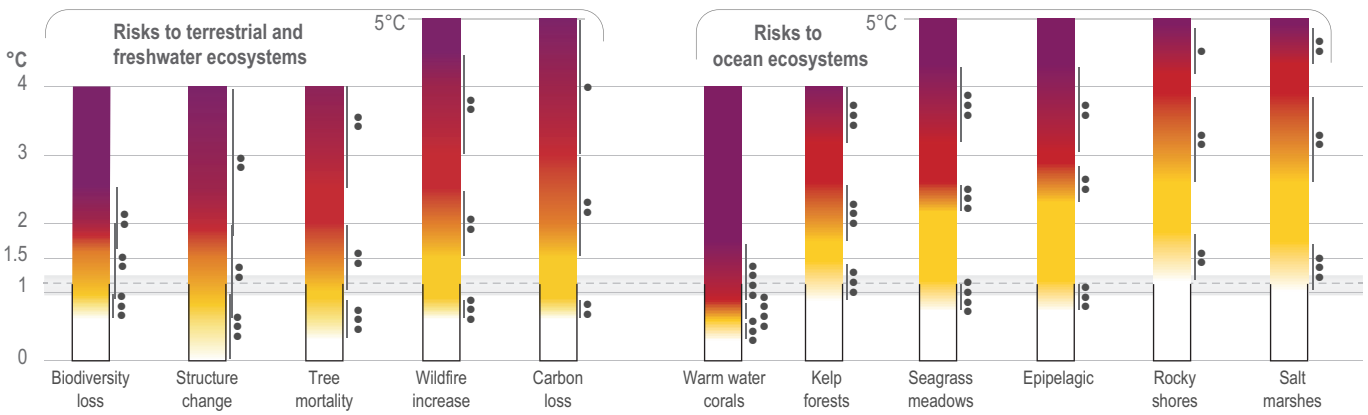

(e) Climate sensitive health outcomes under three adaptation scenarios

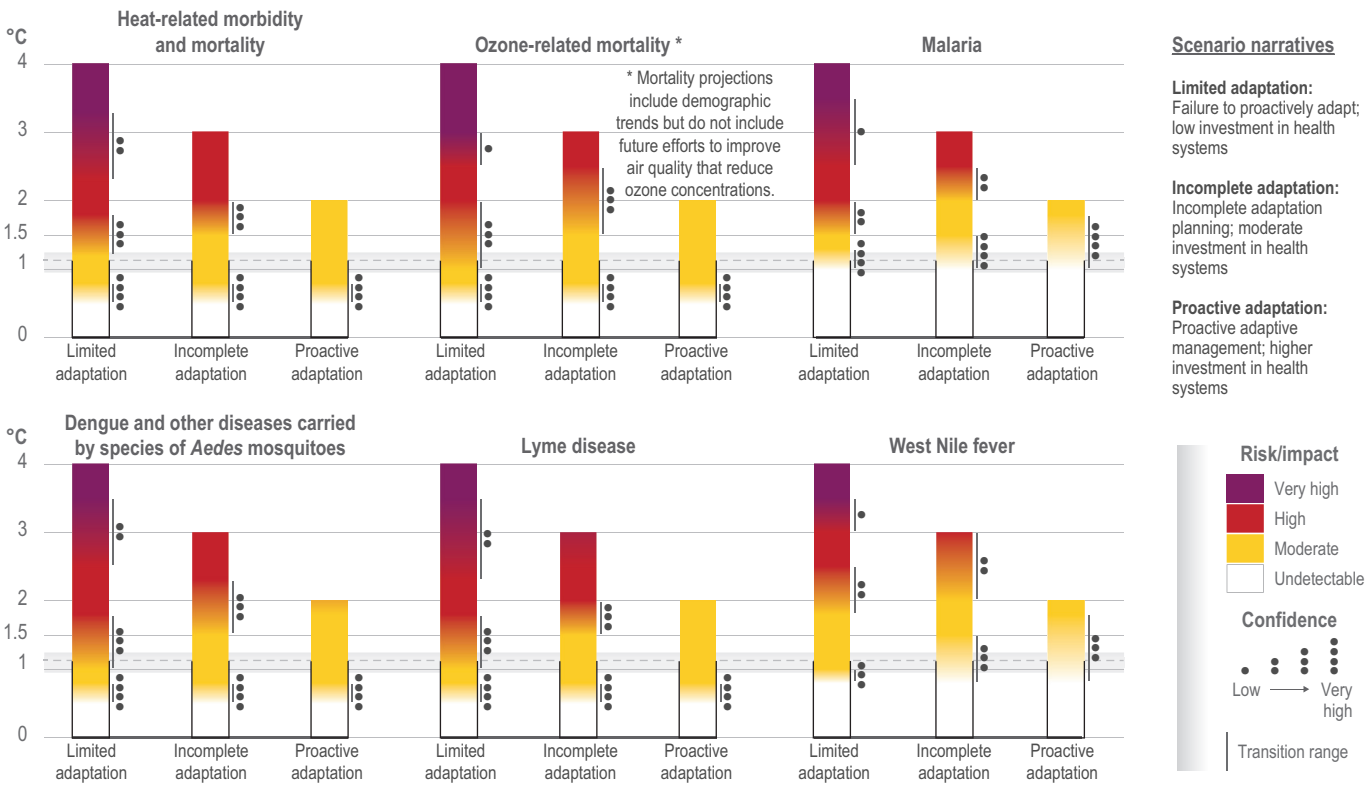

Figure AI.46 | Burning ember diagrams of regional and global risk assessments. {Reasons for concern (RFC): Sections 16.6.3.1–16.6.3.5; 16.6.4; Table SM16.18; SM16.6. Africa: 9.2; Table 9.2; Table SM 9.1. Australia and New Zealand/ Australia: Table 11.14; SM 11.2. Mediterranean: CCP4.3.2–8; SMCCP4.2. Europe: 13.10.2; 13.10.2.1–13.10.2.4; SM13.10. North America: 14.6.2; 14.6.3; Table 14.3, SM14.4. Arctic: CCP6.3.1; Table CCP6.5; SMCCP6.6. Ecosystems: Table 2.5; Table 2.S. 4 Ocean: IPCC (2019). Health: 7.3.1; Ebi et al. (2021).}

AI

AI.2.4 From Adaptation to Climate Resilient Development

Evidence of transformative adaptation by sector and region

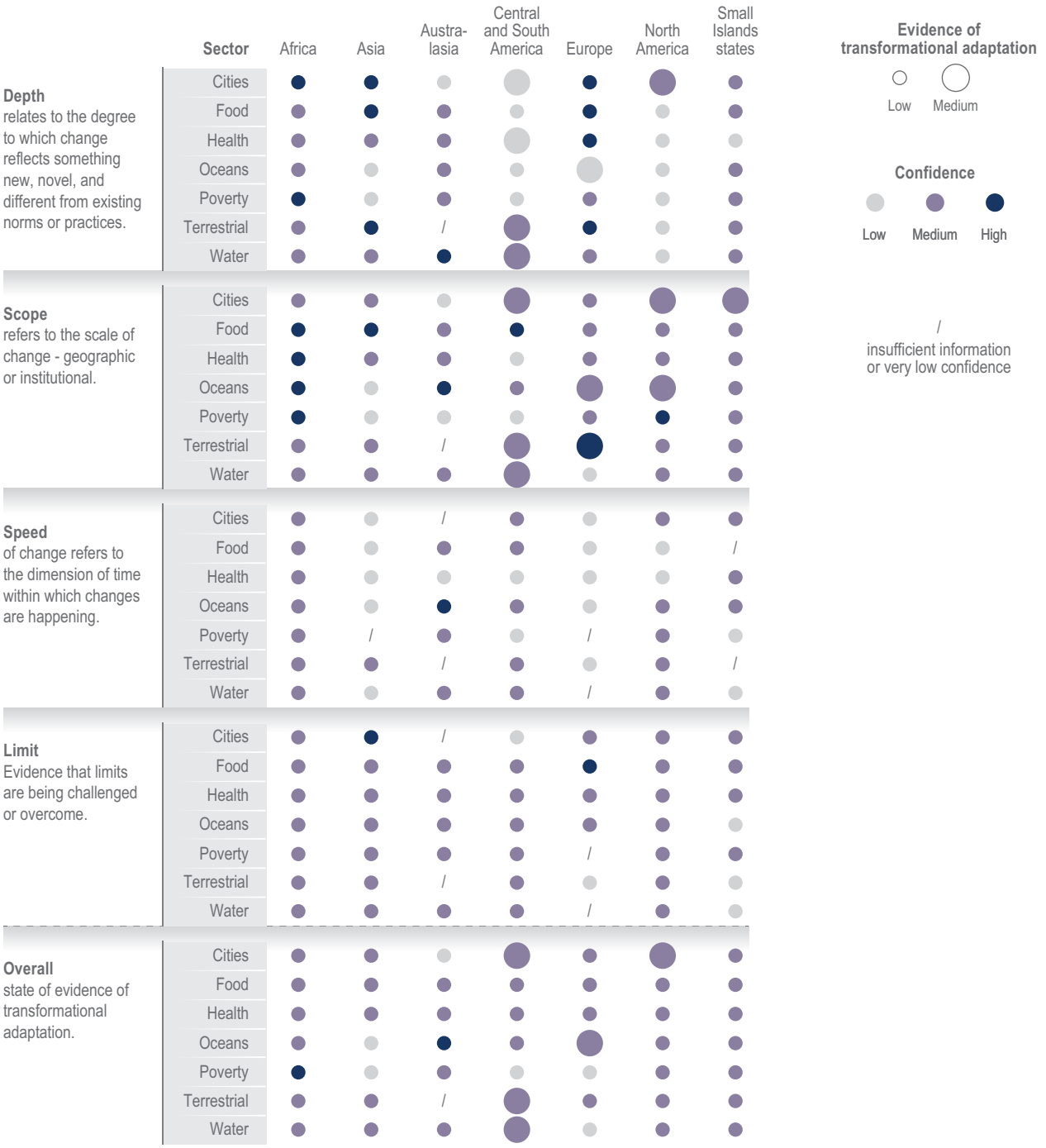

Figure AI.47 | Evidence of transformative adaptation by sector and region. Evidence of transformative adaptation is assessed based on the scope, speed, depth and ability to challenge limits of responses reported in the scientific literature Studies relevant to multiple regions or sectors are included in assessment for each relevant sector/region. Evidence of transformational adaptation does not imply effectiveness, equity or adequacy. {16.3.2; Figure 16.6}

Drought is exacerbating water management challenges which vary across regions with respect to anticipated water scarcity conditions by 2050

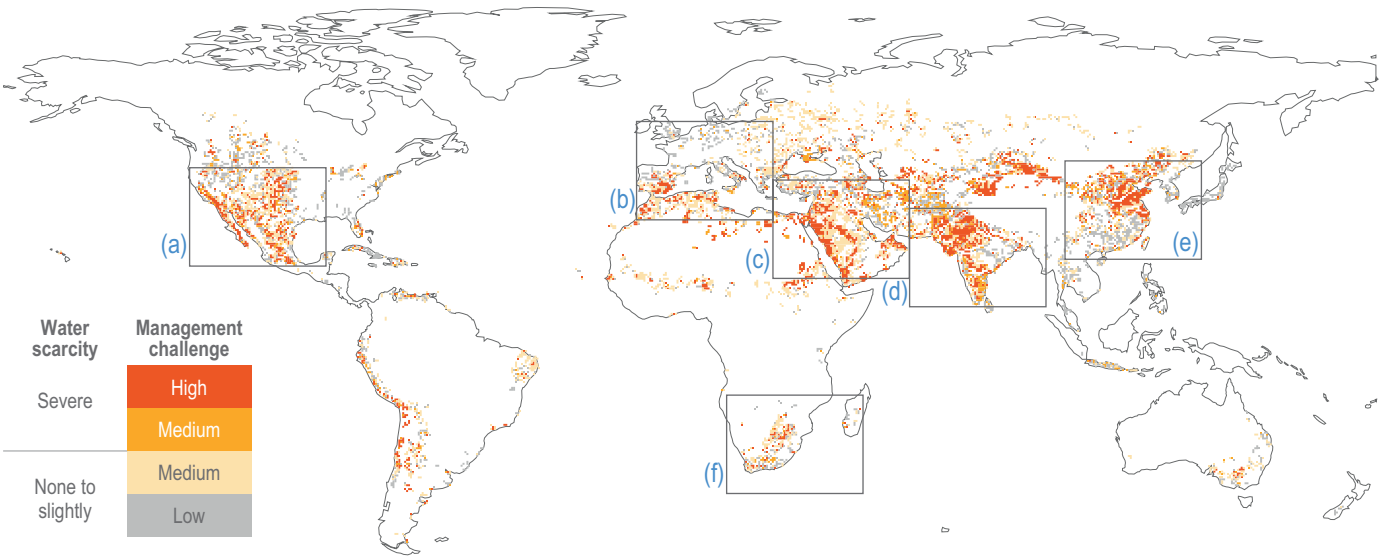

Zoomed-in map segments of six most affected regions of differing management chal- lenges with respect to anticipated water scarcity conditions by 2050.

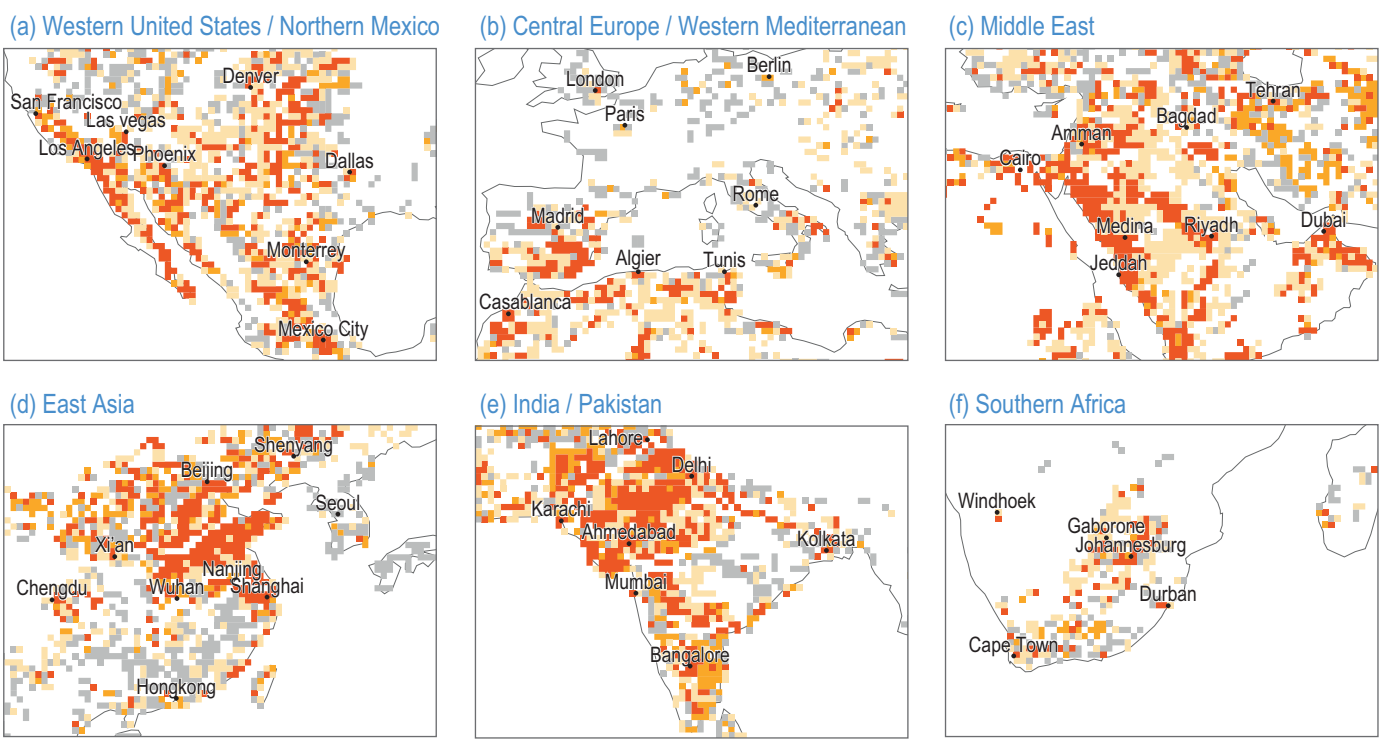

Figure AI.48 | Drought is exacerbating water management challenges which vary across regions with respect to anticipated water scarcity conditions by 2050. Local levels of policy challenges for addressing water scarcity by 2050, considering both the central estimate (median) and the changing uncertainty in projections of the Water Scarcity Index (WSI) from the present day to 2050. Projections used five Coupled Model Intercomparison Project 5 (CMIP5) climate models, three global hydrological models from the Inter-Sectoral Impact Model Intercomparison Project (ISIMIP), and three Shared Socioeconomic Pathways (SSPs). Reproduced from Greve et al. (2018). {Figure Box 4.1.1; Box 4.1}

https://doi.org/10.1017/9781009325844.028

AI

Observed water-related adaptation responses with positive outcomes

(a) Map depicting 319 case studies of current water related adaptation responses with documented beneficial outcomes of adaptation

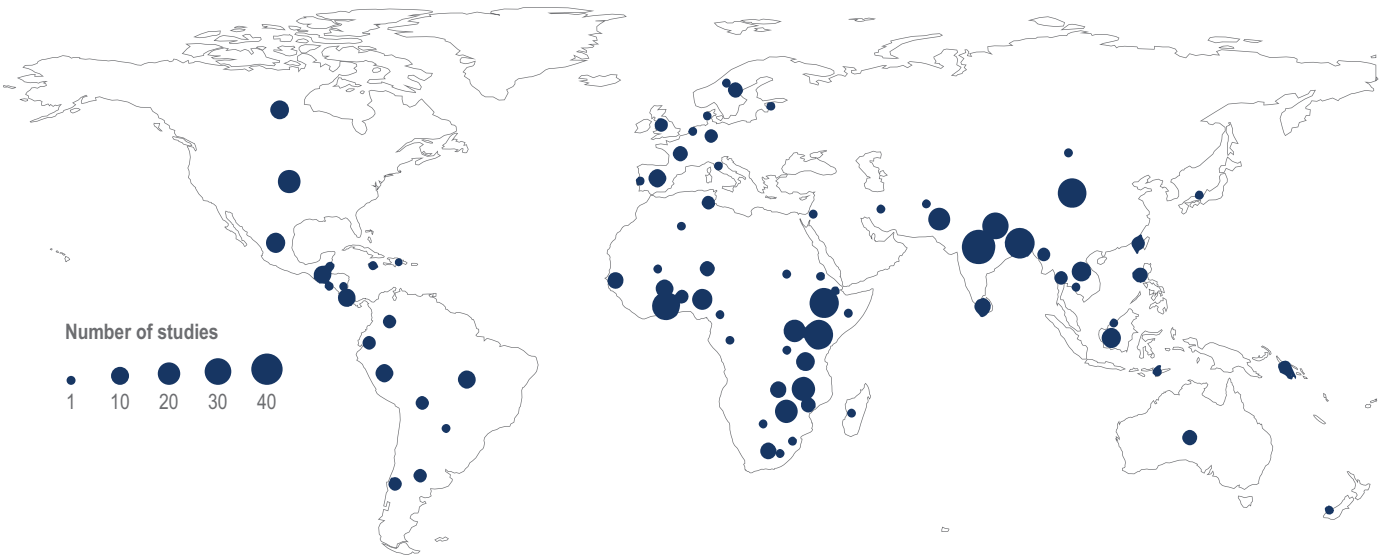

(b) Fraction of top six adaptation responses to total responses

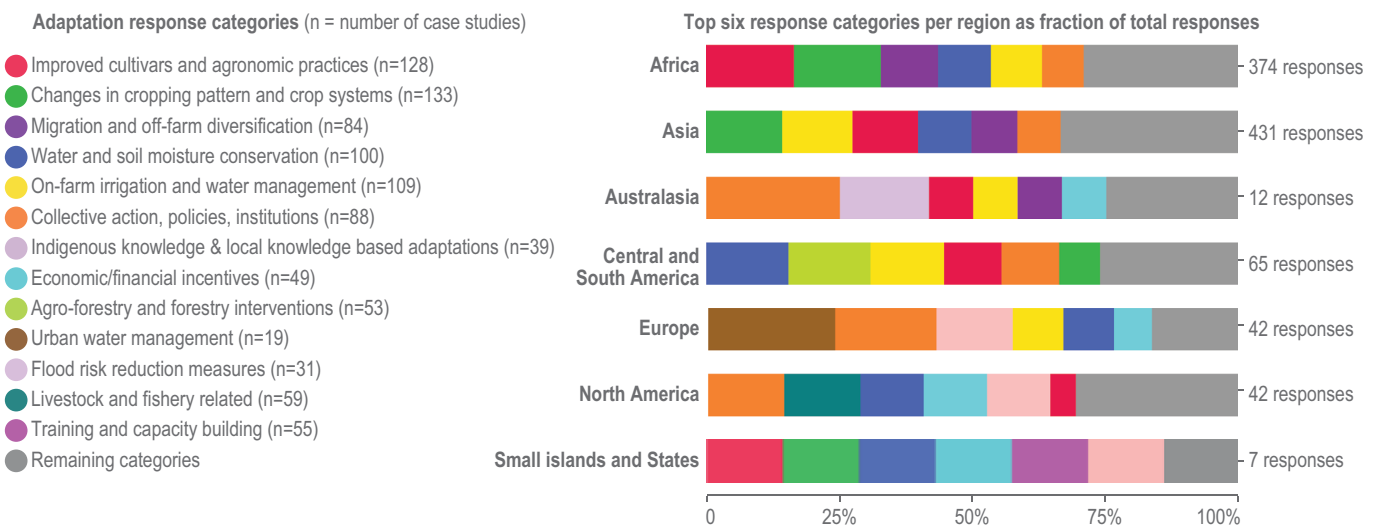

(c) Beneficial outcomes of adaptation per region across five dimensions. Innerlines correspond to the top six adaptation response categories from previous panel.

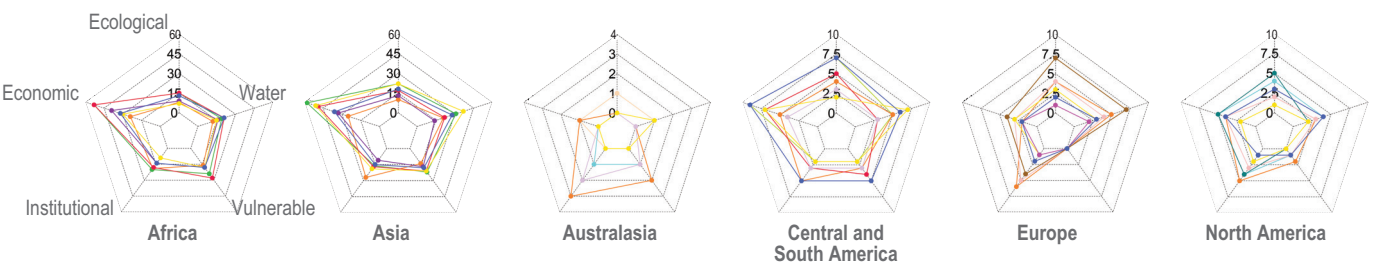

Figure AI.49 | Observed water-related adaptation responses with positive outcomes.

(a) Location of case studies of water-related adaptation responses (996 data points from 319 studies). In these 996 data points, at least one positive outcome was recorded in one of the five outcome indicators. These outcome indicators are economic/financial, outcomes for vulnerable people, ecological/environmental, water-related, and socio-cultural and institutional.

(b) In most instances, the top six adaptation categories include nearly 75% of the studies.

(c) Due to a small number of studies in Small Island States, a spider diagram was not generated. {Figure 4.27}

https://doi.org/10.1017/9781009325844.028

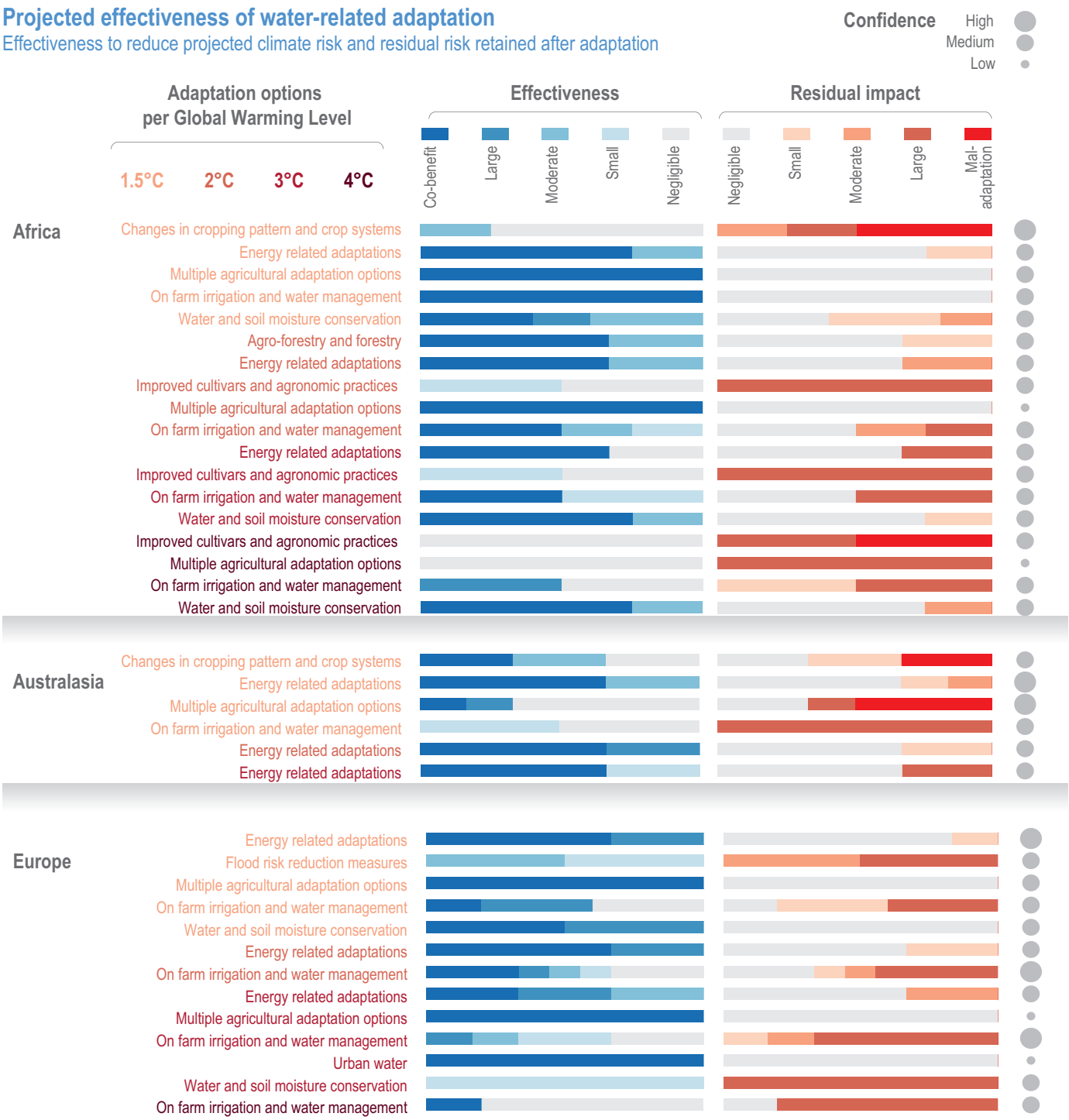

Figure AI.50a | Projected effectiveness of water-related adaptation options. Effectiveness in returning the system to a study-specific baseline state relative to the projected climate impact; and level of residual risk retained after adaptation, relative to baseline conditions. Regional summaries are based on sIPCC regions. Warming levels refer to the global mean temperature (GMT) increase relative to a 1850–1900 baseline. For each data point, the study-specific GMT increase was calculated to show effectiveness at 1.5°C, 2°C, 3°C and 4°C. Based on the ability of an implemented option to return the system to its baseline state, the effectiveness is classified based on the share of risk the option can reduce: large (>80%); moderate (80–50%); small (<50–30%); insufficient (<30%). Where the system state is improved relative to baseline, co-benefits are identified. Residual impacts show the share of remaining impacts after adaptation has been implemented: negligible (<5%); small (5 to <20%); moderate (20 to <50); large (≥50%). Where risks increase after adaptation, data points are shown as maladaptation. All underlying data are provided in SM4.8. {Figure 4.28}

https://doi.org/10.1017/9781009325844.028

Projected effectiveness of water-related adaptation

Effectiveness to reduce projected climate risk and residual risk retained after adaptation

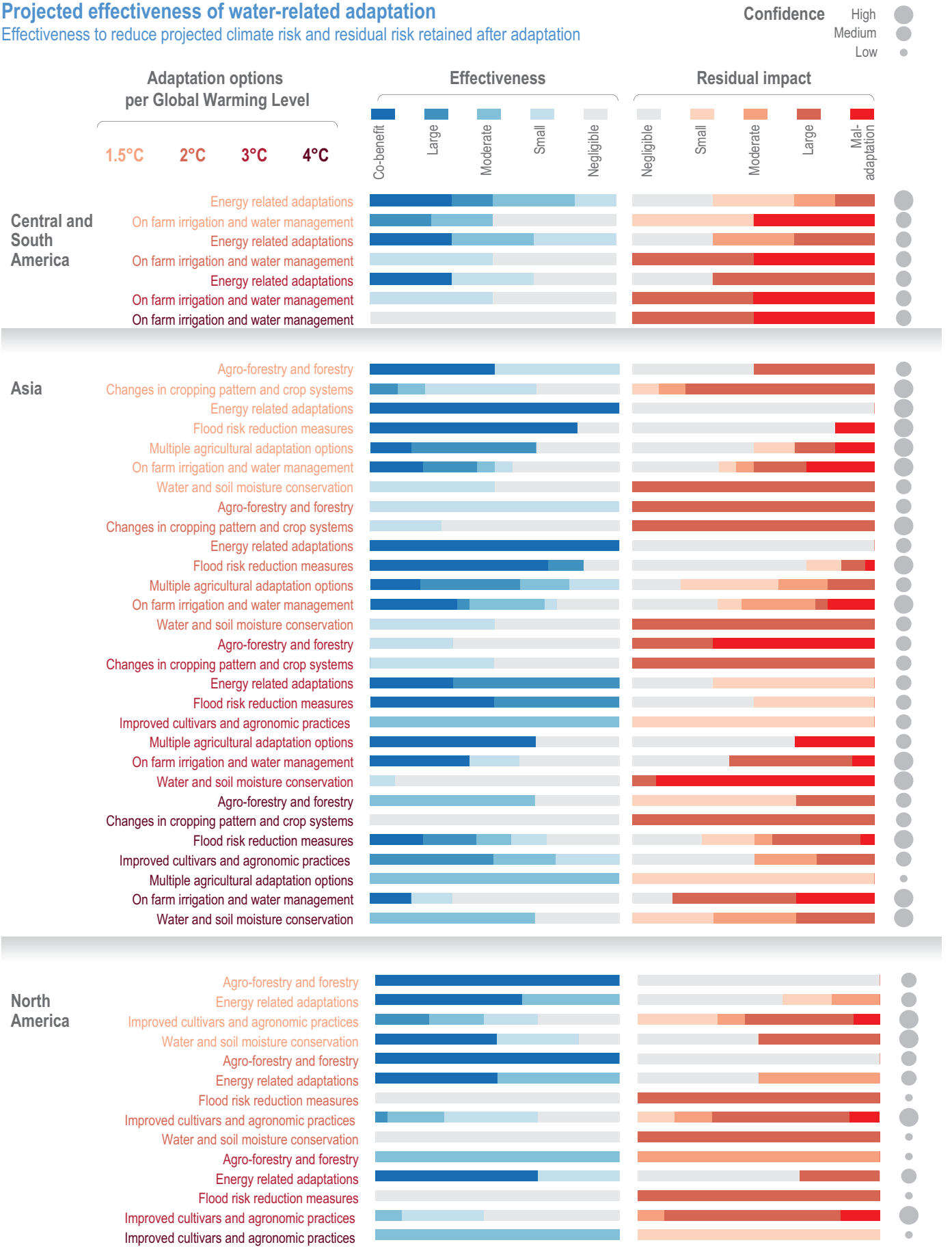

Figure AI.50b | Projected effectiveness of water-related adaptation options.

https://doi.org/10.1017/9781009325844.028

Projected effectiveness of water-related adaptation

Effectiveness to reduce projected climate risk and residual risk retained after adaptation

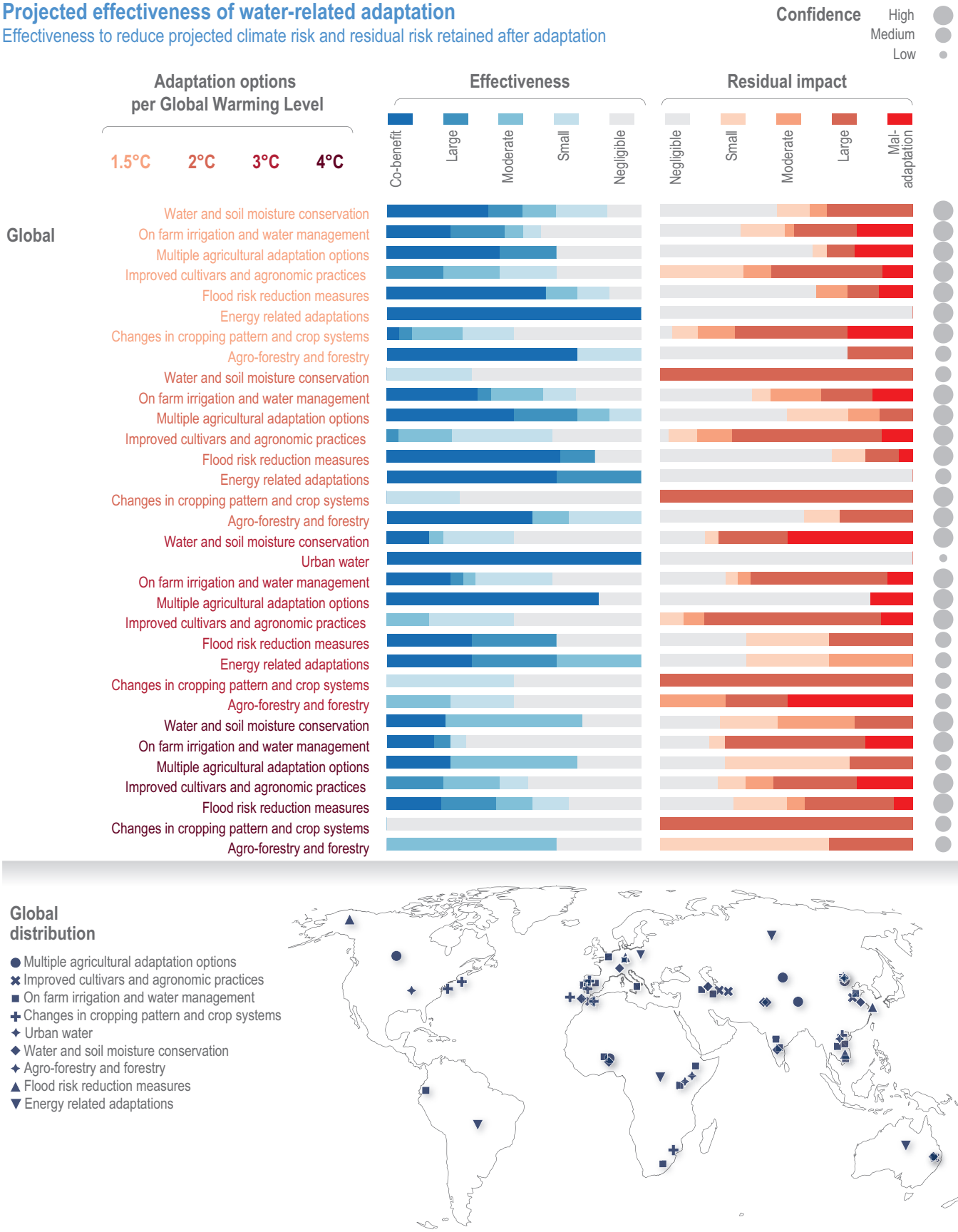

Figure AI.50c | Projected effectiveness of water-related adaptation options.

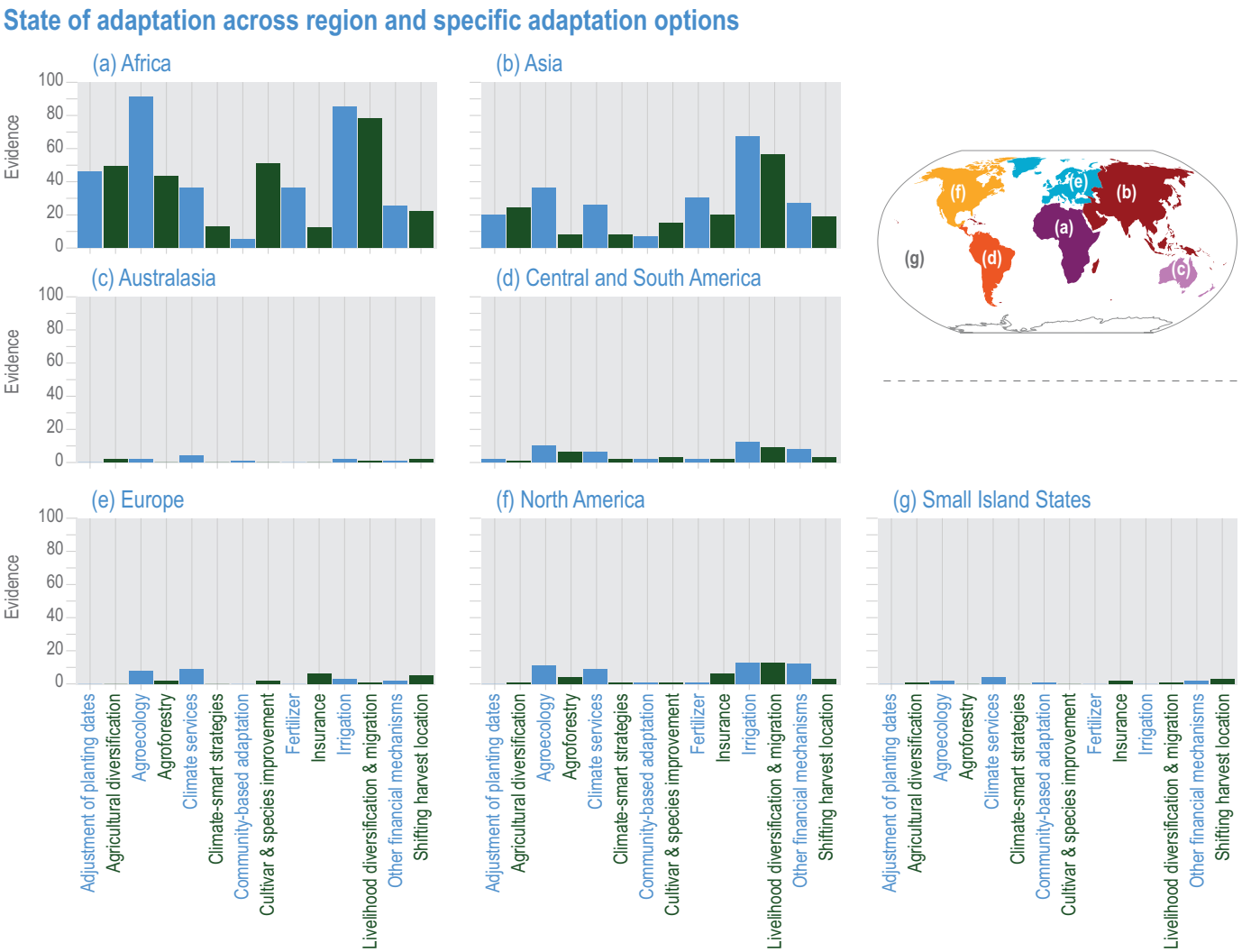

Figure AI.51 | Evidence of observed adaptation across regions in food, fibre and other ecosystem products. Observed adaptation options across regions in food, fibre, and other ecosystem products based on Global Adaptation Mapping Initiative (GAMI) database (Berrang-Ford et al., 2021a). The bars indicate the amount of evidence for the options per region. {Figure 5.20}

https://doi.org/10.1017/9781009325844.028

Who is responding, by geographic region and sector?

(a) Number of publications reporting engagement of each actor in adaptation-related responses during the period (2013–2019)

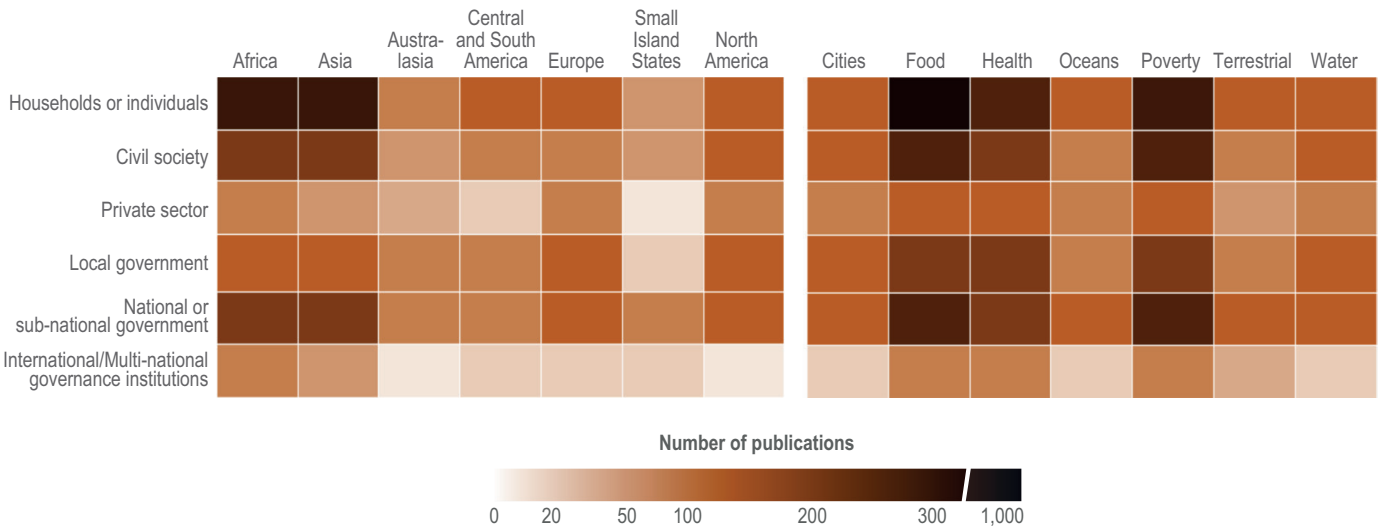

(b) Type of adaptation responses by global region

Percentages reflect the number of articles mentioning each type of adaptation over the total number of articles for that region

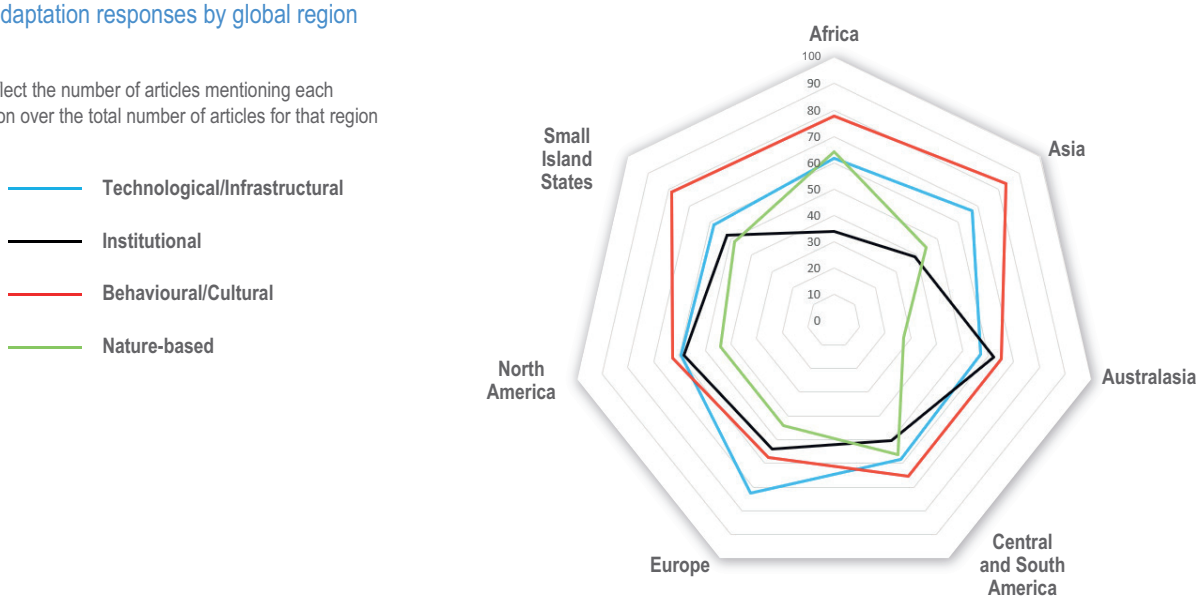

Figure AI.52 | Who is responding, by geographic region and sector?

(a) Cell contents indicate the number of publications reporting engagement of each actor in adaptation-related responses. Darker colours denote a high number of publications.

(b) Percentages reflect the number of articles mentioning each type of adaptation over the total number of articles for that region. Radar values do not total 100% per region since publications frequently report multiple types of adaptation; for example, construction of drainage systems (infrastructural), changing food storage practices by households (behavioural) and planting of tree cover in flood prone areas (nature-based) in response to flood risk to agricultural crops. Data updated and adapted from Berrang-Ford et al. (2021b), based on 1682 scientific publications reporting on adaptation-related responses in human systems. {Figure 16.4; Figure 16.5}

The urban adaptation gap to current climate risks: inequality in all world regions

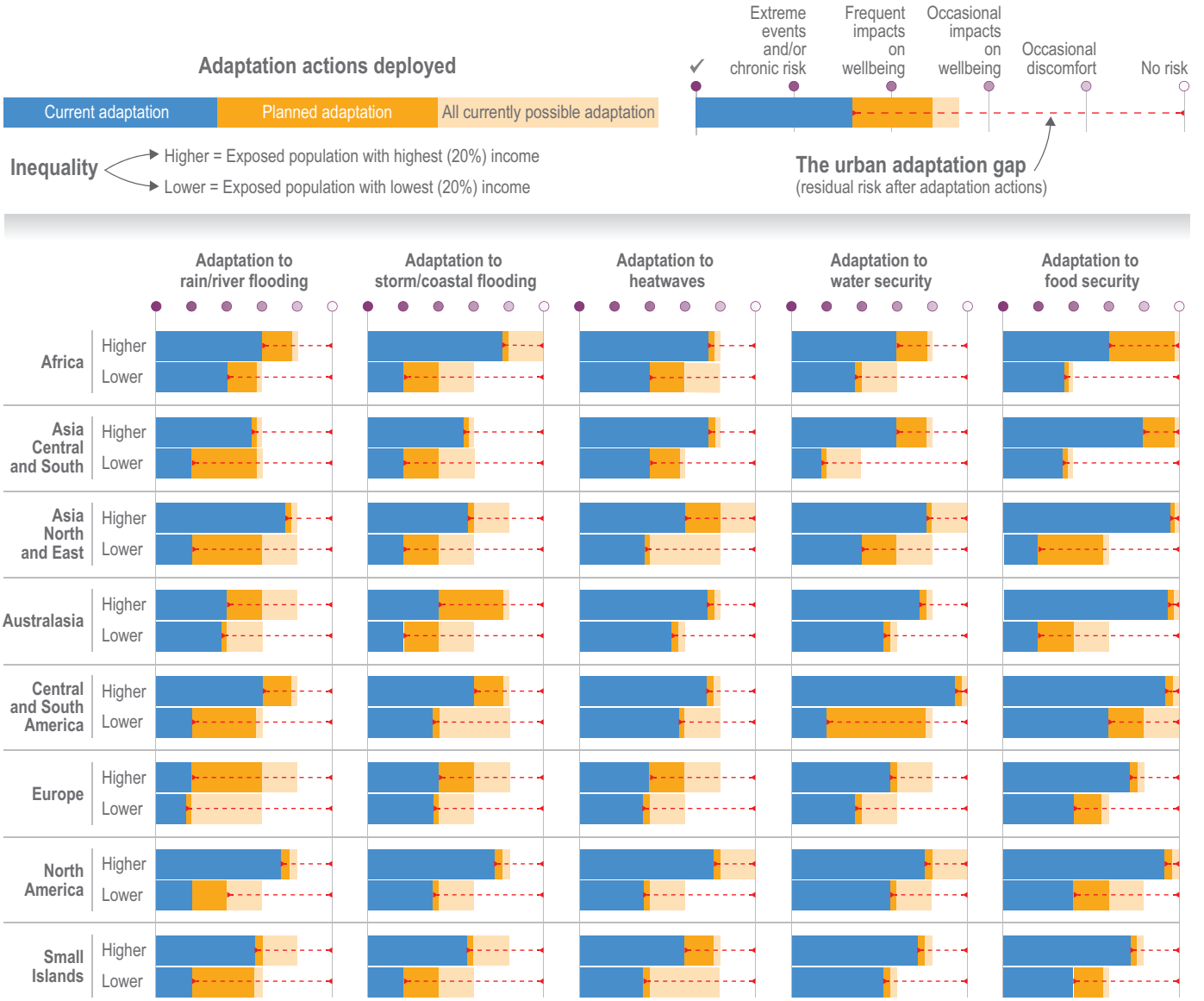

Figure AI.53 | The urban adaptation gap. This is a qualitative assessment presenting individual, non-comparative data for world regions from 25 AR6 Contributing Lead Authors and Lead Authors, the majority from regional chapters. Respondents were asked to make expert summary statements based on the data included within their chapters and across the AR6 report augmented by their expert knowledge. Multiple iterations allowed opportunity for individual and group judgement. Urban populations and risks are very diverse within regions making the presented results indicative only. Variability in data coverage leads to the overall analysis having *medium agreement*, *medium evidence*. Major trends identified in Section 6.3.1 at least meet this level of confidence. Analysis is presented for current observed climate change-associated hazards and for three adaptation scenarios: (1) current adaptation (based on current levels of risk management and climate adaptation), (2) planned adaptation (assessing the level of adaptation that could be realised if all national, city and neighbourhood plans and policies were fully enacted), (3) transformative adaptation (if all possible adaptation measures were to be enacted). Assessments were made for the lowest and highest quintile by income. Residual risk levels achieved for each income class under each adaptation scenario are indicated by five adaptation levels: no risk, occasional discomfort, occasional impacts on well-being, frequent impacts on well-being, extreme events and/or chronic risk. The urban adaptation gap is revealed when levels of achieved adaptation fall short of delivering 'no risk'. The graphic uses IPCC Regions and has split Asia into two regions: North and East Asia, and Central and South Asia. {Figure 6.4}

https://doi.org/10.1017/9781009325844.028

Evidence on constraints and limits to adaptation by region and sector

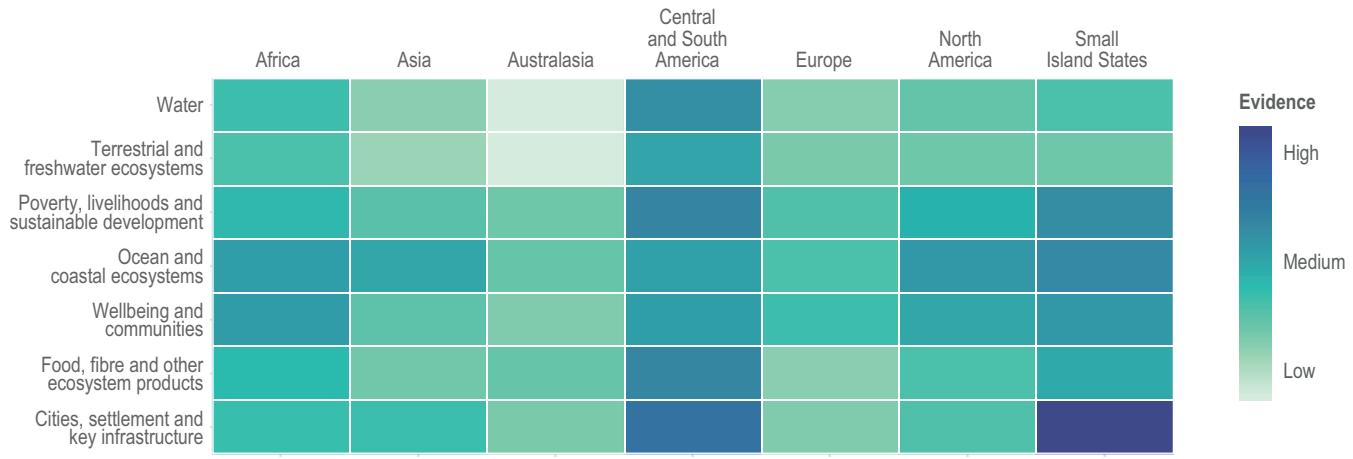

Figure AI.54 | Evidence on constraints and limits to adaptation by region and sector. Low evidence: <20% of assessed literature has information on limits, literature mostly focuses on constraints to adaptation; medium evidence: between 20% and 40% of assessed literature has information on limits, literature provides some evidence of constraints being linked to limits; High evidence: > 40% of assessed literature has information on limits, literature provides broad evidence of constraints being linked to limits. Data from Thomas et al. (2021), based on 1682 scientific publications reporting on adaptation-related responses in human systems. {Figure 16.7; 16.A.1}

https://doi.org/10.1017/9781009325844.028

Constraints to achieve adaptation to climate change by region and sector

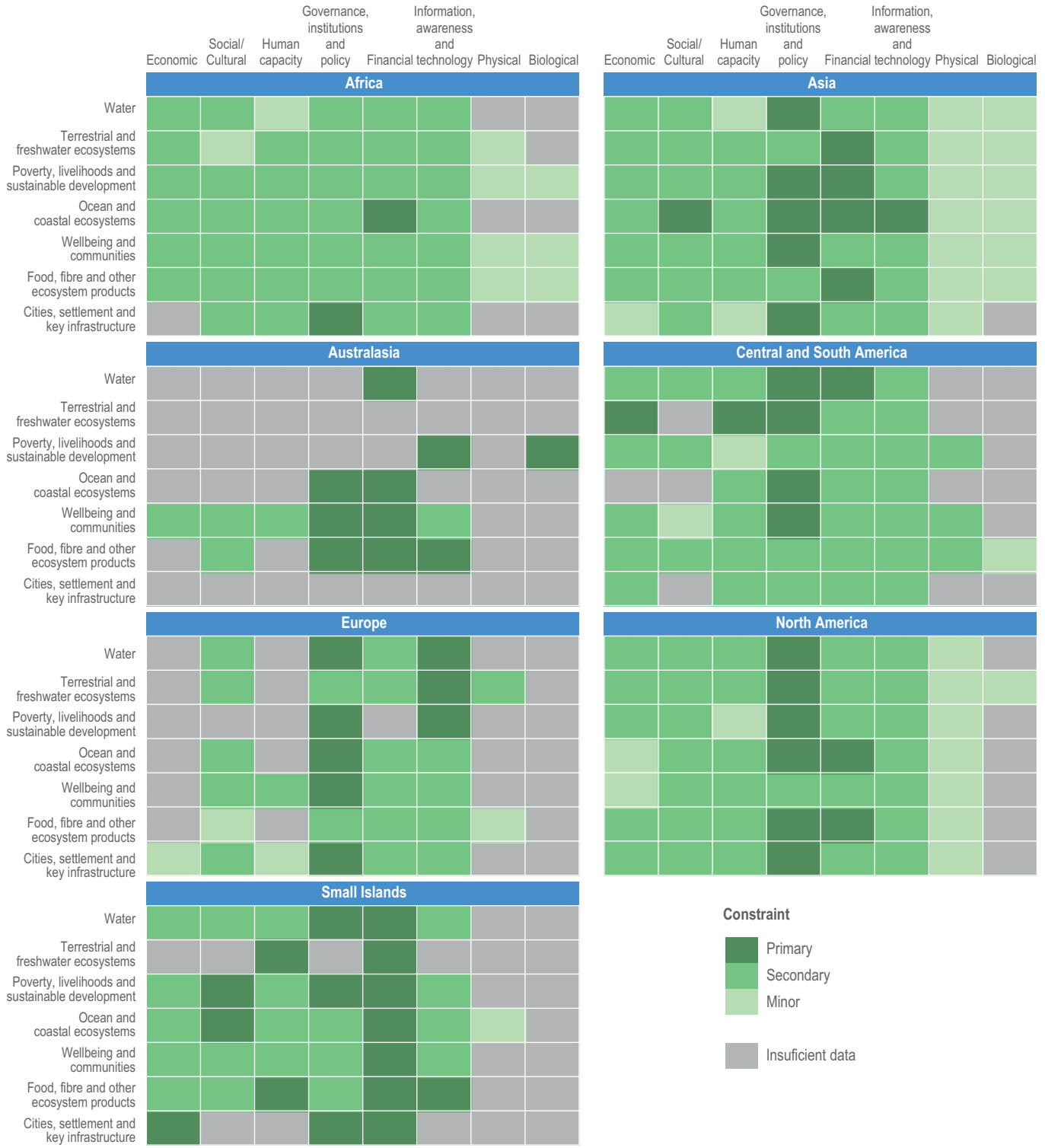

Figure AI.55 | "Constraints to achieve adaptation to climate change by region and sector. Constraints are categorised as: (1) Economic: existing livelihoods, economic structures and economic mobility; (2) Social/cultural: social norms, identity, place attachment, beliefs, worldviews, values, awareness, education, social justice and social support; (3) Human capacity: individual, organisational and societal capabilities to set and achieve adaptation objectives over time including training, education and skill development; (4) Governance, institutions and policy: existing laws, regulations, procedural requirements, governance scope, effectiveness, institutional arrangements, adaptive capacity and absorption capacity; (5) Financial: lack of financial resources; (6) Information/awareness/technology: lack of awareness or access to information or technology; (7) Physical: presence of physical barriers; and (8) Biologic/climatic: temperature, precipitation, salinity, acidity and intensity and frequency of extreme events including storms, drought and wind. Insufficient data: there is not enough literature to support an assessment (fewer than five studies available); Minor constraint: <20% of assessed literature identifies this constraint; secondary constraint: 20–50% of assessed literature identifies this constraint; primary constraint: >50% of assessed literature identifies this constraint. Data from Thomas et al. (2021), based on 1682 scientific publications reporting on adaptation-related responses in human systems. {Figure 16.8; 16.A.1 }

Distribution of adaptation finance across different regions and different types of finance

(a) Distribution of adaptation finance across different regions and different types of finance in 2015–2016

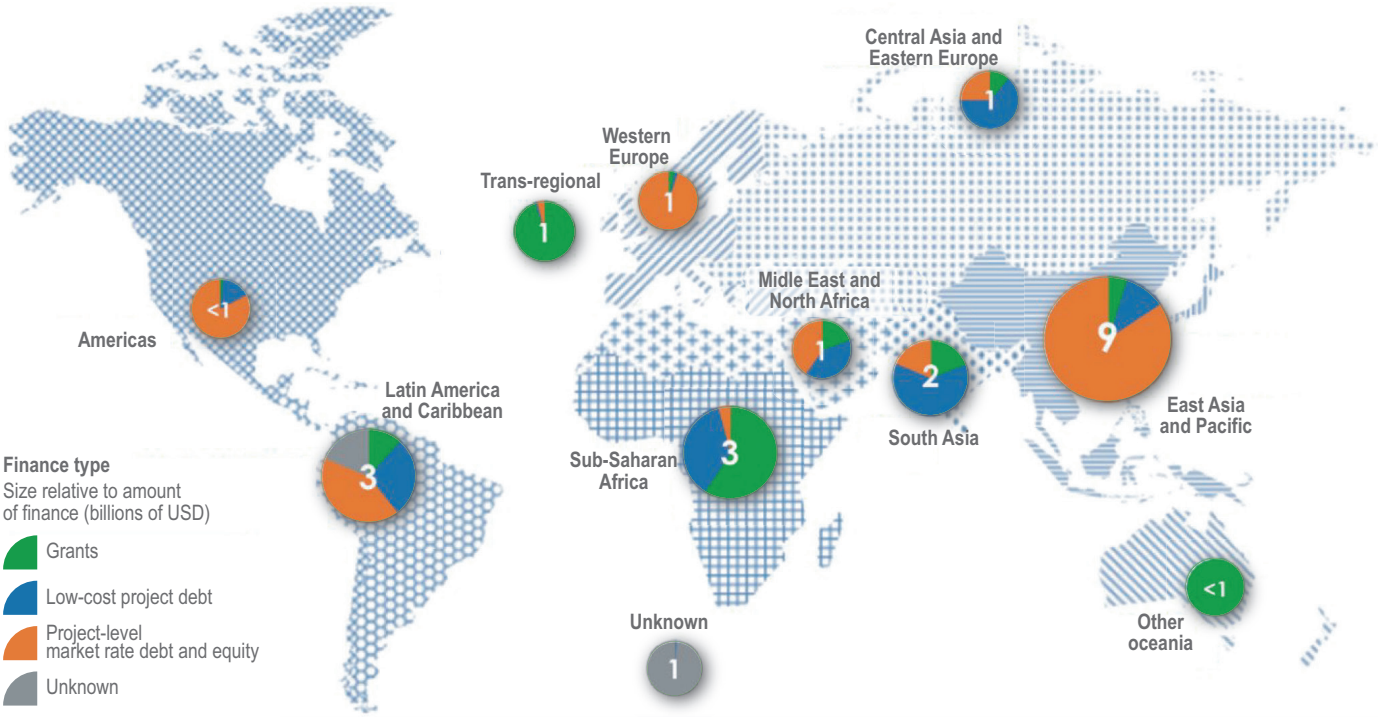

(b) Flow and distribution of globally tracked adaptation and resilience finance in 2018

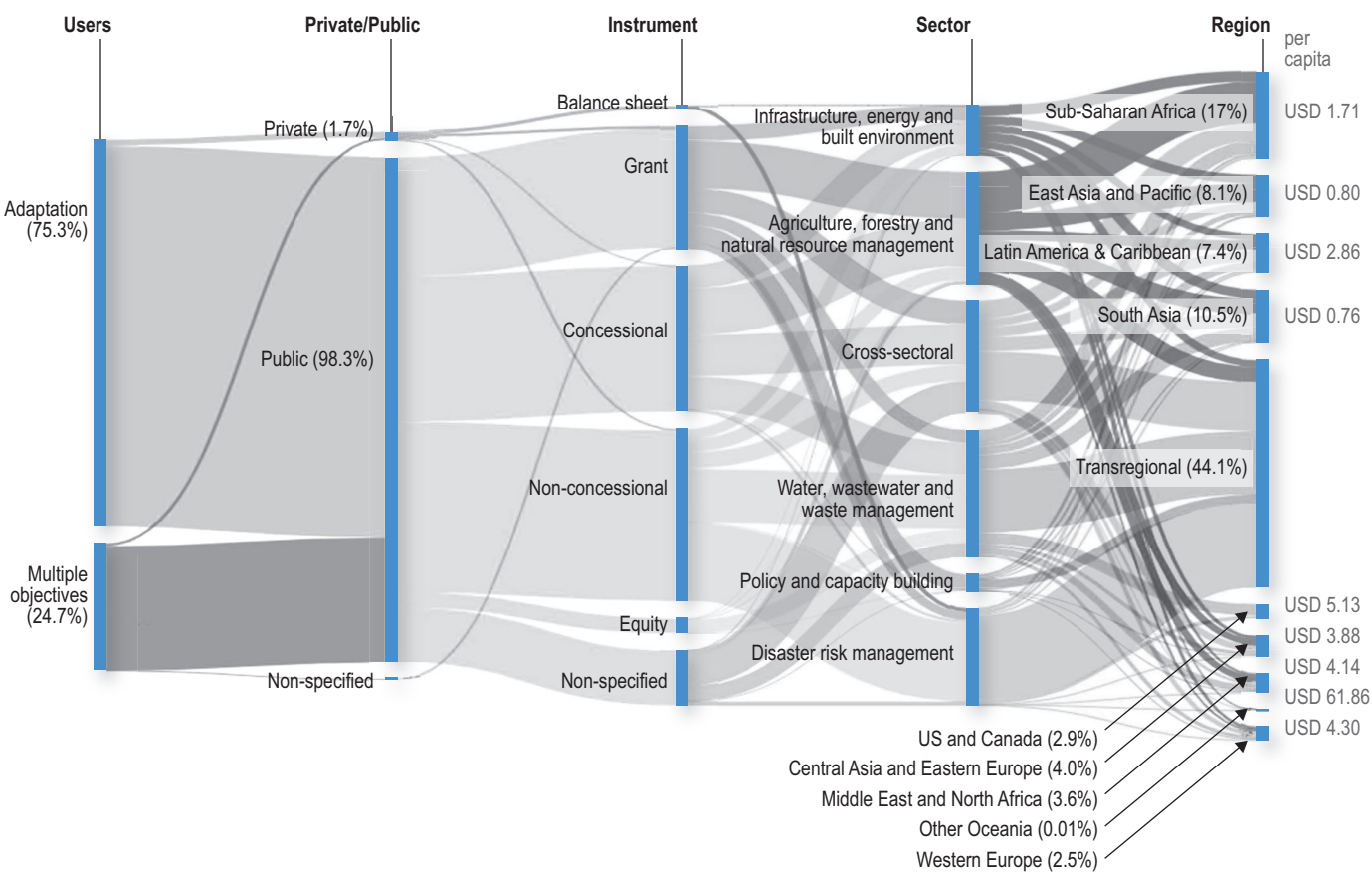

Figure AI.56 | Distribution of adaptation finance across different regions and different types of finance.

(a) Data for period 2015–2016, as tracked by the Climate Policy Initiative (CPI).

(b) Each strand shows the relative proportion of finance flowing from one category to another (for example from private or public sources to different instruments). Categories from left to right are: Use = whether the finance is solely for adaptation or for adaptation and other objectives, including mitigation; Public/Private = whether the finance comes from public or private sources; Instrument, the financing instrument; Sector = the broad sectoral allocation; Region = the geographical distribution of funding (proportion of total in % and per-capita allocation). Data for year 2018 from different sources, through different instruments into different sectors and regions as collated by CPI (2020). {Figure FINANCE.2 in Chapter 17; Figure FAQ17.2.1}

References

Alfieri, L., et al., 2017: Global projections of river flood risk in a warmer world. *Earth's Future*, **5**(2), 171–182, doi:10.1002/2016ef000485.

Assis, J., et al., 2017: Bio-ORACLE v2.0: Extending marine data layers for bioclimatic modelling. *glob. Ecol. Biogeogr.*, **27**, 277–284, doi:10.1111/geb.12693.

Barragán, J.M. and M. de Andrés, 2015: Analysis and trends of the world's coastal cities and agglomerations. *Ocean Coast. Manag.*, **114**, 11–20.

Beal, T., et al., 2017: Global trends in dietary micronutrient supplies and estimated prevalence of inadequate intakes. *PLoS ONE*, **12**(4), e175554, doi:10.1371/journal.pone.0175554.

Bell, J.D., et al., 2018a: Climate change impacts, vulnerabilities and adaptations: Western and Central Pacific Ocean marine fisheries. In: *Impacts of Climate Change on Fisheries and Aquaculture: Synthesis of Current Knowledge, Adaptation and Mitigation Options*. [Barange, M., T. Bahri, M. C. M. Beveridge, K. L. Cochrane, S. Funge-Smith and F. Poulain (eds.)]. Food and Agriculture Organization of the United Nations, Rome, Italy, pp. 305–324. ISBN 978-9251306079.

Berrang-Ford, L., et al., 2021a: The Global Adaptation Mapping Initiative (GAMI): Part 1 – Introduction and overview of methods. *protocolexchange*, doi:10.21203/rs.3.pex-1240/v1.

Berrang-Ford, L., et al., 2021b: A systematic global stocktake of evidence on human adaptation to climate change. *Nat. Clim. Chang.* in press.

Blasiak, R., et al., 2017: Climate change and marine fisheries: Least developed countries top global index of vulnerability. *PLoS ONE*, **12**(6), e179632, doi:10.1371/journal.pone.0179632.

Boone, R., et al., 2018: Climate change impacts on selected global rangeland ecosystem services. *Glob Change Biol*, **24**(3), 1382–1393, doi:10.1111/gcb.13995.

Callaghan, M., et al., 2021: Machine learning-based evidence and attribution mapping of 100,000 climate impact studies. *Nat. Clim. Chang.* **11**, 966–972 (2021). https://doi.org/10.1038/s41558-021-01168-6

Carleton, T., et al., 2018: *Valuing the Global Mortality Consequences of Climate Change Accounting for Adaptation Costs and Benefits*. University of Chicago, Becker Friedman Institute for Economics Working Paper, Vol. 2018-51. doi:10.2139/ssrn.3224365. University of Chicago, Chicago.

Carrão, H., G. Naumann and P. Barbosa, 2016: Mapping global patterns of drought risk: An empirical framework based on sub-national estimates of hazard, exposure and vulnerability. *Glob. Environ. Chang.*, **39**, 108–124, doi:10.1016/j.gloenvcha.2016.04.012.

Cheung William, W.L., G. Reygondeau and T.L. Frölicher, 2016: Large benefits to marine fisheries of meeting the 1.5°C global warming target. *Science (New York NY)*, **354**(6319), 1591–1594, doi:10.1126/science.aag2331.

Cottrell, R.S., et al., 2019: Food production shocks across land and sea. *Nat. Sustain.*, **2**(2), 130–137, doi:10.1038/s41893-018-0210-1.

Cook, W.D., K. Tone and J. Zhu, 2014: Data envelopment analysis: Prior to choosing a model. *Omega*, **44**, 1–4, doi:10.1016/j.omega.2013.09.004.

Cooper, J.A.G., et al., 2020a: Sandy beaches can survive sea-level rise. *Nat. Clim. Chang.*, **10**(11), 993–995, doi:10.1038/s41558-020-00934-2.

Corbane, C., et al., 2018: GHS built-up grid, derived from Landsat, multitemporal (1975-1990-2000-2014), R2018A. European Commission, Joint Research Centre (JRC), Brussels.

CPI, 2020: *Updated View of the Global Landscape of Climate Finance 2019. Rob Macquarie, Baysa Naran, Paul Rosane, Matthew Solomon, Cooper Wetherbee*. Climate Policy, I, London, https://www.climatepolicyinitiative.org/publication/updated-view-on-the-global-landscape-of-climate-finance-2019. Accessed 2021.

Ebi, K., et al., 2021: Burning embers: synthesis of the health risks of climate change. *Environ. Res. Lett.*, **16**(4), doi:10.1088/1748-9326/abeadd.

FAO, 2018b: *The State of World Fisheries and Aquaculture: Meeting the Sustainable Development Goals* [Barange, M., J. Alder, U. Barg, S. Funge-Smith, P. Mannini, M. Taconet and J. Plummer (eds.)]. The State of World Fisheries and Aquaculture (SOFIA), FAO, Rome, Italy. 277 pp.

Fluet-Chouinard, E., S. Funge-Smith and P.B. McIntyre, 2018: Global hidden harvest of freshwater fish revealed by household surveys. *Proc. Natl. Acad. Sci.*, **115**(29), 7623, doi:10.1073/pnas.1721097115.

García Molinos, J., et al., 2016: Climate velocity and the future global redistribution of marine biodiversity. *Nature Clim Change*, **6**, 83–88, doi:10.1038/NCLIMATE2769.

Gilbert, M., Nicolas, G., Cinardi, G., Van Boeckel, T. P., Vanwambeke, S. O., Wint, G. R. W., & Robinson, T. P. (2018). Global distribution data for cattle, buffaloes, horses, sheep, goats, pigs, chickens and ducks in 2010. Scientific Data, 5(1), 180227. doi: 10.1038/sdata.2018.227

Golden, C.D., et al., 2016: Nutrition: Fall in fish catch threatens human health. *Nature*, **534**(7607), 317–320, doi:10.1038/534317a.

Greve, P., et al., 2018: Global assessment of water challenges under uncertainty in water scarcity projections. *Nat. Sustain.*, **1**(9), 486–494, doi:10.1038/s41893-018-0134-9.

Gutiérrez, J.M., R.G. Jones, G.T. Narisma, L.M. Alves, M. Amjad, I. V. Gorodetskaya, M. Grose, N.A.B. Klutse, S. Krakovska, J. Li, D. Martínez-Castro, L.O. Mearns, S.H. Mernild, T. Ngo-Duc, B. van den Hurk, and J.-H. Yoon, 2021: Atlas. In: *Climate Change 2021: The Physical Science Basis. Contribution of Working Group I to the Sixth Assessment Report of the Intergovernmental Panel on Climate Change*. [Masson-Delmotte, V., P. Zhai, A. Pirani, S. L. Connors, C. Péan, S. Berger, N. Caud, Y. Chen, L. Goldfarb, M. I. Gomis, M. Huang, K. Leitzell, E. Lonnoy, J. B. R. Matthews, T. K. Maycock, T. Waterfield, O. Yelekçi, R. Yu and B. Zhou (eds.)]. Cambridge University Press, Cambridge.

Haasnoot, M., et al., 2019a: Generic adaptation pathways for coastal archetypes under uncertain sea-level rise. *Environ. Res. Commun.*, **1**(7), 71006.

Haasnoot, M., et al., 2021: Long-term sea-level rise necessitates a commitment to adaptation: A first order assessment. *Clim. Risk Manag.*, **34**, doi:10.1016/j.crm.2021.100355.

Hirabayashi, Y., et al., 2021b: Global exposure to flooding from the new CMIP6 climate model projections. *Sci Rep*, **11**(1), 3740, doi:10.1038/s41598-021-83279-w.

Hoornweg, D. and K. Pope, 2017: Population predictions for the world's largest cities in the 21st century. *environ urban*, **29**(1), 195–216.

IPCC, 2012: *Managing the Risks of Extreme Events and Disasters to Advance Climate Change Adaptation. A Special Report of Working Groups I and II of the Intergovernmental Panel on Climate Change* [Field, C.B., V. Barros, T.F. Stocker, D. Qin, D.J. Dokken, K.L. Ebi, M.D. Mastrandrea, K.J. Mach, G.-K. Plattner, S.K. Allen, M. Tignor, and P.M. Midgley (eds.)]. Cambridge University Press, Cambridge, UK, and New York, NY, USA, 582 pp

IPCC, 2014: *Climate Change 2014: Impacts, Adaptation, and Vulnerability. Part A: Global and Sectoral Aspects. Contribution of Working Group II to the Fifth Assessment Report of the Intergovernmental Panel on Climate Change* [Field, C.B., V.R. Barros, D.J. Dokken, K.J. Mach, M.D. Mastrandrea, T.E. Bilir, M. Chatterjee, K.L. Ebi, Y.O. Estrada, R.C. Genova, B. Girma, E.S. Kissel, A.N. Levy, S. MacCracken, P.R. Mastrandrea, and L.L. White (eds.)]. Cambridge University Press, Cambridge, UK and New York, NY, USA.

IPCC, 2019: *Special Report on the Ocean and Cryosphere in a Changing Climate* [H.-O. Pörtner, D.C. Roberts, V. Masson-Delmotte, P. Zhai, M. Tignor, E. Poloczanska, K. Mintenbeck, A. Alegría, M. Nicolai, A. Okem, J. Petzold, B. Rama, N.M. Weyer (eds.)]. In press

Jägermeyr, J., et al., 2021: Climate change signal in global agriculture emerges earlier in new generation of climate and crop models. *Nat. Food Press*, doi:10.21203/rs.3.rs-101657/v1.

Jurgilevich, A., A. Räsänen, F. Groundstroem and S. Juhola, 2017: A systematic review of dynamics in climate risk and vulnerability assessments. *Environ. Res. Lett.*, **12**(1), 13002.

Kay, R. and J. Adler, 2017: *Coastal Planning and Management*. CRC Press, London.

Kelly-Gerreyn, B.A., et al., 2014: Benthic biomass size spectra in shelf and deep-sea sediments. *Biogeosciences*, **11**(22), 6401–6416, doi:10.5194/bg-11-6401-2014.

Kienberger, S., T. Blaschke and R.Z. Zaidi, 2013: A framework for spatio-temporal scales and concepts from different disciplines: the 'vulnerability cube'. *Nat. Hazards*, **68**(3), 1343–1369.

Klein Goldewijk, K., A. Beusen and P. Janssen, 2010: Long-term dynamic modeling of global population and built-up area in a spatially explicit way: HYDE 3.1. *Holocene*, **20**(4), 565–573.

Klein Goldewijk, K., A. Beusen, G. Van Drecht and M. De Vos, 2011: The HYDE 3.1 spatially explicit database of human-induced global land-use change over the past 12,000 years. *Glob. Ecol. Biogeogr.*, **20**(1), 73–86.

Kulp, S. and B. Strauss, 2019: New elevation data triple estimates of global vulnerability to sea-level rise and coastal flooding. *Nat Commun*, **10**(4844), doi:10.1038/s41467-019-12808-z.

Kwiatkowski, L., O. Aumont and L. Bopp, 2019: Consistent trophic amplification of marine biomass declines under climate change. *Glob Change Biol*, **25**(1), 218–229, doi:10.1111/gcb.14468.

Meredith, M., M. Sommerkorn, S. Cassotta, C. Derksen, A. Ekaykin, A. Hollowed, G. Kofinas, A. Mackintosh, J. Melbourne-Thomas, M.M.C. Muelbert, G. Ottersen, H. Pritchard, and E.A.G. Schuur, 2019: Polar Regions. In: *IPCC Special Report on the Ocean and Crysosphere in a Changing Climate* [Pörtner, H. O., D. C. Roberts, V. Vmasson-Delmotte, P. Zhai, M. Tignor, E. Poloczanska, K. Mintenbeck, A. Alegría, M. Nicolai, A. Okem, J. Petzold, B. Rama and N. M. Weyer (eds.)], In press. pp. 203–320.

Meza, I., et al., 2020: Global-scale drought risk assessment for agricultural systems. *Nat. Hazards Earth Syst. Sci.*, **20**(2), 695–712, doi:10.5194/nhess-20-695-2020.

Miller, K. A., G.R. Munro, U.R. Sumaila and W.W.L. Cheung, 2013: Governing marine fisheries in a changing climate: a game-theoretic perspective. *Can. J. Agric. Econ.*, **61**(2), 309–334, doi:10.1111/cjag.12011.

Mills, G., et al., 2018: Closing the global ozone yield gap: quantification and cobenefits for multistress tolerance. *Glob Chang Biol*, **24**(10), 4869–4893, doi:10.1111/gcb.14381.

Mora, C., et al., 2017b: Global risk of deadly heat. *Nature Clim Change*, **7**, 501.

Nyboer, E.A., C. Liang and L.J. Chapman, 2019: Assessing the vulnerability of Africa's freshwater fishes to climate change: A continent-wide trait-based analysis. *Biol. Conserv.*, **236**, 505–520, doi:10.1016/j.biocon.2019.05.003.

Østhagen, A., J. Spijkers and O.A. Totland, 2020: Collapse of cooperation? The North-Atlantic mackerel dispute and lessons for international cooperation on transboundary fish stocks. *Marit. Stud.*, **19**(2), 155–165, doi:10.1007/s40152-020-00172-4.

Robinson, L.M., et al., 2015: Rapid assessment of an ocean warming hotspot reveals "high" confidence in potential species' range extensions. *Glob. Environ. Change.*, **31**, 28–37, doi:10.1016/j.gloenvcha.2014.12.003.

Rufat, S., E. Tate, C.G. Burton and A.S. Maroof, 2015: Social vulnerability to floods: review of case studies and implications for measurement. *Int. J. Disaster Risk Reduct.*, **14**, 470–486.

Scussolini, P., et al., 2016: FLOPROS: an evolving global database of flood protection standards. *Nat. Hazards Earth Syst. Sci.*, **16**(5), 1049–1061, doi:10.5194/nhess-16-1049-2016.

Selig, E.R., et al., 2019: Mapping global human dependence on marine ecosystems. *CONSERVATION LETTERS*, **12**(2), e12617, doi:10.1111/conl.12617.

Sharps, K., et al., 2020: *Yield Constraint Score (YCS) for the effect of five crop stresses on global production of four staple food crops*. NERC Environmental Information Data Centre, https://doi.org/10.5285/d347ed22-2b57-4dce-88e3-31a4d00d4358. Accessed on 2020-11-26 17:25

Spielman, S.E., et al., 2020: Evaluating social vulnerability indicators: criteria and their application to the Social Vulnerability Index. *Nat Hazards*, **100**(1), 417–436.

Stuart-Smith, J., et al., 2018: Southernmost records of two Seriola species in an Australian ocean-warming hotspot. *Mar. Biodivers.*, **48**(3), 1579–1582, doi:10.1007/s12526-016-0580-4.

Taberna, A., T. Filatova, D. Roy and B. Noll, 2020: Tracing resilience, social dynamics and behavioral change: a review of agent-based flood risk models. *Socio-Environ. Syst. Model.*, **2**, 17938.

Tanoue, M., Y. Hirabayashi and H. Ikeuchi, 2016: Global-scale river flood vulnerability in the last 50 years. *Sci Rep*, **6**, 36021, doi:10.1038/srep36021.

Tanoue, M., R. Taguchi, H. Alifu and Y. Hirabayashi, 2021: Residual flood damage under intensive adaptation. *Nat. Clim. Chang.* In Press.

Thomas, A., et al., 2021: Global evidence constraints and limits to human adaptation. *Reg Environ Change*, **21**, doi:10.1007/s10113-021-01808-9.

Thornton, P.K., G.C. Nelson, D. Mayberry and M. Herrero, 2021: Increases in extreme heat stress in domesticated livestock species during the twenty-first century. *Glob. Chang. Biol.*, doi:10.1111/gcb.15825.

Tittensor, D.P., et al., 2018: A protocol for the intercomparison of marine fishery and ecosystem models: Fish-MIP v1.0. *Geosci. Model Dev.*, **11**(4), 1421–1442, doi:10.5194/gmd-11-1421-2018.

Tittensor, D.P., et al., 2021: Next-generation ensemble projections reveal higher climate risks for marine ecosystems. *Nat. Clim. Chang.* Accepted.

Trisos, C.H., C. Merow and A.L. Pigot, 2020: The projected timing of abrupt ecological disruption from climate change. *Nature*, **580**(7804), 496–501, doi:10.1038/s41586-020-2189-9.

UNISDR, 2004: Living with risk: A global review of disaster reduction initiatives: Version 1. In: Living with risk: A global review of disaster reduction initiatives: Version 1. UN. International Strategy for Disaster Reduction (ISDR). Secretariat; World ….

Viviroli, D., et al., 2020: Increasing dependence of lowland populations on mountain water resources. *Nat. Sustain.*, doi:10.1038/s41893-020-0559-9.

Vousdoukas, M.I., et al., 2020a: Reply to: Sandy beaches can survive sea-level rise. *Nat. Clim. Chang.*, **10**(11), 996–997, doi:10.1038/s41558-020-00935-1.

Vousdoukas, M.I., et al., 2020b: Sandy coastlines under threat of erosion. *Nat. Clim. Chang.*, **10**(3), 260–263, doi:10.1038/s41558-020-0697-0.

World Bank, 2019: *The World Governance Indicators*. https://info.worldbank.org/governance/wgi/.

World Bank, 2020: *The World Development Indicators: GDP (current US$)*. https://data.worldbank.org/indicator/NY.GDP.MKTP.CD.

Xu, C., et al., 2020: Future of the human climate niche. *Proc. Natl. Acad. Sci.*, **117**(21), 11350–11355, doi:10.1073/pnas.1910114117.

Yool, A., et al., 2017: Big in the benthos: future change of seafloor community biomass in a global, body size-resolved model. *Glob Change Biol*, **23**(9), 3554–3566, doi:10.1111/gcb.13680.